Applications of genetically engineered *Bacillus subtilis* in biocatalysis and functional materials

Thesis by

Yue Hui

In Partial Fulfillment of the Requirements for

the Degree of

Doctor of Philosophy in Chemical

Engineering

CALIFORNIA INSTITUTE OF TECHNOLOGY

Pasadena, California

2023

(Defended July 22, 2022)

Yue Hui
ORCID: 0000-0002-0354-0382

ACKNOWLEDGEMENTS

First, I would like to thank my advisor, Prof. David Tirrell for his guidance throughout my graduate studies. I deeply appreciate the intellectual freedom that Dave has given me to explore ideas that I found interesting. I greatly enjoy conversations with Dave for his unique insights on scientific topics and lively stories. The independent and critical thinking that I strive to acquire under Dave's guidance helps shape my way of approaching science and far beyond. I'm grateful for everything Dave has taught me.

I would like to thank my committee members: Prof. Mikhail Shapiro, Prof. Dianne Newman, and Prof. Zhen-Gang Wang. They provided me with new perspectives on my work through their constructive comments and suggestions during meetings. I also appreciate Prof. Zhen-Gang Wang for letting me TA for the graduate-level thermodynamics course. It was a great learning opportunity and a lot of fun.

I would like to thank the current and previous members of the Tirrell lab for fostering the fantastic lab culture that I greatly enjoyed over the years. I would like to thank the MCME subgroup members for their valuable suggestions on my work, Dr. Samuel Ho for teaching me western blot and protein purification, Dr. Bradley Silverman for letting me use some of his bacterial strains, and Elliot Mackrell for fun discussions about project ideas on *Bacillus.* I would also like to thank the rest of the Caltech community for their support over the years: Dr. Andres Collazo and Dr. Giada Spigolon for their kind assistance on the usage of the confocal microscopes at BIF, Allison Kinard and Irina Meininger for supporting the graduate program, Laura Kim and Daniel Yoder at ISP for their guidance on immigration-related issues.

I would like to thank all my friends and collaborators. I always feel so lucky to have these people in my life. I'd like to thank Prof. Seunghyun Sim, who I collaborated with throughout my graduate studies (Chapter 4). Besides her sharp insights on scientific topics, I also learned from her good habits of preparing weekly summaries and marking calendars for the most efficient use of my time during grad school. She is both a mentor and a friend. I'd like to

thank Dr. Xinran Liu, my officemate and project-mate, for her neat BONCAT specialties and friendship. I'd like to thank Ziyu Cui, for her hard work, which became part of Chapter 3 and the many long days (including some holidays when we were the only people in the building) we had trouble-shooting together. Special thanks to my best friend Dr. Hyuna Jo for all the chats, meals, and trips to Starbucks that we had together, and for always being there for me when I needed a listener. To me, doing science with friends is the #1 happiest experience I had during grad school.

I would like to thank mentors and friends from before I came to Caltech, especially Prof. Young-Shin Jun, who advised me during college. My journey with science started in the Jun lab. I am deeply grateful to Prof. Jun's mentorship that led me to pursue my PhD and her continued support during my graduate studies. I would also like to thank Prof. Lijie Zhang, Amanda Lin, Zhiyan Jiang, and Dr. Yanzhe Zhu for their continued friendship.

Finally, I would like to thank my family for their love throughout my life. Thanks to my parents for funding my education and for their unconditional support for me to pursue my life goals despite being thousands of miles away. I will always be grateful for the faith and trust they place in me. I would also like to thank my cousins, Zihan Wen and Jiehao Yan, who often come visit me and bring me the feeling of family.

ABSTRACT

Bacillus subtilis is a gram-positive model bacterium that forms endospores as a response to nutrient limitation and other environmental stresses. The *B. subtilis* spore contains a dehydrated core, where the bacterial genome is safely stored, and multilayer proteinaceous coats, protecting the spore from various physical and chemical insults. Because of the outstanding resilience of the *B. subtilis* spore, it has attracted increasing interest for application in biotechnology. In this thesis, we demonstrate the utilization of genetically engineered *B. subtilis* cells and spores for heterologous protein display and functional material synthesis and characterization.

In Chapter 1, we review the fundamentals of sporulation and germination in *B. subtilis*. We highlight notable biotechnological applications of native and engineered *B. subtilis* spores in recent years. We also discuss limitations associated with prior studies that inspire us to pursue the work in this thesis.

In Chapter 2, we describe the T7 RNA polymerase (RNAP) enabled high density protein display on *B. subtilis* spores (TIED) method. The TIED constructs employ a coat protein promoter – P_{cotG}, P_{cotV}, or P_{cotZ} – to drive the expression of the T7 RNAP. Target proteins are fused to the C-terminus of a spore crust protein – CotY or CotZ – and subjected to amplification by the T7 promoter. We prepare the endogenous constructs in which coat protein promoters directly regulate fusion protein expression for comparison with TIED. In addition, we develop a supplementary procedure to harvest spores before mother cell lysis, further improving the loading density of the target proteins. We verify the performance of the TIED architectures with a fluorescent reporter protein, mWasabi. Together with the early harvest protocol, the TIED method substantially enhances the total expression level and loading density of the crust-mWasabi fusion proteins relative to the endogenous expression system, as evidenced by bulk fluorescence measurements and microscopy.

In Chapter 3, we implement the TIED architectures described in Chapter 2 for enzyme display on *B. subtilis* spores. We demonstrate the spore-based biocatalyst platform with three enzymes – lipase A and lipase B secreted by vegetative *B. subtilis*, and an engineered

peroxidase, APEX2. We manifest that TIED enables massive accumulation of all three enzymes on the spore surface, with loading densities in the range of 10^6-10^7 enzymes per spore. Further, TIED-enzymes show comparable catalytic performance to the respective free-form enzymes, enhanced catalytic activity in methanol, and increased temperature stability. We conduct Michaelis-Menten studies to elucidate the kinetic characteristics of TIED-enzymes and their free form counterparts. Finally, we demonstrate that TIED-enzymes are not only recyclable, but also fully renewable after loss of activity through induction of germination and sporulation, demonstrating the potential for perpetual regeneration of the immobilized biocatalysts.

In Chapter 4, we describe a new class of living composite materials (LCMs), in which genetically engineered *B. subtilis* cells and spores are effectively crosslinked into the surrounding polymeric scaffold. The resulting LCMs can be dried to yield portable materials. When re-immersed in aqueous media, entrapped cells and spores in previously-dried LCMs exhibit metabolic activity, including synthesis and secretion of recombinant proteins. Notably, we show that the scaffold based on photopolymerization of *N*-(hydroxymethyl) acrylamide (NHMAA) achieves effective cellular confinement, showing no evidence of cellular leakage over a period of 72 hours. We envision that the design principles elucidated in this work can provide a promising route to functional living materials engineered for biomedical and other applications.

PUBLISHED CONTENT AND CONTRIBUTIONS

1. S. Sim*, Y. Hui*, and D. A. Tirrell, 3D-printable cellular composites for production of recombinant proteins. *Manuscript submitted*.
   Y. H. contributed to the preparation of new bacterial strains, experimental work, microscopic image analysis, and manuscript writing.

2. Y. Hui, Z. Cui, and S. Sim, Stress-tolerant, recyclable, and renewable biocatalyst platform enabled by engineered bacterial spores. *ACS Synthetic Biology, ASAP*, DOI: 10.1021/acssynbio.2c00256
   Y. H. contributed to the conception of the project, experimental work, data analysis, and manuscript writing.

TABLE OF CONTENTS

Acknowledgements……...iii
Abstract ……v
Published Content and Contributions…….....vii
Table of Contents……. viii
List of Illustrations and/or Tables……x

Chapter I: The *Bacillus subtilis* Spore and its Application in Biotechnology 1
1.1 Introduction 1
1.2 Genetic Regulation of Spore Formation.....2
1.3 Structure and Properties of the Spore.....4
1.4 Germination.....5
1.5 Engineered Spores as Platforms for Heterologous Protein Display.....5
1.6 Application of Spores in Functional Materials 8
1.7 References 10

Chapter II: T7 RNA Polymerase Enabled High Density Protein Display on *Bacillus subtilis* Spores 23
2.1 Introduction 24
2.2 Results and Discussion 25
2.3 Conclusions 30
2.4 Materials and Methods 31
2.5 Supplementary Tables and Figures 33
2.6 Acknowledgements 38
2.7 References 39

Chapter III: Stress-Tolerant, Recyclable, and Renewable Biocatalyst Platform by Engineered *Bacillus subtilis* Spores 42

3.1 Introduction 43

3.2 Results and Discussion 44

3.2.1 Catalytic Performance of TIED-LipB 44

3.2.2 Catalytic Performance of TIED-LipA 48

3.2.3 Catalytic Performance of TIED-APEX2 51

3.2.4 Recycling and Renewal of TIED-Enzymes 54

3.3 Conclusions 57

3.4 Materials and Methods 59

3.5 Supplementary Tables and Figures 66

3.6 Acknowledgements 79

3.7 References 80

Chapter IV: Leak-Free Cellular Composites for Production of Recombinant Proteins 86

4.1 Introduction 87

4.2 Results and Discussion 88

4.3 Conclusions 97

4.4 Materials and Methods 98

4.5 Supplementary Tables and Figures 103

4.6 Acknowledgements 114

4.7 References 115

LIST OF ILLUSTRATIONS AND/OR TABLES

Number *Page*

1. Figure 1.1: Sporulation and Germination in *B. subtilis* 2
2. Figure 1.2: Genetic Regulation of the *B. subtilis* Spore Formation 3
3. Figure 1.3: Structure of the *B. subtilis* Spore 4
4. Figure 2.1: Genetic Constructs 25
5. Figure 2.2: Total Expression Level of the Fusion Proteins 26
6. Figure 2.3: Microscopic Images 27
7. Figure 2.4: Spore Fluorescence of TIED-mWasabi 28
8. Figure 2.5: Distribution of the Fusion Proteins 29
9. Table S2.1: Protein and Peptide Sequences 33
10. Table S2.2: Genetic Constructs.....34
11. Figure S2.1: Early Harvest and Natural Maturation.....35
12. Figure S2.2: Cells and Spores Before Early Harvest.....36
13. Figure S2.3: Spore Fluorescence 37
14. Figure 3.1: Catalytic Performance of TIED-LipB.....45
15. Figure 3.2: Michaelis Menten Analysis of LipB 46
16. Figure 3.3: Resilience of TIED-LipB.....48
17. Figure 3.4: Catalytic Performance of TIED-LipA 49
18. Figure 3.5: Michaelis Menten Analysis of LipA.....50
19. Figure 3.6: Resilience of TIED-LipA 51
20. Figure 3.7: Catalytic Performance of TIED-APEX2 53
21. Figure 3.8: Recycling and Renewal of TIED-LipA 55
22. Figure 3.9: Recycling and Renewal of TIED-LipA in Methanol 56
23. Figure 3.10: Illustration of the TIED Method 57
24. Table S3.1: Protein Sequences.....66
25. Table S3.2: Genetic Constructs.....67
26. Figure S3.1: Spores of TIED-Enzymes.....69

27. Figure S3.2: Calibration Curves 70
28. Figure S3.3: Western Blot Images 71
29. Figure S3.4: Quantitative Western Blot Analysis 72
30. Figure S3.5: Kinetics Study of LipB.....73
31. Figure S3.6: Free Form lipases in Organic Solvents 74
32. Figure S3.7: Kinetics Study of LipA 75
33. Figure S3.8: Kinetics Study of APEX2.....76
34. Figure S3.9: Recycling of TIED-LipA 77
35. Figure S3.10: Recycling of TIED-LipB.....78
36. Figure S3.11: Recycling of TIED-APEX2.....79
37. Figure 4.1: Characterization of the Pristine LCMs.....89
38. Figure 4.2: Characterization of the Re-swollen LCMs.....91
39. Figure 4.3: Characterization of the Spore-based LCMs 93
40. Figure 4.4: Protein Secretion by the Re-swollen LCMs.....96
41. Figure 4.5: Illustration of the LCMs 95
42. Table S4.1: Primer Sequences 103
43. Figure S4.1: CFU Analysis.....104
44. Figure S4.2: Viability Analysis of the Cell-based LCMs.....105
45. Figure S4.3: Protein Production in the Cell-based LCMs 106
46. Figure S4.4: Characterization of $PNIPAM_{Spore}$ 107
47. Figure S4.5: Characterization of $PNHMAA_{cell}$ 108
48. Figure S4.6: Viability Analysis of the Spore-based LCMs 109
49. Figure S4.7: Characterization of $PNHMAA_{mRFP}$ 110
50. Figure S4.8: Characterization of $PNIPAM_{mRFP}$.....111
51. Figure S4.9: Characterization of $PNHMAA_{mRFP\_S}$.....112
52. Figure S4.10: Characterization of $PNIPAM_{mRFP\_S}$.....113

Chapter 1

THE BACILLUS SUBTILIS SPORE AND ITS APPLICATION IN BIOTECHNOLOGY

1.1 Introduction

Bacteria have developed a wide variety of strategies to survive in harsh environments. Sporulation, a cell differentiation process undertaken by *B. subtilis*, is an adaptive response to environmental stresses, such as starvation.[1-7] When nutrients available in an environment are insufficient to support binary fission, *B. subtilis* responds by entering sporulation. The result of the process is a metabolically dormant and partially dehydrated endospore, where the genome is safely stored for germination in the future, should conditions improve. Sporulation in *B.subtilis* has long been a model system in the study of developmental biology, such as gene regulation,[8-10] chromosome segregation,[11-13] membrane restructuring,[14-16] and intercellular quorum sensing.[17-19] Other research focuses on the structure and properties of *B. subtilis* spores. The multilayer proteinaceous coat structure provides the spores with strong resistance to many environmental stresses, such as heat, desiccation, and radiation, among others.[4,6,20-23] Because of this, *B.subtilis* spores have been engineered and utilized for various applications in biotechnology.[24-26] In this chapter, we review the physiology related to sporulation and germination in *B. subtilis*. We then discuss recent applications of *B. subtilis* cells and spores in biomedicine, biocatalysis, and functional materials.

1.2 Genetic Regulation of Spore Formation

Sporulation begins with asymmetric division into a smaller forespore compartment and a larger mother cell, separated by a septum. Then, the forespore is engulfed by the mother cell through a phagocytosis-like process. The engulfment is followed by synthesis of the cortex, which consists mainly of peptidoglycan, and by assembly of coat proteins. As the forespore fully matures, it is released into the environment, accompanied by mother cell lysis (**Figure 1.1**). A spore can remain dormant for decades until it senses nutrients in the environment and returns to the vegetative state through germination. Spores exhibit extraordinary environmental persistence, owing to the layers of protective protein coats and the partially dehydrated nature. Spores withstand high temperatures, desiccation, radiation, and chemical insults, such as antibiotics and hydrogen peroxide.[22,23,27-31]

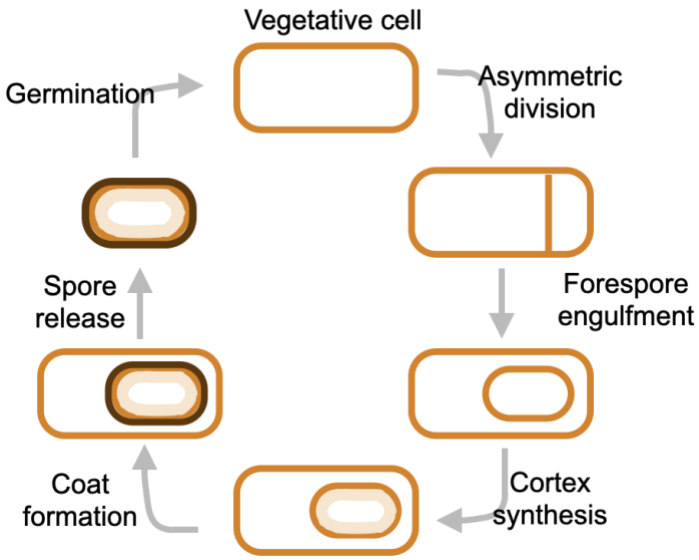

Figure 1.1. Sporulation and germination in *B. subtilis*

To make the decision to enter sporulation, *B. subtilis* employs a sophisticated apparatus for evaluation of a wide range of external signals, such as nutrient depletion and high population density. The commitment to sporulation is governed by several independent regulatory pathways, with the most critical one involving the master regulator, Spo0A (**Figure 1.2**). It

is estimated that more than 10% of *B. subtilis* genes are under control, directly or indirectly, of Spo0A.[1,32] Activation of a set of histidine sensor kinases (KinA, KinB, and KinC) transfers a phosphoryl group to Spo0A via a multicomponent phosphorelay.[33-35] An increased level of Spo0A phosphorylation is required for triggering sporulation, as it activates transcription of important regulators – *spoIIA*, *spoIIE*, and *spoIIG* –, induces asymmetric cell division, and promotes early mother-cell development.[35-37]

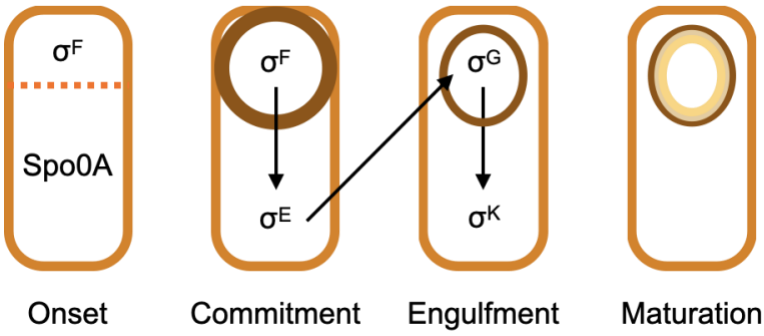

Figure 1.2. Compartment-specific genetic regulation of spore formation in *B. subtilis* (Figure adapted from Ref 38).[38]

Following asymmetric septum formation, distinct gene expression programs occur in the forespore and mother-cell compartments to drive further morphological development **(Figure 1.2)**. Cell-specific transcription is achieved by two σ-factors – σ^F in the forespore compartment and σ^E in the mother-cell compartment.[39-41] An elaborate genetic regulation system is in place to ensure high-resolution spatiotemporal control of the σ-factors' activity. Hydrolysis of cell wall components in the septum leads to wrapping of its membrane around the forespore. The complete enclosure of the forespore sets the beginning of late-stage spore development. Another set of compartment specific σ-factors – σ^G in the forespore compartment and σ^K in the mother-cell compartment – become active as early-phase σ-factors are removed by proteases. σ^G and σ^K, together with other transcriptional regulators orchestrate cortex synthesis and coat protein assembly, resulting in formation of the mature spore (**Figure 1.2**).[42-44]

1.3 Structure and Properties of the Spore

Application of electron microscopy to sporulating *B. subtilis* has revealed the details of spore structure (**Figure 1.3**).[45] The bacterial genome is safely stored in the partially dehydrated core, where water has mostly been replaced with Ca^{2+}-dipicolinic acid. Surrounding the core are the inner membrane, germ cell wall, cortex, and outer membrane. Most importantly, three morphologically distinct layers of coat proteins – a laminar inner coat, a rough outer coat, and an outermost crust – together protect spores from various environmental stresses and define their interaction with different surfaces (**Figure 1.3**). A complex genetic regulation network defines the protein-protein interactions and orchestrates the assembly of the coat layers. Studies utilizing reverse genetics approaches have identified critical morphogenic proteins that serve as hubs for the assembly of others.[46-48] SafA was identified as the interaction center for inner coat proteins, including CotD, CotP, CotT, OxdD, among many others; while CotE governs the assembly of the outer coat layer, consisting of CotA, CotB, CotC, CotG, etc.[49,50] Recently, the composition and assembly of the crust layer have been elucidated. CotX, CotY and CotZ, individually or in conjunction, are necessary for crust assembly.[49,51] Notably, N-glycosylation motifs have been identified in multiple proteins in the crust layer (CotX, and potentially CotV, CotY, and CotZ), suggesting its potential involvement in the polysaccharide coating.[52]

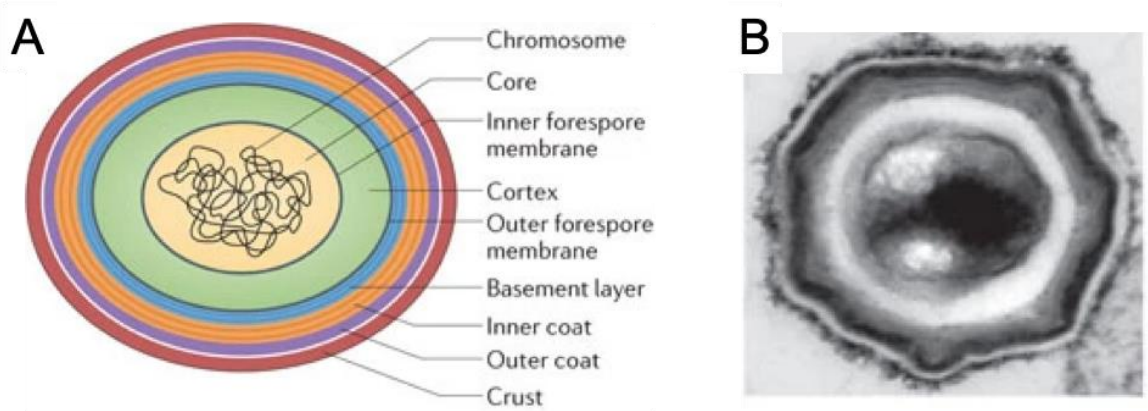

Figure 1.3. Structure of *B.subtilis* spore. (**A**) Cartoon illustration of a typical *B. subtilis* spore consisting of multiple layers (**B**) Thin section transmission electron micrograph of a *B. subtilis* spore stained with ruthenium red (Figure adapted from Ref 45).[45]

The structural features of the *B. subtilis* spore are essential to its resistance to various environmental stresses. The partially dehydrated nature of the core, in conjunction with the small acid soluble proteins that bind to the genome, provide the spore with strong tolerance for heat and desiccation. CotA, a copper dependent laccase, produces a dark pigment, effectively protecting the spore from UV radiation.[53] In addition, the pigment resembles melanin, which is known to provide resistance to peroxide in many microbes.[54] A recent study has found that major cystine-rich crust proteins, CotY and CotZ, in purified form, can each self-assemble into highly ordered secondary structures, implicating their importance for the structural integrity of the spore.[55] In addition, the formation of a crust polysaccharide layer is thought to further protect the spore against biological degradation and scavenging.[52]

1.4 Germination

Once spores are formed, they can remain dormant for years. Yet spores are able to germinate rapidly, on the minute timescale, to return to a metabolically active state once nutrients become available again. Environmental conditions are under constant monitoring of germinant receptors located in the inner spore membrane. Although macromolecules are largely excluded, small germinants, such as sugars, amino acids, and peptidoglycan fragments, are able to traverse the coat and cortex layers to reach the germinant receptors. Once the germination process begins, the coat layers open and eventually shed to allow outgrowth of a vegetative cell, resuming binary fission.

1.5 Engineered Spores as Platforms for Heterologous Protein Display

Spores of *B. subtilis* have emerged as versatile platforms for displaying heterologous proteins because of several reasons: 1) *B. subtilis* is generally recognized as safe (GRAS), which allows its wide applications in synthesis of food enzymes and additives.[56,57] 2) tight assembly of coat proteins endows spores with outstanding structural stability and resistance to harsh conditions commonly used in industrial processes. 3) industry-scale, streamlined production of spores can be achieved in an economic manner.[56,57] The most reported method to display proteins on the spore surface is via genetically encoded expression of the target for display

fused to an anchor protein located in the coat or crust layer. Usually, the fusion protein is placed under the same transcriptional regulation as the anchor protein, allowing its expression and assembly on spore surface. As more coat and crust proteins are identified and characterized, many have been examined as fusion partners for display, such as CotB,[58-64] CotC,[65-73] CotG,[74-80] CotZ,[81-84] CotY,[84,85] CgeA,[83,84] among others. Relying on this approach, many studies have demonstrated success in the display of bioactive molecules on *B.subtilis* spores.

One major application of the platform is for engineering novel whole-cell biocatalysts with surface displayed enzymes. Multiple studies have demonstrated the display of β-galactosidase (β-Gal).[70,78,84,86,87] Kwon et al. successfully installed β-Gal via C-terminal fusion with a spore coat protein, CotG. As a result, the displayed enzymes can catalyze the transgalactosylation of ONPG (ortho-nitrophenyl-β-galactoside) in aqueous biphasic systems, with 27.7% conversion yield. The tightly attached enzymes showed enhanced stability in a panel of organic solvents compared with the native enzyme.[78] Similarly, Wang et al. investigated crust proteins – CotY and CotZ – as fusion partners for β-Gal. Enzyme activity (0.12 and 0.25 U/mg spores for CotY and CotZ fusion, respectively) was confirmed for both constructs, further expanding choices of anchors offered by spores.[84] Besides β-Gal, many industrial enzymes have been shown to be compatible with the platform. Hinc et al. attached subunit A of urease (UreA) from *Helicobater acinonychis* to *B. subtilis* spores via fusion with CotB. Similar constructs with CotC and CotG as fusion partners led to issues with accessibility and protease cleavage of the displayed target despite positive expression, suggesting a need for target-specific anchor selection.[59] In Wang et al., the *Bombyx mori* alcohol dehydrogenase (BmADH) was installed via C-terminal fusion with CotC. Compared to the free enzyme, the immobilized BmADH showed stable catalytic activity in a wider range of temperature and pH.[71]

In addition to biocatalysis, the spore platform has found applications in the field of vaccine development. With displayed antigens, many examples of spore-enabled vaccines have been shown to trigger immune responses *in vivo*. In 2001, Isticato and coworkers presented the

first evidence of heterologous protein expression on the *B. subtilis* spore surface. The 495-amino-acid C-terminal fragment of tetanus toxin (TTFC) was successfully installed with the aid of CotB.[61] Surface presentation of TTFC was confirmed by western blot and flow cytometry analysis. Immunogenicity of the engineered spores in mice further suggests the displayed proteins retained their bioactive form. Following this pioneering work, many antigens have been investigated for display via CotB fusion, including the envelope protein VP28 of white spot syndrome virus (WSSV),[62] the VP1 protein of Enterovirus 71 (EV71),[58] influenza virus M2 protein,[88] *Streptococcus mutans* P1 protein,[64] MPT64 of TB virus,[63] *Clostridium perfringens* alpha toxin,[60] among others.

While most previous research on platform development has focused on screening and selection of fusion partners, several studies investigated the effect of linker sequence and structure. Hinc et al. compared a peptide linker that forms a strong α-helical structure (−GGGEAAAKGGG-) to one that does not (-GGGGS-). Fusion of UreA to CotB via the helical linker showed an approximately 100-fold improvement in loading density relative to the standard linker, suggesting linker sequence as another factor contributing to the display efficiency of heterologous proteins.[82] The reported linker sequence was adopted by many following studies, including the work to be discussed in Chapter 2 and 3.[81,89-91]

In summary, the engineering of *B. subtilis* spores as platforms for heterologous protein display has been under extensive investigation. Exploration of a wide variety of anchoring motifs in the spore coat and crust layers, as well as the linker sequences has enabled installation of enzymes, antigens, and other therapeutic proteins on the spore surface. Despite a great number of proof-of-concept demonstrations, applications of the technology are often limited by insufficient protein loading density, typically 10^2–10^5 proteins per spore.[92-94] In Chapter 2 and 3, we discuss a set of novel genetic architectures that employ the T7 RNA polymerase for high density enzyme display on *B. subtilis* spores.

1.6 Applications of Spores in Functional Materials

Functional soft materials with living cells or spores embedded in a structural scaffold have gained increasing research interest. The incorporation of metabolically active cells, genetically engineered in many examples, enables the composite materials to gain dynamic functions, such as self-healing,[95,96] self-cleaning,[97] and self-gluing.[98] These materials have found wide applications in the development of biosensors,[97,99-101] actuators, and robotics.[102,103] Among numerous microbes, *B. subtilis* appears to be well-suited for this purpose. The robust structure of spores allows them to survive harsh and unpredictable conditions often required by material applications. Switching the level of nutrient supply can trigger transitions between dormant and active state to meet specific needs. Diverse synthetic biology tools made available for *B.subtilis* by recent studies further enable genetic encoding of various functions for creating responsive materials. Because of these advantages, *B.subtilis* has attracted increasing interest for use in advanced materials.

Chen and coworkers presented the first example of utilizing *B.subtilis* for generating water-responsive materials.[104] The spore cortex surrounding the dehydrated core swells upon absorbing water. As a result, spores respond to changes in the relative humidity through contraction and expansion in volume. Harnessing this feature, the authors demonstrated the changing mechanical patterns of spores in response to water gradients by atomic force microscopy (AFM). The use of an engineered strain (mutations in *cotE* and *gerE*) further enhanced the energy density of the spores two-fold. Self-assembly of the engineered spores in monolayer fashion on silicon microcantilevers demonstrates their potential in producing bio-hybrid hygromorph actuators. Based on this work, Cakmak et al. developed another system with water-resistant UV-curable adhesives, which greatly improved the work density of the spore-enabled actuator compared to previous work.[105] In addition, 3-D printing aided by lithographic approaches led to rapid preparation of water-resistant actuators with various geometries.

Another major application of spores is for biosensing and remediation. *B. subtilis* spores embedded in polymer scaffolds can respond to external signals as soon as they germinate

and return to the metabolically active state. Thus, the resulting materials can benefit from the strong persistence of spores for increased robustness, as well as their ability to sense, respond, and produce useful chemicals. Schönhagen et al. developed a composite material with genetically engineered spores embedded in a poly(vinyl alcohol) matrix.[106] The authors demonstrated the resulting biohybrid hydrogel produced fluorescent proteins upon induction with β-d-1-thiogalactopyranoside (IPTG). The spore-based sensor was then tested against different conditions, showing stable fluorescence production after being treated at up to 60 °C or stored at room temperature for 28 days. Recently, González and coworkers developed a customized 3-D printable system with engineered spores and shear-thinning agarose.[107] Similar to the previous work, the embedded spores responded to IPTG and xylose by expressing fluorescent proteins. The authors showed the materials can be completely desiccated and then rehydrated in rich medium without the cells losing metabolic function. The spore-based materials were treated with organic solvents, high osmolarity, high pH, ultraviolet light, and γ-radiation. Under all conditions, the embedded spores were able to germinate and grow despite delayed onset of germination. Finally, the authors prepared materials with two engineered strains that can respectively sense a quorum signal from *S. aureus* (autoinducer peptide, AIP-I and AIP-IV) and produce MRSA-(lysostaphin and thiocillin)-specific antibiotics as a remediation strategy. The resulting materials generated fluorescent signals when in contact with *S. aureus*. Antibiotics secreted by the embedded bacteria eventually cleared the pathogens.

In summary, *B.subtilis* spores have enabled the development of various functional materials. Their high resistance to environmental stresses makes them superior candidates compared to other nonpathogenic microbes. The introduction of inducible genetic circuits into the *B.subtilis* genome endows composite materials with advanced functionality, encouraging their application as biosensors and actuators. Despite recent progress in this field, effective containment of *B.subtilis* cells once germinated from spores in rich medium remains an unsolved challenge. Vegetative growth of *B.subtilis* outside the scaffold gives rise to contamination and biosafety concerns, and thus limits the utility of this technology. In Chapter 4, we discuss a new class of living composite materials, where protein producing

B.subtilis cells are effectively crosslinked with the surrounding polymer scaffold and show no cellular leakage for 72 hours.

1.7 References

1 Errington, J. Regulation of endospore formation in Bacillus subtilis. *Nature Reviews Microbiology* **1**, 117-126 (2003).

2 Stragier, P. & Losick, R. Molecular genetics of sporulation in Bacillus subtilis. *Annual Review of Genetics* **30**, 297-341 (1996).

3 Tan, I. S. & Ramamurthi, K. S. Spore formation in Bacillus subtilis. *Environmental Microbiology Reports* **6**, 212-225 (2014).

4 Henriques, A. O. & Moran, J., Charles P. Structure, assembly, and function of the spore surface layers. *Annual Review of Microbiology* **61**, 555-588 (2007).

5 Setlow, P. I will survive: DNA protection in bacterial spores. *Trends in Microbiology* **15**, 172-180 (2007).

6 Setlow, P. & Johnson, E. A. Spores and their significance. *Food Microbiology: Fundamentals and Frontiers*, 23-63 (2019).

7 Eichenberger, P. *et al.* The program of gene transcription for a single differentiating cell type during sporulation in Bacillus subtilis. *PLoS Biology* **2**, e328 (2004).

8 Piggot, P. J. & Losick, R. Sporulation genes and intercompartmental regulation. *Bacillus subtilis and its Closest Relatives: from Genes to Cells*, 483-517 (2001).

9 Rothfield, L., Taghbalout, A. & Shih, Y.-L. Spatial control of bacterial division-site placement. *Nature Reviews Microbiology* **3**, 959-968 (2005).

10 Sonenshein, A. L. Control of sporulation initiation in Bacillus subtilis. *Current Opinion in Microbiology* **3**, 561-566 (2000).

11 Wu, L. J. & Errington, J. RacA and the Soj-Spo0J system combine to effect polar chromosome segregation in sporulating Bacillus subtilis. *Molecular Microbiology* **49**, 1463-1475 (2003).

12 Wu, L. J. & Errington, J. Coordination of cell division and chromosome segregation by a nucleoid occlusion protein in Bacillus subtilis. *Cell* **117**, 915-925 (2004).

13 Ireton, K., Gunther 4th, N. & Grossman, A. D. spo0J is required for normal chromosome segregation as well as the initiation of sporulation in Bacillus subtilis. *Journal of Bacteriology* **176**, 5320-5329 (1994).

14 Beek, A. T. *et al.* Transcriptome analysis of sorbic acid-stressed Bacillus subtilis reveals a nutrient limitation response and indicates plasma membrane remodeling. *Journal of Bacteriology* **190**, 1751-1761 (2008).

15 Doan, T. *et al.* FisB mediates membrane fission during sporulation in Bacillus subtilis. *Genes & Development* **27**, 322-334 (2013).

16 Morlot, C., Uehara, T., Marquis, K. A., Bernhardt, T. G. & Rudner, D. Z. A highly coordinated cell wall degradation machine governs spore morphogenesis in Bacillus subtilis. *Genes & Development* **24**, 411-422 (2010).

17 Jabbari, S., Heap, J. T. & King, J. R. Mathematical modelling of the sporulation-initiation network in Bacillus subtilis revealing the dual role of the putative quorum-sensing signal molecule PhrA. *Bulletin of Mathematical Biology* **73**, 181-211 (2011).

18 Lazazzera, B. A. Quorum sensing and starvation: signals for entry into stationary phase. *Current Opinion in Microbiology* **3**, 177-182 (2000).

19 Pottathil, M. & Lazazzera, B. A. The extracellular Phr peptide-Rap phosphatase signaling circuit of Bacillus subtilis. *Frontiers in Bioscience-Landmark* **8**, 32-45 (2003).

20 Henriques, A. O. & Moran Jr, C. P. Structure and assembly of the bacterial endospore coat. *Methods* **20**, 95-110 (2000).

21 Setlow, P. Spores of Bacillus subtilis: their resistance to and killing by radiation, heat and chemicals. *Journal of Applied Microbiology* **101**, 514-525 (2006).

22 Setlow, P. Resistance of bacterial spores. *Bacterial Stress Responses*, 319-332 (2010).

23 Setlow, P. Spore resistance properties. *Microbiology Spectrum* **2**, 2.5. 11 (2014).

24 Zhang, X., Al-Dossary, A., Hussain, M., Setlow, P. & Li, J. Applications of Bacillus subtilis spores in biotechnology and advanced materials. *Applied and Environmental Microbiology* **86**, e01096-01020 (2020).

25 Guoyan, Z. *et al.* Bacillus subtilis spore surface display technology: a review of its development and applications. 179-190 (2019).

26 Su, Y., Liu, C., Fang, H. & Zhang, D. Bacillus subtilis: a universal cell factory for industry, agriculture, biomaterials and medicine. *Microbial Cell Factories* **19**, 1-12 (2020).

27 Ghosh, S., Zhang, P., Li, Y.-q. & Setlow, P. Superdormant spores of Bacillus species have elevated wet-heat resistance and temperature requirements for heat activation. *Journal of Bacteriology* **191**, 5584-5591 (2009).

28 Granger, A. C., Gaidamakova, E. K., Matrosova, V. Y., Daly, M. J. & Setlow, P. Effects of Mn and Fe levels on Bacillus subtilis spore resistance and effects of Mn2+,

other divalent cations, orthophosphate, and dipicolinic acid on protein resistance to ionizing radiation. *Applied and Environmental Microbiology* **77**, 32-40 (2011).

29 Leggett, M. J., McDonnell, G., Denyer, S. P., Setlow, P. & Maillard, J. Y. Bacterial spore structures and their protective role in biocide resistance. *Journal of Applied Microbiology* **113**, 485-498 (2012).

30 PALOP, A., Manas, P. & Condon, S. Sporulation temperature and heat resistance of Bacillus spores: a review. *Journal of Food Safety* **19**, 57-72 (1999).

31 Sunde, E. P., Setlow, P., Hederstedt, L. & Halle, B. The physical state of water in bacterial spores. *Proceedings of the National Academy of Sciences* **106**, 19334-19339 (2009).

32 Molle, V. *et al.* The Spo0A regulon of Bacillus subtilis. *Molecular Microbiology* **50**, 1683-1701 (2003).

33 Perego, M., Cole, S. P., Burbulys, D., Trach, K. & Hoch, J. A. Characterization of the gene for a protein kinase which phosphorylates the sporulation-regulatory proteins Spo0A and Spo0F of Bacillus subtilis. *Journal of Bacteriology* **171**, 6187-6196 (1989).

34 Pompeo, F., Foulquier, E. & Galinier, A. Impact of serine/threonine protein kinases on the regulation of sporulation in Bacillus subtilis. *Frontiers in Microbiology* **7**, 568 (2016).

35 Fujita, M. & Losick, R. Evidence that entry into sporulation in Bacillus subtilis is governed by a gradual increase in the level and activity of the master regulator Spo0A. *Genes & Development* **19**, 2236-2244 (2005).

36 Fujita, M., González-Pastor, J. E. & Losick, R. High-and low-threshold genes in the Spo0A regulon of Bacillus subtilis. *Journal of Bacteriology* **187**, 1357-1368 (2005).

37 Fawcett, P., Eichenberger, P., Losick, R. & Youngman, P. The transcriptional profile of early to middle sporulation in Bacillus subtilis. *Proceedings of the National Academy of Sciences* **97**, 8063-8068 (2000).

38 Eijlander, R. T. *et al.* SpoVT: from fine-tuning regulator in Bacillus subtilis to essential sporulation protein in Bacillus cereus. *Frontiers in Microbiology* **7**, 1607 (2016).

39 Hilbert, D. W. & Piggot, P. J. Compartmentalization of gene expression during Bacillus subtilis spore formation. *Microbiology and Molecular Biology Reviews* **68**, 234-262 (2004).

40 Eichenberger, P. *et al.* The σE regulon and the identification of additional sporulation genes in Bacillus subtilis. *Journal of Molecular Biology* **327**, 945-972 (2003).

41 Potúčková, L. *et al.* A new RNA polymerase sigma factor, σF is required for the late stages of morphological differentiation in Streptomyces spp. *Molecular Microbiology* **17**, 37-48 (1995).

42 Sun, G., Yang, M., Jiang, L. & Huang, M. Regulation of pro-σK activation: a key checkpoint in Bacillus subtilis sporulation. *Environmental Microbiology* **23**, 2366-2373 (2021).

43 Errington, J. *et al.* Structure and function of the spoIIIJ gene of Bacillus subtilis: a vegetatively expressed gene that is essential for σG activity at an intermediate stage of sporulation. *Microbiology* **138**, 2609-2618 (1992).

44 Serrano, M., Neves, A., Soares, C. M., Moran Jr, C. P. & Henriques, A. O. Role of the anti-sigma factor SpoIIAB in regulation of σG during Bacillus subtilis sporulation. *Journal of Bacteriology* **186**, 4000-4013 (2004).

45 McKenney, P. T., Driks, A. & Eichenberger, P. The Bacillus subtilis endospore: assembly and functions of the multilayered coat. *Nature Reviews Microbiology* **11**, 33-44 (2013).

46 Donovan, W., Zheng, L., Sandman, K. & Losick, R. Genes encoding spore coat polypeptides from Bacillus subtilis. *Journal of Molecular Biology* **196**, 1-10 (1987).

47 Beall, B., Driks, A., Losick, R. & Moran Jr, C. Cloning and characterization of a gene required for assembly of the Bacillus subtilis spore coat. *Journal of Bacteriology* **175**, 1705-1716 (1993).

48 Zheng, L., Donovan, W. P., Fitz-James, P. C. & Losick, R. Gene encoding a morphogenic protein required in the assembly of the outer coat of the Bacillus subtilis endospore. *Genes & Development* **2**, 1047-1054 (1988).

49 McKenney, P. T. *et al.* A distance-weighted interaction map reveals a previously uncharacterized layer of the Bacillus subtilis spore coat. *Current Biology* **20**, 934-938 (2010).

50 Kim, H. *et al.* The Bacillus subtilis spore coat protein interaction network. *Molecular Microbiology* **59**, 487-502 (2006).

51 Imamura, D., Kuwana, R., Takamatsu, H. & Watabe, K. Proteins involved in formation of the outermost layer of Bacillus subtilis spores. *Journal of Bacteriology* **193**, 4075-4080 (2011).

52 Bartels, J. *et al.* The Bacillus subtilis endospore crust: protein interaction network, architecture and glycosylation state of a potential glycoprotein layer. *Molecular Microbiology* **112**, 1576-1592 (2019).

53 Hullo, M.-F. o., Moszer, I., Danchin, A. & Martin-Verstraete, I. CotA of Bacillus subtilis is a copper-dependent laccase. *Journal of Bacteriology* **183**, 5426-5430 (2001).

54 Liu, G. Y. & Nizet, V. Color me bad: microbial pigments as virulence factors. *Trends in Microbiology* **17**, 406-413 (2009).

55 Jiang, S. *et al.* Diverse supramolecular structures formed by self-assembling proteins of the B acillus subtilis spore coat. *Molecular Microbiology* **97**, 347-359 (2015).

56 Hoa, N. T. *et al.* Characterization of Bacillus species used for oral bacteriotherapy and bacterioprophylaxis of gastrointestinal disorders. *Applied and Environmental Microbiology* **66**, 5241-5247 (2000).

57 Green, D. H. *et al.* Characterization of two Bacillus probiotics. *Applied and Environmental Microbiology* **65**, 4288-4291 (1999).

58 Cao, Y.-G. *et al.* Construction and evaluation of a novel Bacillus subtilis spores-based enterovirus 71 vaccine. *Journal of Applied Biomedicine* **11**, 105-113 (2013).

59 Hinc, K. *et al.* Expression and display of UreA of Helicobacter acinonychis on the surface of Bacillus subtilis spores. *Microbial Cell Factories* **9**, 1-11 (2010).

60 Hoang, T. H., Hong, H. A., Clark, G. C., Titball, R. W. & Cutting, S. M. Recombinant Bacillus subtilis expressing the Clostridium perfringens alpha toxoid is a candidate orally delivered vaccine against necrotic enteritis. *Infection and Immunity* **76**, 5257-5265 (2008).

61 Isticato, R. *et al.* Surface display of recombinant proteins on Bacillus subtilis spores. *Journal of Bacteriology* **183**, 6294-6301 (2001).

62 Nguyen, A. T. *et al.* Bacillus subtilis spores expressing the VP28 antigen: a potential oral treatment to protect Litopenaeus vannamei against white spot syndrome. *FEMS Microbiology Letters* **358**, 202-208 (2014).

63 Sibley, L. *et al.* Recombinant Bacillus subtilis spores expressing MPT64 evaluated as a vaccine against tuberculosis in the murine model. *FEMS Microbiology Letters* **358**, 170-179 (2014).

64 Tavares Batista, M. *et al.* Gut adhesive Bacillus subtilis spores as a platform for mucosal delivery of antigens. *Infection and Immunity* **82**, 1414-1423 (2014).

65 Feng, F. *et al.* Display of human proinsulin on the Bacillus subtilis spore surface for oral administration. *Current Microbiology* **67**, 1-8 (2013).

66 Lian, C. *et al.* Surface display of human growth hormone on Bacillus subtilis spores for oral administration. *Current Microbiology* **68**, 463-471 (2014).

67 Mao, L. *et al.* Surface display of human serum albumin on Bacillus subtilis spores for oral administration. *Current Microbiology* **64**, 545-551 (2012).

68 Mauriello, E. M. *et al.* Display of heterologous antigens on the Bacillus subtilis spore coat using CotC as a fusion partner. *Vaccine* **22**, 1177-1187 (2004).

69 Sun, H. *et al.* Bacillus subtilis spore with surface display of paramyosin from Clonorchis sinensis potentializes a promising oral vaccine candidate. *Parasites & Vectors* **11**, 1-15 (2018).

70 Tavassoli, S., Hinc, K., Iwanicki, A., Obuchowski, M. & Ahmadian, G. Investigation of spore coat display of Bacillus subtilis β-galactosidase for developing of whole cell biocatalyst. *Archives of Microbiology* **195**, 197-202 (2013).

71 Wang, N. *et al.* Display of Bombyx mori alcohol dehydrogenases on the Bacillus subtilis spore surface to enhance enzymatic activity under adverse conditions. *PLoS One* **6**, e21454 (2011).

72 Wang, X. *et al.* Surface display of Clonorchis sinensis enolase on Bacillus subtilis spores potentializes an oral vaccine candidate. *Vaccine* **32**, 1338-1345 (2014).

73 Zhou, Z. *et al.* Oral administration of a Bacillus subtilis spore-based vaccine expressing Clonorchis sinensis tegumental protein 22.3 kDa confers protection against Clonorchis sinensis. *Vaccine* **26**, 1817-1825 (2008).

74 Chen, H. *et al.* Display of Thermotoga maritima MSB8 nitrilase on the spore surface of Bacillus subtilis using out coat protein CotG as the fusion partner. *Journal of Molecular Catalysis B: Enzymatic* **123**, 73-80 (2016).

75 Gao, C. *et al.* Chemoenzymatic synthesis of N-acetyl-D-neuraminic acid from N-acetyl-D-glucosamine by using the spore surface-displayed N-acetyl-D-neuraminic acid aldolase. *Applied and Environmental Microbiology* **77**, 7080-7083 (2011).

76 Hwang, B.-Y., Kim, B.-G. & Kim, J.-H. Bacterial surface display of a co-factor containing enzyme, ω-transaminase from Vibrio fluvialis using the Bacillus subtilis spore display system. *Bioscience, Biotechnology, and Biochemistry* **75**, 1862-1865 (2011).

77 Kim, J.-H., Lee, C.-S. & Kim, B.-G. Spore-displayed streptavidin: a live diagnostic tool in biotechnology. *Biochemical and Biophysical Research Communications* **331**, 210-214 (2005).

78 Kwon, S. J., Jung, H.-C. & Pan, J.-G. Transgalactosylation in a water-solvent biphasic reaction system with β-galactosidase displayed on the surfaces of Bacillus subtilis spores. *Applied and Environmental Microbiology* **73**, 2251-2256 (2007).

79 Qu, Y. *et al.* Catalytic transformation of HODAs using an efficient meta-cleavage product hydrolase-spore surface display system. *Journal of Molecular Catalysis B: Enzymatic* **102**, 204-210 (2014).

80 Rostami, A. *et al.* Display of B. pumilus chitinase on the surface of B. subtilis spore as a potential biopesticide. *Pesticide Biochemistry and Physiology* **140**, 17-23 (2017).

81 He, W., Jiang, B., Mu, W. & Zhang, T. Production of d-allulose with d-psicose 3-epimerase expressed and displayed on the surface of Bacillus subtilis spores. *Journal of Agricultural and Food Chemistry* **64**, 7201-7207 (2016).

82 Hinc, K., Iwanicki, A. & Obuchowski, M. New stable anchor protein and peptide linker suitable for successful spore surface display in B. subtilis. *Microbial Cell Factories* **12**, 1-8 (2013).

83 Iwanicki, A. *et al.* A system of vectors for Bacillus subtilis spore surface display. *Microbial Cell Factories* **13**, 1-9 (2014).

84 Wang, H., Yang, R., Hua, X., Zhao, W. & Zhang, W. Functional display of active β-galactosidase on Bacillus subtilis spores using crust proteins as carriers. *Food Science and Biotechnology* **24**, 1755-1759 (2015).

85 Kim, J. Surface display of lipolytic enzyme, Lipase A and Lipase B of Bacillus subtilis on the Bacillus subtilis spore. *Biotechnology and Bioprocess Engineering* **22**, 462-468 (2017).

86 Hwang, B.-Y., Pan, J.-G., Kim, B.-G. & Kim, J.-H. Functional display of active tetrameric β-galactosidase using Bacillus subtilis spore display system. *Journal of Nanoscience and Nanotechnology* **13**, 2313-2319 (2013).

87 Wang, H., Yang, R., Hua, X., Zhang, W. & Zhao, W. An approach for lactulose production using the CotX-mediated spore-displayed β-galactosidase as a biocatalyst. *Journal of Microbiology and Biotechnology* **26**, 1267-1277 (2016).

88 Zhao, G. *et al.* Development of a heat-stable and orally delivered recombinant M2e-expressing B. subtilis spore-based influenza vaccine. *Human Vaccines & Immunotherapeutics* **10**, 3649-3658 (2014).

89 Hosseini-Abari, A. *et al.* Surface display of bacterial tyrosinase on spores of Bacillus subtilis using CotE as an anchor protein. *Journal of Basic Microbiology* **56**, 1331-1337 (2016).

90 Guo, Q. *et al.* Enhanced D-tagatose production by spore surface-displayed L-arabinose isomerase from isolated Lactobacillus brevis PC16 and biotransformation. *Bioresource Technology* **247**, 940-946 (2018).

91 Jiang, H. *et al.* Immune response induced by oral delivery of Bacillus subtilis spores expressing enolase of Clonorchis sinensis in grass carps (Ctenopharyngodon idellus). *Fish & Shellfish Immunology* **60**, 318-325 (2017).

92 Chen, L., Holmes, M., Schaefer, E., Mulchandani, A. & Ge, X. Highly active spore biocatalyst by self-assembly of co-expressed anchoring scaffoldin and multimeric enzyme. *Biotechnology and Bioengineering* **115**, 557-564 (2018).

93 Wang, F. *et al.* Bacillus subtilis spore surface display of haloalkane dehalogenase DhaA. *Current Microbiology* **76**, 1161-1167 (2019).

94 Gashtasbi, F., Ahmadian, G. & Noghabi, K. A. New insights into the effectiveness of alpha-amylase enzyme presentation on the Bacillus subtilis spore surface by adsorption and covalent immobilization. *Enzyme and Microbial Technology* **64**, 17-23 (2014).

95 Duraj-Thatte, A. M. *et al.* Genetically programmable self-regenerating bacterial hydrogels. *Advanced Materials* **31**, 1901826 (2019).

96 Chen, A. Y., Zhong, C. & Lu, T. K. Engineering living functional materials. *ACS Synthetic Biology* **4**, 8-10 (2015).

97 Gerber, L. C., Koehler, F. M., Grass, R. N. & Stark, W. J. Incorporating microorganisms into polymer layers provides bioinspired functional living materials. *Proceedings of the National Academy of Sciences* **109**, 90-94 (2012).

98 Zhang, C. *et al.* Engineered Bacillus subtilis biofilms as living glues. *Materials Today* **28**, 40-48 (2019).

99 Ravikumar, S., Baylon, M. G., Park, S. J. & Choi, J.-i. Engineered microbial biosensors based on bacterial two-component systems as synthetic biotechnology platforms in bioremediation and biorefinery. *Microbial Cell Factories* **16**, 1-10 (2017).

100 Liu, S. & Xu, W. Engineered living materials-based sensing and actuation. *Frontiers in Sensors* **1**, 586300 (2020).

101 Tang, T.-C. *et al.* Hydrogel-based biocontainment of bacteria for continuous sensing and computation. *Nature Chemical Biology* **17**, 724-731 (2021).

102 Guo, S. *et al.* Engineered living materials based on adhesin-mediated trapping of programmable cells. *ACS Synthetic Biology* **9**, 475-485 (2020).

103 Wangpraseurt, D., You, S., Sun, Y. & Chen, S. Biomimetic 3D living materials powered by microorganisms. *Trends in Biotechnology* (2022).

104 Chen, X., Mahadevan, L., Driks, A. & Sahin, O. Bacillus spores as building blocks for stimuli-responsive materials and nanogenerators. *Nature Nanotechnology* **9**, 137-141 (2014).

105 Cakmak, O., El Tinay, H. O., Chen, X. & Sahin, O. Spore-based water-resistant water-responsive actuators with high power density. *Advanced Materials Technologies* **4**, 1800596 (2019).

106 Schulz-Schönhagen, K., Lobsiger, N. & Stark, W. J. Continuous production of a shelf-stable living material as a biosensor platform. *Advanced Materials Technologies* **4**, 1900266 (2019).

107 González, L. M., Mukhitov, N. & Voigt, C. A. Resilient living materials built by printing bacterial spores. *Nature Chemical Biology* **16**, 126-133 (2020).

Chapter 2

T7 RNA POLYMERASE ENABLED HIGH DENSITY PROTEIN DISPLAY ON BACILLUS SUBTILIS SPORES

Content from this chapter is adapted with permission from:

Y. Hui, Z. Cui, and S. Sim, Stress-tolerant, recyclable, and renewable biocatalyst platform enabled by engineered bacterial spores. *ACS Synthetic Biology, ASAP*

Abstract

In this chapter, we describe a new set of genetic architectures enabled by bacteriophage-derived T7 RNA polymerase (T7 RNAP) for high-density protein display (TIED) on *B. subtilis* spores. Target proteins are fused to a spore crust protein – CotY or CotZ – for spore localization. The TIED constructs employ coat protein promoters to drive expression of the T7 RNAP, amplifying expression of the target proteins. Endogenous architectures, in which coat protein promoters directly trigger target protein expression were constructed for comparison. We selected a fluorescent reporter protein, mWasabi, as the target to evaluate expression levels in both TIED and endogenous expression systems. We further studied the localization of mWasabi on spores by fluorescence microscopy. Strains harboring TIED constructs formed spores with considerably higher surface fluorescence. The substantial enhancement in loading density of mWasabi suggests potential application of TIED to immobilization of enzymes and other bioactive molecules on *B. subtilis* spores.

2.1 Introduction

Bacterial spores have emerged as novel platforms for displaying heterologous proteins. In particular, spores of *Bacillus subtilis* have attracted wide research interests for such purpose. They can tolerate environmental stresses likely present in industrial settings, such as high temperature, nutrient deprivation, and organic solvents.[1] In addition, a complex network of structural proteins comprising the outer layers of *B. subtilis* spores provides a plethora of possible anchoring motifs for enzyme loading.[2,3] So far, a range of heterologous proteins, including enzymes and antigens, have been installed on the surface of *B. subtilis* spores.[4-9] Nevertheless, relying on endogenous transcriptional machinery, previous work often suffered from low protein loading density, thus limiting wide application of the technology. In this chapter, we report a set of new genetic architectures leveraging the T7 RNA polymerase (T7 RNAP) for high density protein display (TIED) on *B. subtilis* spores. We demonstrate that, compared to endogenous transcriptional machinery, TIED architectures led to substantial enhancement in loading density of a fluorescent reporter protein, mWasabi, on the spore surface.

2.2 Results and Discussion

TIED combines the amplified expression of recombinant proteins by bacteriophage-derived T7 RNA polymerase (T7 RNAP), spore-specific promoters for activation of T7 RNAP, and spontaneous assembly of recombinant proteins on the *B. subtilis* spore surface (**Figure 2.1A**). We hypothesized that implementing T7 RNAP in the engineered genetic circuit designed to be active during late-stage sporulation would amplify the expression of fusion proteins, which subsequently assemble on the spore surface. We devised a panel of TIED constructs with three endogenous, σ_K-specific promoters, P_{cotG}, P_{cotV}, and P_{cotZ}. Target proteins were fused to the C-terminus of a coat protein, which assembles with other coat proteins to form the outer protein layers of *B. subtilis* spores. We chose the two morphogenic coat proteins suggested to play a crucial role in the assembly of the outermost crust layer, CotY and CotZ,[2,3,10,11] for our design of TIED. An epitope tag, 3×FLAG, was incorporated on the C-terminus for immunolabeling and quantification of target proteins. To evaluate the performance of the TIED platform, we built genetic constructs with the endogenous promoters directly driving the expression of the fusion protein (**Figure 2.1B**), analogous to the genetic architectures reported in previous studies.[4-9] We selected a fluorescent reporter protein, mWasabi, as the first target to observe its overall expression level and spore localization in both TIED and endogenous expression systems.

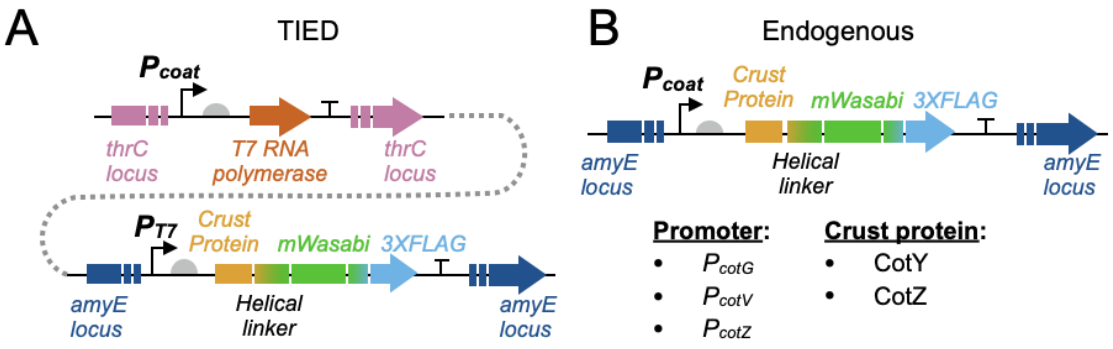

Figure 2.1. Genetic constructs for expression of crust-mWasabi fusion proteins. (**A**), TIED architectures. (**B**), endogenous architectures. Six constructs with combinations of three promoters (P_{cotG}, P_{cotV}, and P_{cotZ}) and two crust proteins (CotY and CotZ) were built for both systems.

Upon inducing sporulation of *B. subtilis* cells, total expression levels of the fluorescent fusion protein were recorded for all 12 strains (**Figures 2.2A and 2.2B**). In general, TIED constructs resulted in higher total expression of fluorescent fusion proteins and earlier activation compared to their endogenous counterparts. In particular, P_{cotG}- and P_{cotV}-driven TIED variants showed a more dynamic increase in fluorescence compared to P_{cotZ}-driven ones (**Figure 2.2A**). Meanwhile, P_{cotZ}-driven constructs outperform the rest in the endogenous constructs (**Figure 2.2B**). The difference in the promoter behavior of P_{cotZ} in TIED and endogenous counterparts may be attributed to the level of expression of T7 RNAP and fusion proteins. We speculate that the amount of T7 RNAP produced in P_{cotZ}-driven TIED constructs is higher than in others, creating a more burdensome and toxic environment for individual cells,[12,13] which could lead to suboptimal output for fusion proteins.

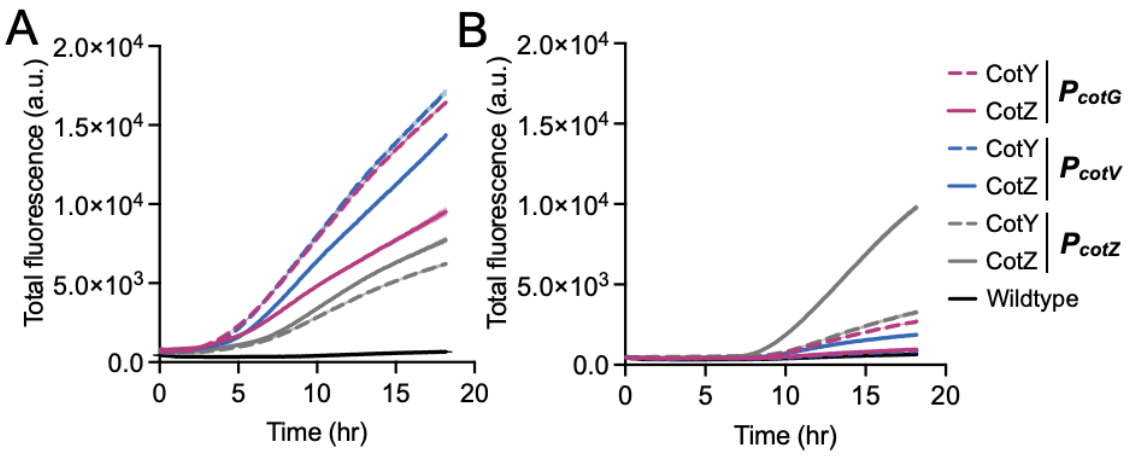

Figure 2.2. Total expression level of crust-mWasabi fusion proteins. (**A**), TIED-mWasabi variants. (**B**), endogenous constructs. Each variant was grown to OD_{600} of 0.5 in LB and resuspended in an equal volume of SM medium. Fluorescence was continuously monitored after resuspension for 18 h. (n = 3 biological replicates).

We further investigated the distribution of the fluorescent fusion proteins through microscopic analysis and bulk fluorescence measurement of purified spore solutions. Despite the TIED system exhibiting a higher total expression level of the fluorescent fusion proteins (**Figure 2.2A**), as forespores approach maturation, the fluorescence emission from the spore

surface was significantly reduced, and most of the fluorescence emission was detected in the residual vegetative cells (**Figure S2.1A**). We hypothesized that a group of proteases active upon completion of mature spore formation to lyse the mother cell could have degraded fluorescent fusion proteins on the spore surface.[14]

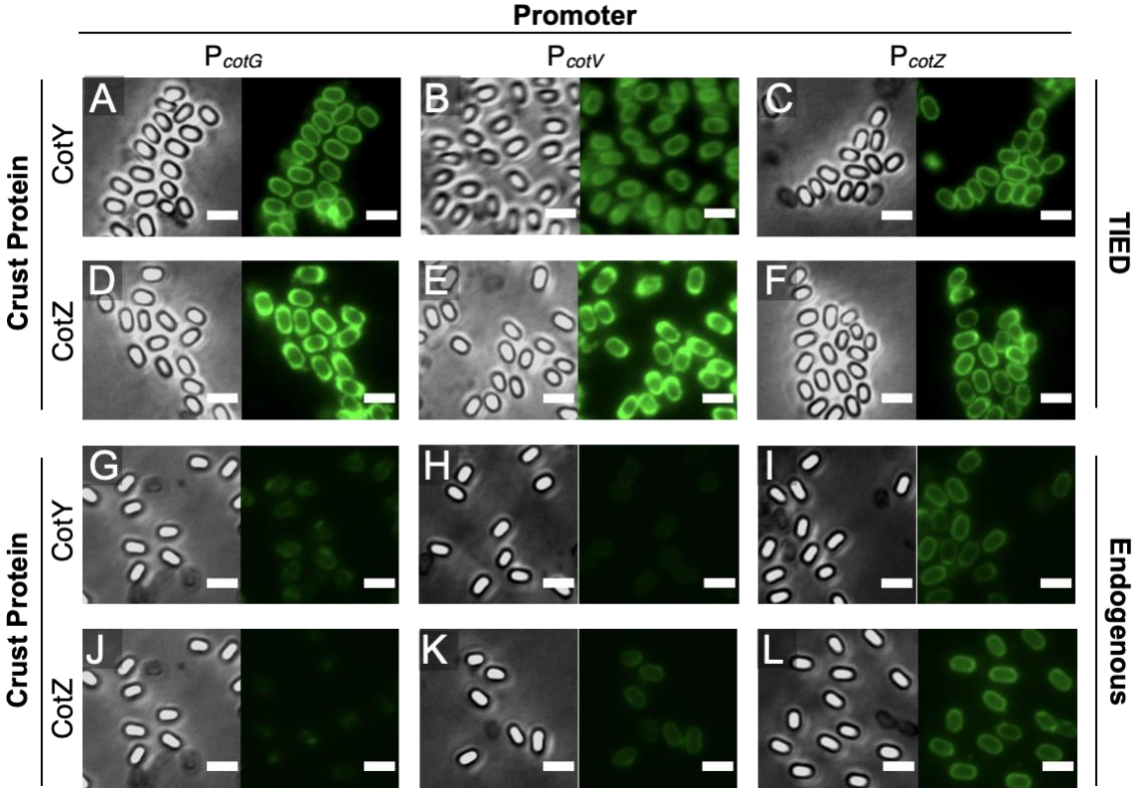

Figure 2.3. Microscopic images of mWasabi displaying spores**.** (**A-L**), Representative phase-contrast and fluorescent microscopic images of spores of each variant. Fluorescence (green) of each sample was measured with 488 nm laser (100 ms exposure time, 3% laser, n = 3 biological replicates). See **Figure S2.2** for images of the corresponding cells before lysozyme digestion. Scale bars, 2 μm.

Based on this hypothesis, we set out to improve the retention of fusion proteins on spores by developing an early harvest protocol to collect mature spores while they are still inside their mother cells. Compared to natural maturation and spontaneous release from the mother cells, spores harvested with our protocol showed higher spore fluorescence in both endogenous and TIED constructs (**Figure S2.3**). Based on the bulk fluorescence intensities of the spore solutions normalized by the optical density at 600 nm (**Figure 2.4**) and microscopic analysis

(**Figure 2.3A-F**), TIED generally outperformed its endogenous counterparts. In particular, TIED constructs with P_{cotG} and P_{cotV} promoters show expression levels two orders of magnitude higher than their endogenous counterparts as measured by fluorescence.

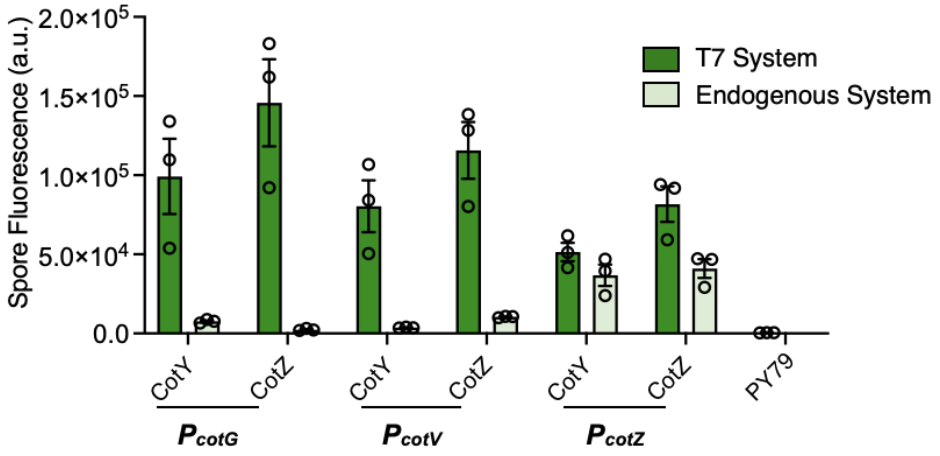

Figure 2.4. Spore fluorescence of the TIED variants, the endogenous counterparts, and their parental strain (PY79). Spores were harvested by lysozyme digestion (50 μg mL^{-1}) of the sporulating cells. Spores were washed twice and resuspended in an equal volume of PBS for fluorescence measurement.

In endogenous constructs, the expression level of the fluorescent fusion protein from the entire population has a positive correlation with the spore-specific fluorescence emission, suggesting that the total production of the fluorescent fusion protein is the determining factor for the number of fusion proteins on the spore surface (**Figures 2.5A and 2.5B**). In TIED, the expression level of the fluorescent fusion protein did not show any correlation with the spore-specific emission (**Figures 2.5C and 2.5D**), indicating the production yield of the fusion protein is not the determining factor for the spore display. We speculate that T7 RNAP-based expression of fusion proteins saturates the available translation machinery in sporulating cells. As a result, the interplay between the timing of the fusion protein expression, coat-protein assembly, and protease-mediated control of the late-stage sporulation determines the density of the displayed fusion proteins.

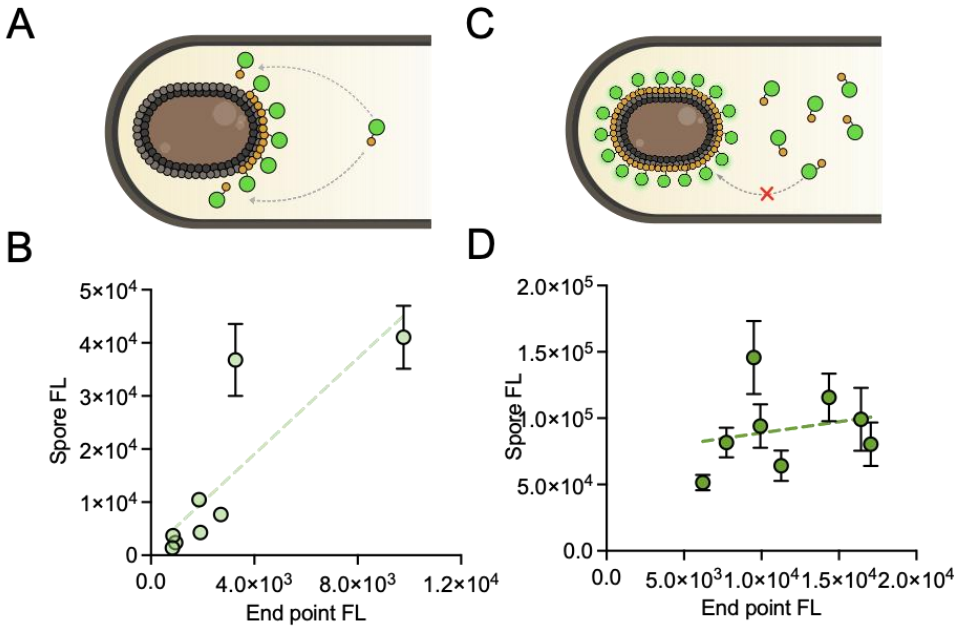

Figure. 2.5. Distribution of crust-mWasabi fusion proteins. (**A**), Illustration of fusion protein synthesis and localization on forming spores harboring endogenous expression system. (**B**), Bulk spore fluorescence of the endogenous counterparts prepared through the early-harvest method as a function of total fluorescent protein expression. Data were fitted with linear regression (dotted line). (n = 3 biological replicates). (**C**), Illustration of fusion protein synthesis and localization on forming spores harboring TIED expression system. (**D**), Bulk spore fluorescence of the TIED variants prepared through the early-harvest method as a function of total fluorescent protein expression. (n = 3 biological replicates. See Fig. 1b and 1c for endpoint fluorescence). Data were fitted with linear regression (dotted line).

2.3 Conclusions

In this work, we developed a set of novel genetic architectures leveraging the T7 RNAP to enable high density protein display (TIED) of mWasabi on *B. subtilis* spore surface. Three promoters natively present in the *B. subtilis* genome for coat protein expression – P_{cotG}, P_{cotV}, and P_{cotZ} – were screened for regulating the expression of T7 RNAP. For each promoter, two abundant crust proteins on the outermost layer of spore– CotZ and CotY – were examined for fusion with mWasabi. In total, six TIED combinations and their endogenous counterparts, where the coat protein promoters directly drive the expression of the fusion protein were constructed. To protect displayed recombinant proteins from increased proteolytic activities in late-stage sporulation, maturing forespores were harvested from mother cells by lysozyme digestion. Together, the TIED genetic architectures and the early harvest protocol allow significant improvement in expression and display density of mWasabi, as shown in bulk fluorescence measurement and microscopy.

2.4 Materials and Methods

Design and cloning of genetic constructs in *B. subtilis*. Gene sequences of CotY and CotZ were obtained from the genes *cotY* and *cotZ*, respectively, from the genome of *B. subtilis* PY79. The gene sequence of mWasabi was codon-optimized (IDT Codon Optimization Tool) based on their protein sequences.[15] Gene sequences of T7 RNAP and the T7 promoter, along with the lac operator and hammerhead ribozyme were amplified from a previously reported construct (GenBank MN005204).[16] The endogenous promoters, P_{cotG}, P_{cotZ}, and P_{cotV}, were amplified from the genome of *B. subtilis* PY79. A strong synthetic ribosomal binding site (RBS), MF001, was inserted between the promoter region and start codon.[16] Between the target protein and the C terminus of CotY/CotZ, an 11-amino-acid spacer that forms a stable α-helical structure was placed.[17] Three repeats of the FLAG tag were introduced to the C terminus of the fusion construct for immunostaining.

PCR-amplified DNA fragments were assembled using Golden Gate Assembly and inserted into plasmid backbones (New England Biolabs).[18] The T7 driven gene circuits for fusion protein expression were inserted into vector PBS1C,[19] which carries homology sites of the *amyE* locus and a chloramphenicol resistance selection marker. The T7 RNAP expression circuit was cloned into the PBS4S backbone,[20] which contains the spectinomycin resistance gene, flanked by sequences homologous to the *thrC* locus. The resultant plasmids were transformed into *E. coli* DH10B (New England Biolabs, C3019) through electroporation and selected by carbenicillin resistance (100 μg mL^{-1}). Clones carrying plasmids with correct sequences were isolated for DNA extraction (QIAGEN, 56604785).

Purified plasmids were linearized by restriction enzyme digestion for the transformation of *B. subtilis*. Chromosomal integration into the *B. subtilis* PY79 genome via double cross-over was performed according to the reported two-step method.[21] The resulting *B. subtilis* clones were selected on lysogeny broth (LB) agar plates supplemented with chloramphenicol (5 μg mL^{-1}) or (and) spectinomycin (100 μg mL^{-1}). To generate strains carrying TIED constructs with engineered circuits in two loci, *B. subtilis* PY79 was transformed first with the T7-

driven fusion protein expression circuit into the *amyE* locus. Competence was induced in selected clones for the subsequent transformation of the construct for T7 RNAP expression.

Bacterial growth and sporulation. Sporulation of wild-type and mutant *B. subtilis* strains was induced by the resuspension method.[22] Starter cultures of *B. subtilis* cells were grown till saturation in LB medium. The starter culture was diluted 1:100 into a 50 mL fresh LB medium in a 250 mL Erlenmeyer flask and allowed to grow at 37 °C until the optical density at 600 nm (OD_{600}) reached 0.5. Culturing time for different variants depended on their respective growth rates and was optimized for each. Cells were harvested by centrifugation (3000 g, 8 min), and the cell pellets were resuspended in an equal volume of SM medium (0.046 mg $FeCl_2$, 4.8 g $MgSO_4$, 12.6 mg $MnCl_2$, 535 mg NH_4Cl, 106 mg Na_2SO_4, 68 mg KH_2PO_4, 96.5 mg NH_4NO_3, 219 mg $CaCl_2$, 2g L-glutamic acid, 20 mg L-tryptophan, pH 7.1). The resuspended cells were transferred back to Erlenmeyer flasks and grown for 14 h with agitation (37 °C, 250 rpm). The resulting cells were collected (4000 g, 10 min) and treated with 50 μg mL^{-1} lysozyme (Sigma-Aldrich, L6876) in phosphate buffered saline (PBS, pH 7.2, gentrox, 30-025). The harvested spores were washed with PBS twice and checked for morphology using an ECHO Revolve Microscope (inverted).

Fluorescence microscopy and image analysis. A 2 μL aliquot of a TIED-mWasabi spore suspension in PBS was dropped on a microscope slide, topped with a cover glass, and mounted on an ECHO Revolve Microscope (inverted mode). A 60x phase contrast lens and a 488 nm laser line (100 ms exposure time, 3% laser) were used for the imaging of spores. Images were exported and processed with Image J (NIH).

2.5 Supplementary Tables and Figures

Table S2.1 Protein and peptide sequences

CotY	MSCGKTHGRHENCVCDAVEKILAEQEAVEEQCPTGCYTNLLNPTIA GKDTIPFLVFDKKG GLFSTFGNVGGFVDDMQCFESIFFRVEKLCDCCATLSILRPVDVKGD TLSVCHPCDPDFF GLEKTDFCIEVDLGCFCAIQCLSPELVDRTSPHKDKKHHHNG
CotZ	MSQKTSSCVREAVENIEDLQNAVEEDCPTGCHSKLLSVSHSLGDTV PFAIFTSKSTPLVA FGNVGELDNGPCFNTVFFRVERVHGSCATLSLLIAFDEHKHILDFTD KDTVCEVFRLEKT NYCIEVDLDCFCAINCLNPRLINRTHHH
mWasabi	MVSKGEETTMGVIKPDMKIKLKMEGNVNGHAFVIEGEGEGKPYDG TNTINLEVKEGAPLPFSYDILTTAF SYGNRAFTKYPDDIPNYFKQSFPEGYSWERTMTFEDKGIVKVKSDIS MEEDSFIYEIHLKGENFPPNGPV MQKETTGWDASTERMYVRDGVLKGDVKMKLLLEGGGHHRVDFK TIYRAKKAVKLPDYHFVDHRIEILNHD KDYNKVTVYEIAVARNSTDGMDELYK
Helical linker	GGGEAAAKGGGGS
3XFLAG	DYKDDDDKGDYKDDDDKIDYKDDDDK

Table S2.2 Genetic constructs

Plasmid name	Description	Promoter	Tags	Integration
PBS1C-CotY-mWasabi-3XFLAG	TIED-mWasabi fused to CotY	P_{T7}, LacO	3XFLAG at C terminus; helical linker between CotY and mWasabi	*amyE*
PBS1C-CotZ-mWasabi-3XFLAG	TIED-mWasabi fused to CotZ	P_{T7}, LacO	3XFLAG at C terminus; helical linker between CotZ and mWasabi	*amyE*
PBS4S-P_{cotG}-T7 RNAP	T7 RNAP expression	P_{cotG}		*thrC*
PBS4S-P_{cotV}-T7 RNAP	T7 RNAP expression	P_{cotV}		*thrC*
PBS4S-P_{cotZ}-T7 RNAP	T7 RNAP expression	P_{cotZ}		*thrC*

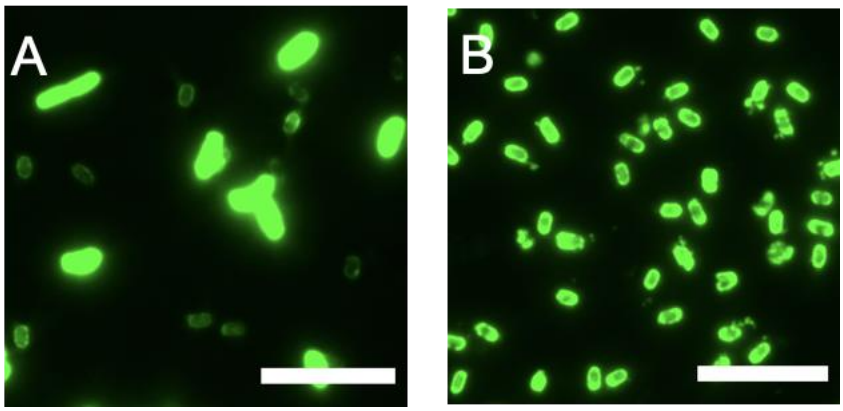

Figure S2.1. Cells and spores by early harvest and natural maturation. (**A**), A representative fluorescence microscopic image of TIED-mWasabi (combination of P_{cotV} promoter and CotZ fusion partner) spores prepared by natural maturation after 24 h in SM medium. (**B**), A representative fluorescence microscopic image of TIED-mWasabi (combination of P_{cotV} promoter and CotZ fusion partner) spores prepared by the early-harvest method with lysozyme digestion after growing in SM medium for 12 h. Same laser (3%) and exposure time (100 ms) were used for imaging. Scale bars, 10 μm.

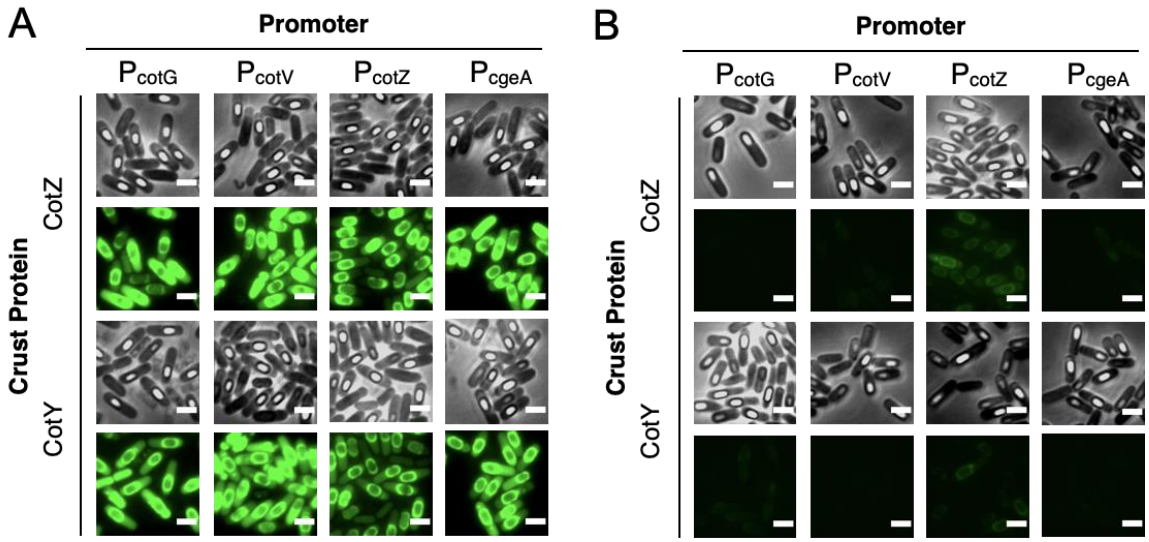

Figure S2.2. Cells and spores before early harvest. (**A**), Representative fluorescence and phase-contrast microscopic images of sporulating cells of TIED-mWasabi variants before spores were harvested. (**B**), Representative fluorescence and phase-contrast microscopic images of sporulating cells of endogenous constructs before spores were harvested. Scale bars, 2 μm.

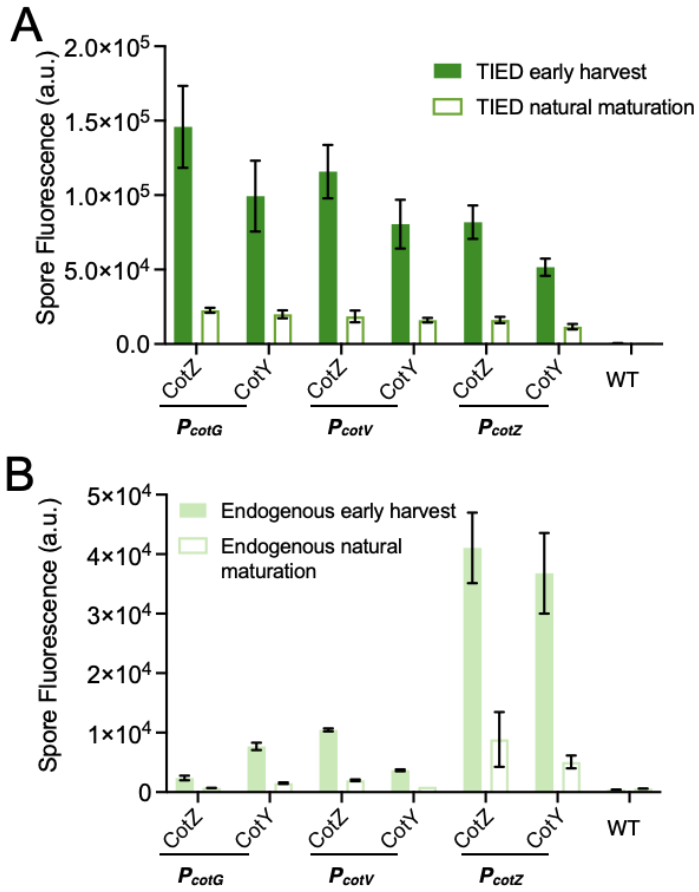

Figure S2.3. Spore fluorescence by early harvest versus natural maturation. (**A**), Bulk spore fluorescence of the TIED variants prepared through the early-harvest method as a function of total fluorescent protein expression. (n = 3 biological replicates. See Fig. 1b and 1c for endpoint fluorescence) Data were fitted with linear regression (dotted line). (**B**), Bulk spore fluorescence of the endogenous counterparts prepared through the early-harvest method as a function of total fluorescent protein expression. Data were fitted with linear regression (dotted line). (n = 3 biological replicates).

2.6 Acknowledgements

We thank Professors David Tirrell and Jennifer Prescher for their helpful comments. This work was supported by Defense Advanced Research Projects Agency Engineered Living Materials Agreement HR0011-17-2-0037, by the Institute for Collaborative Biotechnologies through cooperative agreement W911NF-19-2-0026 from the U.S. Army Research Office, and by the start-up funds (S. S.) from the University of California, Irvine. The content of the information does not necessarily reflect the position or the policy of the Government, and no official endorsement should be inferred.

2.7 References

1 Ugwuodo, C. J. & Nwagu, T. N. Stabilizing enzymes by immobilization on bacterial spores: A review of literature. *International Journal of Biological Macromolecules* **166**, 238-250 (2021).

2 McKenney, P. T., Driks, A. & Eichenberger, P. The Bacillus subtilis endospore: assembly and functions of the multilayered coat. *Nature Reviews Microbiology* **11**, 33-44 (2013).

3 McKenney, P. T. *et al.* A distance-weighted interaction map reveals a previously uncharacterized layer of the Bacillus subtilis spore coat. *Current Biology* **20**, 934-938 (2010).

4 Bartels, J., López Castellanos, S. N., Radeck, J. & Mascher, T. Sporobeads: The utilization of the Bacillus subtilis endospore crust as a protein display platform. *ACS Synthetic Biology* **7**, 452-461 (2018).

5 Chen, L., Holmes, M., Schaefer, E., Mulchandani, A. & Ge, X. Highly active spore biocatalyst by self-assembly of co-expressed anchoring scaffoldin and multimeric enzyme. *Biotechnology and Bioengineering* **115**, 557-564 (2018).

6 Wang, F. *et al.* Bacillus subtilis spore surface display of haloalkane dehalogenase DhaA. *Current Microbiology* **76**, 1161-1167 (2019).

7 Gashtasbi, F., Ahmadian, G. & Noghabi, K. A. New insights into the effectiveness of alpha-amylase enzyme presentation on the Bacillus subtilis spore surface by adsorption and covalent immobilization. *Enzyme and Microbial Technology* **64**, 17-23 (2014).

8 Kim, J. Surface display of lipolytic enzyme, Lipase A and Lipase B of Bacillus subtilis on the Bacillus subtilis spore. *Biotechnology and Bioprocess Engineering* **22**, 462-468 (2017).

9 Kwon, S. J., Jung, H.-C. & Pan, J.-G. Transgalactosylation in a water-solvent biphasic reaction system with β-galactosidase displayed on the surfaces of Bacillus subtilis spores. *Applied and Environmental Microbiology* **73**, 2251-2256 (2007).

10 Bartels, J. *et al.* The Bacillus subtilis endospore crust: protein interaction network, architecture and glycosylation state of a potential glycoprotein layer. *Molecular Microbiology* **112**, 1576-1592 (2019).

11 Imamura, D., Kuwana, R., Takamatsu, H. & Watabe, K. Proteins involved in formation of the outermost layer of Bacillus subtilis spores. *Journal of Bacteriology* **193**, 4075-4080 (2011).

12 Davanloo, P., Rosenberg, A. H., Dunn, J. J. & Studier, F. W. Cloning and expression of the gene for bacteriophage T7 RNA polymerase. *Proceedings of the National Academy of Sciences* **81**, 2035-2039 (1984).

13 Tan, S.-I. & Ng, I.-S. New insight into plasmid-driven T7 RNA polymerase in Escherichia coli and use as a genetic amplifier for a biosensor. *ACS Synthetic Biology* **9**, 613-622 (2020).

14 Dancer, B. & Mandelstam, J. Production and possible function of serine protease during sporulation of Bacillus subtilis. *Journal of Bacteriology* **121**, 406-410 (1975).

15 Kozlowski, M. T., Silverman, B. R., Johnstone, C. P. & Tirrell, D. A. Genetically Programmable Microbial Assembly. *ACS Synthetic Biology* **10**, 1351-1359 (2021).

16 Castillo-Hair, S. M., Fujita, M., Igoshin, O. A. & Tabor, J. J. An engineered B. subtilis inducible promoter system with over 10 000-fold dynamic range. *ACS Synthetic Biology* **8**, 1673-1678 (2019).

17 Hinc, K., Iwanicki, A. & Obuchowski, M. New stable anchor protein and peptide linker suitable for successful spore surface display in B. subtilis. *Microbial Cell Factories* **12**, 1-8 (2013).

18 Engler, C., Gruetzner, R., Kandzia, R. & Marillonnet, S. Golden gate shuffling: a one-pot DNA shuffling method based on type IIs restriction enzymes. *PloS One* **4**, e5553 (2009).

19 Popp, P. F., Dotzler, M., Radeck, J., Bartels, J. & Mascher, T. The Bacillus BioBrick Box 2.0: expanding the genetic toolbox for the standardized work with Bacillus subtilis. *Scientific Reports* **7**, 1-13 (2017).

20 Radeck, J. *et al.* The Bacillus BioBrick Box: generation and evaluation of essential genetic building blocks for standardized work with Bacillus subtilis. *Journal of Biological Engineering* **7**, 1-17 (2013).

21 Bennallack, P. R., Burt, S. R., Heder, M. J., Robison, R. A. & Griffitts, J. S. Characterization of a novel plasmid-borne thiopeptide gene cluster in Staphylococcus epidermidis strain 115. *Journal of Bacteriology* **196**, 4344-4350 (2014).

22 Sterlini, J. M. & Mandelstam, J. Commitment to sporulation in Bacillus subtilis and its relationship to development of actinomycin resistance. *Biochemical Journal* **113**, 29-37 (1969).

Chapter 3

STRESS-TOLERANT, RECYCLABLE, AND RENEWABLE BIOCATALYST PLATFORM ENABLED BY ENGINEERED BACILLUS SUBTILIS SPORES

Content from this chapter is adapted with permission from:

Y. Hui, Z. Cui, and S. Sim, Stress-tolerant, recyclable, and renewable biocatalyst platform enabled by engineered bacterial spores. *ACS Synthetic Biology, ASAP*

Abstract

In this chapter, we describe a stress-tolerant, recyclable, and renewable biocatalyst platform based on T7 RNA polymerase-enabled high-density protein display on bacterial spores (TIED). TIED uses high-level T7 RNA polymerase-driven expression of recombinant proteins specifically in sporulating cells to allow spontaneous assembly of recombinant fusion proteins on the *B. subtilis* spore surface. TIED enables a high loading density in the range of 10^6–10^7 recombinant enzymes per spore, robust catalytic activity of displayed enzymes comparable to the respective free enzymes, and enhanced kinetic stability of displayed enzymes in methanol and elevated temperatures. Further, we demonstrate TIED-enzymes to be not only recyclable, but fully renewable after loss of activity through induction of germination and sporulation, enabling perpetual regeneration of these immobilized biocatalysts.

3.1 Introduction

Enzymatic catalysis offers unique advantages for a wide range of chemical transformations because of its specificity, efficiency, and environmental friendliness.[1-4] With advances in computational tools and directed evolution in recent years, enzyme engineering has expanded the portfolio of available biocatalysts beyond nature's repertoire.[5-8] Despite their apparent merits in chemical and pharmaceutical manufacturing processes, using enzymes in a scalable and economical manner remains challenging for a wide range of applications. In addition to costly purification, enzymes are less attractive in terms of stability and reusability compared to synthetic catalysts. Subjecting them to common reaction conditions, such as organic solvents or high temperature, often leads to denaturation and subsequent loss of function.[9,10]

Immobilizing enzymes on solid supports has been shown to alleviate these limitations and is considered essential for installing enzyme biocatalysts in large-scale production because it enables the recycling of enzymes.[11] *In situ* immobilization of enzymes on bacterial spores features additional benefits by leveraging the autonomous biological process of protein synthesis and assembly on the spore surface. So far, a range of enzymes, including α-amylase, lipase, and β-galactosidase, have been installed on the surface of *B. subtilis* spores.[12-17] However, despite a number of successful proof-of-concept studies, none so far have fully addressed major limitations of this system for practical applications: (1) low enzyme loading density, typically 10^2–10^5 enzymes per spore, leading to insufficient catalytic activity, and (2) loss of activity over time and in harsh conditions. Furthermore, quantitative and substrate-specific characterizations of catalytic behavior of spore-immobilized enzymes in comparison to their respective free-forms remain elusive.

This work demonstrates a novel biocatalyst platform that is stress-tolerant, recyclable, and renewable. This development was made possible by T7 RNA polymerase-enabled high-density protein display on bacterial spores (TIED) technology. We achieved 10^6–10^7 enzymes per spore loading density with comparable catalytic performance to the respective free-form enzymes, enhanced catalytic activity in methanol, and increased temperature

stability. In addition to being recyclable for multiple uses, enzyme-displaying spores can also be fully renewed upon attrition of their activity, allowing unlimited reuse of immobilized biocatalysts.

3.2 Results and Discussion

3.2.1 Catalytic Performance of TIED-LipB

Leveraging the TIED technology combined with an early harvest strategy, we devised a versatile platform for displaying recombinant proteins in high density on bacterial spores. After validating the performance of TIED with a fluorescent protein, we sought to display functional enzymes on *B. subtilis* spores (**Figure 3.1A**). We chose *B. subtilis* lipase B (LipB) as our first target because of its relatively small size (19.5 kDa) and the general importance of lipases in industrial applications, including bulk production of food ingredients, detergents, and pharmaceuticals.[18] Six TIED combinations with three promoters and two anchor proteins resulted in phase-bright spores (**Figures 3.1B**, **S3.1A**). Loading densities achieved by previous studies in spore-based enzyme display typically ranged from 10^2 to 10^5 enzymes per spore, based on enzymatic activities or dot blot experiments. Loading densities of LipB on each TIED construct were determined by quantitative western blot using spore lysate containing the crust and coat proteome. The impermeability of spores makes complete lysis difficult. As such, a decoating procedure was used to extract the insoluble crust and coat fractions from spores (**Section 3.4**). Among all TIED variants, P_{cotG} and CotZ fusion partner combination resulted in the highest loading density of LipB, 1.75×10^7 LipB per spore (**Figures 3.1C**, **S3.3A**, and **S3.4A**). Corresponding to the relative loading densities of the TIED constructs, normalized lipase activity assessed by colorogenic *p*-nitrophenol palmitate (C16) substrate conversion (**Figure 3.1D**) shows that the P_{cotG} and CotZ combination exhibits the highest substrate conversion compared to all other TIED constructs by orders of magnitude (**Figure 3.1E**). Subsequent enzymatic analyses of TIED-LipB, compared to the free-form LipB, were performed with this variant.

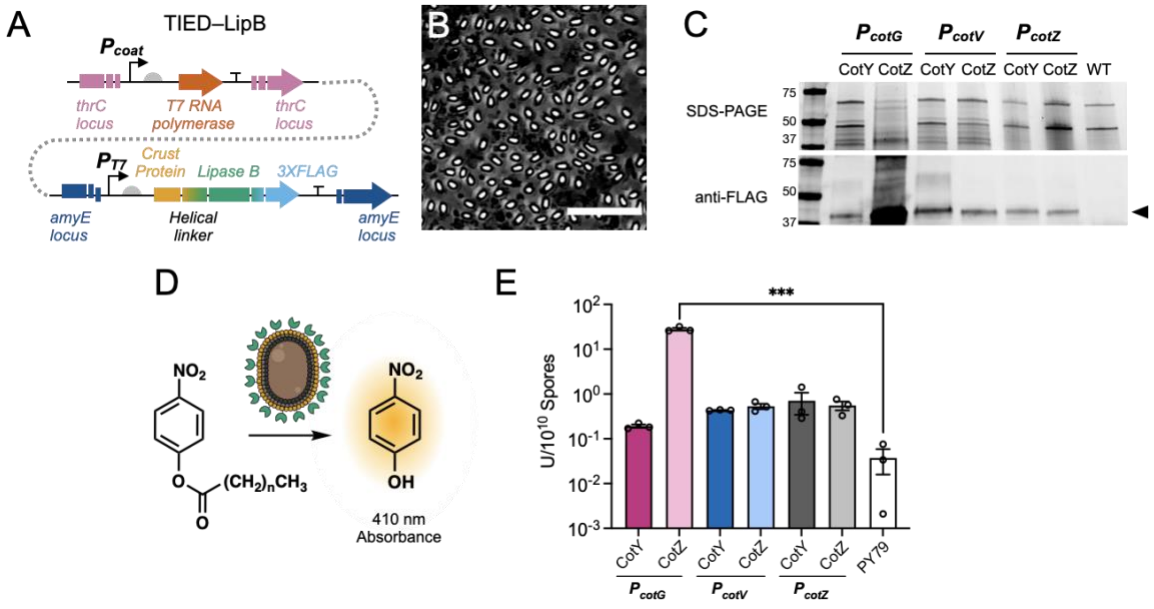

Figure 3.1. Catalytic performance of TIED-LipB. (**A**), Genetic constructs of TIED-LipB. (**B**), A representative phase-contrast image of TIED-LipB (with the combination of promoter P_{cotG} and CotZ fusion partner) after lysozyme digestion. Scale bar, 10 μm. (**C**), SDS-PAGE gel and western blot images of spore lysates of each variant and their parental strain PY79 (WT). Lysate of PY79 (WT) was included as a negative control. The protein content of each lysate, measured by BCA assay, was normalized to 20 μg for loading in each lane. Resolved proteins were transferred for western blot analysis with primary anti-FLAG and secondary Alexa Fluor 647-conjugated antibodies. Bands corresponding to monomers of the respective fusion proteins were indicated by the black triangle. (**D**), Schematic illustration of the colorimetric assay for TIED-lipase activity. (**E**), Enzymatic activity of TIED-LipB variants and PY79 spores for hydrolysis of *p*-nitrophenol palmitate (C16, 1 mM). The enzyme activity unit, U, is defined as the conversion of 1 μmol of a substrate into *p*-nitrophenol in 1 h at 42 °C.

We investigated the effect of substrate bulkiness on the overall efficiency of TIED-LipB on spores with three substrates: C16, *p*-nitrophenyl dodecanoate (C12), and *p*-nitrophenyl octanoate (C8). Both TIED-LipB and the free-form LipB convert substrate with shorter alkyl chains more efficiently, and TIED-LipB showed hydrolysis activity for these substrates on-par with that of free-form LipB (**Figure 3.2A**). We performed a traditional Michaelis-Menten kinetic study to evaluate the overall catalytic performance. Both TIED-LipB (**Figures 3.2B**, **S3.5A**) and the free-form LipB (**Figures 3.2C**, **S3.5B**) showed a similar substrate-dependent, hyperbolic Michaelis-Menten kinetics with no apparent signs of substrate inhibition in the

experimental concentration range. The apparent Michaelis-Menten constants (K_m) of TIED-LipB and the free-form LipB were similar to each other for all substrates (**Figures 3.2D**, **S3.5C**). Taken together, these results show the high efficiency and substrate binding affinity of the TIED-LipB to be comparable to free-form LipB.

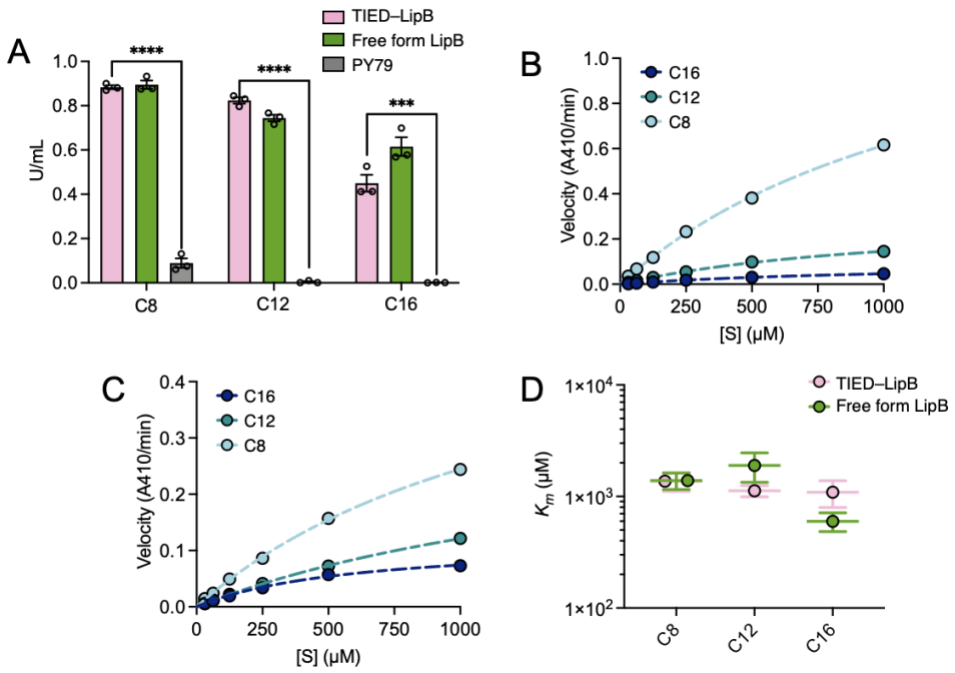

Figure 3.2. Michaelis Menten analysis of TIED-LipB and free form LipB. (**A**), Normalized activity of TIED-LipB (combination of P_{CotG} and CotZ fusion partner) and free-form LipB for hydrolysis of *p*-nitrophenyl palmitate (C16), *p*-nitrophenyl dodecanoate (C12), and *p*-nitrophenyl octanoate (C8). Spores of PY79 (OD_{600} of 0.5) analyzed with the same method were included as a negative control. (**B**), Reaction velocities of TIED-LipB (combination of P_{CotG} and CotZ fusion partner, OD_{600} of 0.5) as a function of substrate concentration. (**C**), Reaction velocities of the free-form LipB (1 μg mL^{-1}) as a function of substrate concentration. Dotted lines indicate fitting with the Michaelis Menten model (n = 3 biological replicates, see full kinetics data in Extended Data Fig. 6). (**D**), The Michaelis Menten constant, K_m, of TIED-LipB (combination of P_{CotG} and CotZ fusion partner) and the free-form LipB for hydrolysis of each substrate, determined from Michaelis Menten fitting. (Error bar indicates ± 90% confidence interval).

We tested whether the densely arranged, immobilized TIED-LipB exhibits better tolerance towards common stressors: organic solvents and elevated temperature. Polar organic solvents are substantially more destructive for enzyme activity because they penetrate and exchange

tightly bound water from enzyme active sites.[19-21] In particular, methanol deactivates lipases from various origins,[22-24] which is a major limitation for industrially-relevant reactions, such as enzymatic biodiesel synthesis.[25] We subjected TIED-LipB to a series of water-miscible and polar organic solvents.[26] In contrast to the free-form LipB, to our surprise, a positive correlation between solvent polarity and relative enzymatic activity of TIED-LipB is observed (**Figures 3.3A**, **3.3B**, and **S3.6A**). Strikingly, TIED-LipB retains approximately 60% of its catalytic activity in methanol, whereas the free-form LipB only showed 6% activity in the same condition (**Figure 3.3A**). TIED-LipB and the free-form LipB likely experience different local environments – TIED-LipB is surface-bound and constitutes a densely packed protein layer, whereas the free-form LipB is in a bulk organic solvent. Solvent polarity, orientation, and solvated substrate anisotropy at the interface differ from those of the bulk solution and affect heterogeneous catalysis.[27-29] We attribute this unique solvent polarity–activity trend to the heterogeneous nature and dense protein layers of the TIED system. In addition, TIED-LipB showed better temperature stability than the free-form LipB, increasing the half-inactivation temperature from 45 to 50 °C (**Figure 3.3C**). Studies have shown that increasing the structural rigidity of enzymes is an effective strategy to improve the kinetic stability towards elevated temperatures.[25,30-32] As such, the enhanced thermal stability is likely due to the increased rigidity of individual enzymes in densely packed protein layers on the spores. Taken together, these results demonstrate that TIED-LipB shows robust enzyme activity, comparable to the free-form LipB, and enables the use of LipB in traditionally harsh conditions.

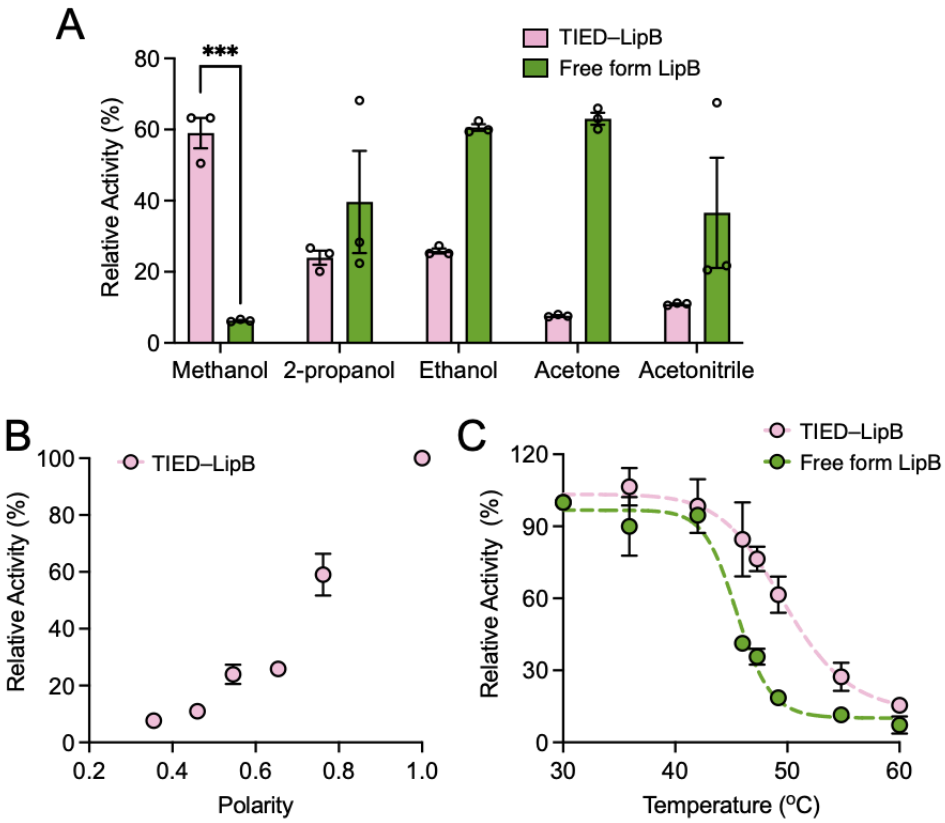

Figure 3.3. Resilience of TIED-LipB. (**A**), Relative activities of TIED-LipB (combination of P_{CotG} and CotZ fusion partner, OD_{600} of 0.5) and the free-form LipB (100 μg mL^{-1}) for hydrolysis of C16 in organic solvents, normalized to their respective activities in Tris-HCl (pH 8.0) buffer. (**B**), Relative activities of TIED-LipB (combination of P_{CotG} and CotZ fusion partner) as a function of solvent polarity (n = 3 biological replicates). (**C**), Relative activities of TIED-LipB (combination of P_{CotG} and CotZ fusion partner, OD_{600} of 0.5) and the free-form LipB (100 μg mL^{-1}) for hydrolysis of C16 at temperatures from 30 to 60 °C, normalized to their respective activities at 30 °C. The half inactivation temperature was determined by fitting a simple Boltzmann sigmoid function (n = 3 biological replicates). P values were determined by two-tail t-tests. *P < 0.05, **P < 10^{-2}, ***P < 10^{-3}, ****P < 10^{-4}.

3.2.2 Catalytic Performance of TIED-LipA

We selected lipase A (LipA), another extracellular lipase secreted by *B. subtilis* during vegetative growth, as our next target. Despite the high homology to LipB and similar α/β hydrolase core structure, LipA shows differences in substrate specificity, activity, and stability.[33] Four TIED-LipA constructs were built, and each spore morphology was

confirmed by phase-contrast optical microscopy (**Figures 3.4A**, **3.4B**, and **S3.1A**). With the exception of the P_{cotG} and CotZ combination TIED construct, all other TIED combinations resulted in high levels of expression and assembly of LipA on the spore surface (**Figure 3.4C**). The loading densities of the three successful TIED constructs are between 9.49×10^6 and 2.93×10^7 (**Figures S3.3** and **S3.4B-D**). Consistent with their high loading density, the three TIED-LipA constructs all exhibited robust hydrolysis activity towards C16 substrate (**Figure 3.4D**).

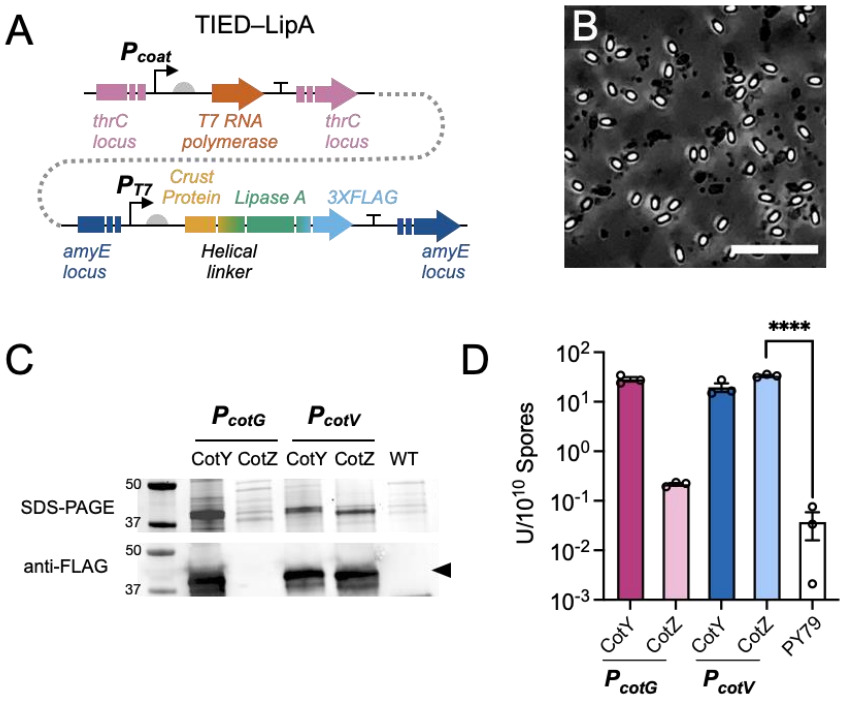

Figure 3.4 Catalytic performance of TIED-LipA. (**A**), Genetic constructs of TIED-LipA. (**B**), A representative phase-contrast image of TIED-LipA (with the combination of promoter P_{cotV} and CotZ fusion partner) after lysozyme digestion. Scale bar, 10 μm. (**C**), SDS-PAGE gel and western blot images of spore lysates of each variant and their parental strain PY79 (WT). Lysate of PY79 (WT) was included as a negative control. Protein content of each lysate, measured by BCA assay, was normalized to 20 μg for loading in each lane. Resolved proteins were transferred for western blot analysis with primary anti-FLAG and secondary Alexa Fluor 647-conjugated antibodies. Bands corresponding to monomers of the respective fusion proteins were indicated by the black triangle. (**D**), Enzymatic activity of TIED-LipA variants and PY79 spores for hydrolysis of *p*-nitrophenol palmitate (C16, 1 mM). The enzyme activity unit, U, is defined as the conversion of 1 μmol of a substrate into *p*-nitrophenol in 1 h at 42 °C.

We chose the TIED-LipA variant with the highest enzymatic activity (P_{cotV} and CotZ combination) for evaluating the enzymatic performance along with the free-form LipA. Enzymatic hydrolysis kinetics of TIED-LipA and the free-form LipA were measured and fitted to the Michaelis Menten model (**Figures 3.5A**, **3.5B**, **S3.7A**, and **S3.7B**). Similar to LipB, both TIED-LipA and the free-form LipA show faster kinetics for smaller substrates. Higher values of K_m in the case of TIED-LipA indicate that the substrate affinities to the enzyme are lower than those of the free-form LipA (**Figures 3.5C**, **S3.7C**). We attribute this trend to the local environment on the spore surface where the active site of immobilized LipA could be distorted due to orientational restrictions, resulting in less favorable substrate access.

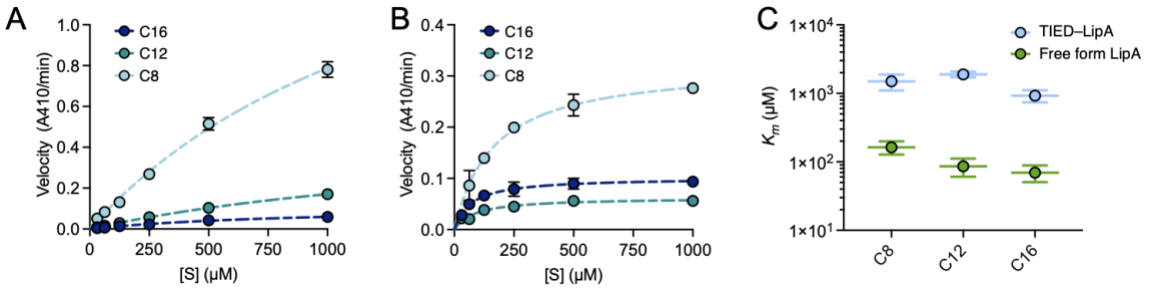

Figure 3.5. Michaelis Menten analysis of TIED-LipA and free form LipA. (**A**), Reaction velocities of TIED-LipA (combination of P_{CotV} and CotZ fusion partner, OD_{600} of 0.5) as a function of substrate concentrations. (**B**), Reaction velocities of the free-form LipA (1 μg mL^{-1}) as a function of substrate concentrations. Dotted lines indicate fitting with Michaelis Menten model (n = 3 biological replicates, see full kinetics data in Extended Data Fig. 7). (**C**), The Michaelis Menten constant, K_m, of TIED-LipA (combination of P_{CotV} and CotZ fusion partner) and the free-form LipB for hydrolysis of each substrate, determined from Michaelis Menten fitting. (Error bar indicates ± 90% confidence interval).

TIED-LipA also showed significantly higher activity in methanol compared to the free-form LipA (**Figure 3.6A**) and a positive correlation between solvent polarity and enzyme activity (**Figure 3.6B**). No such correlation was observed for the free-form LipA (**Figure S3.6B**). Furthermore, TIED-LipA exhibited superior thermal stability than the free-form LipA, with the half-inactivation temperature increased from 51 to 57 °C, likely due to the increased enzyme rigidity in the restricted local environment (**Figure 3.6C**).

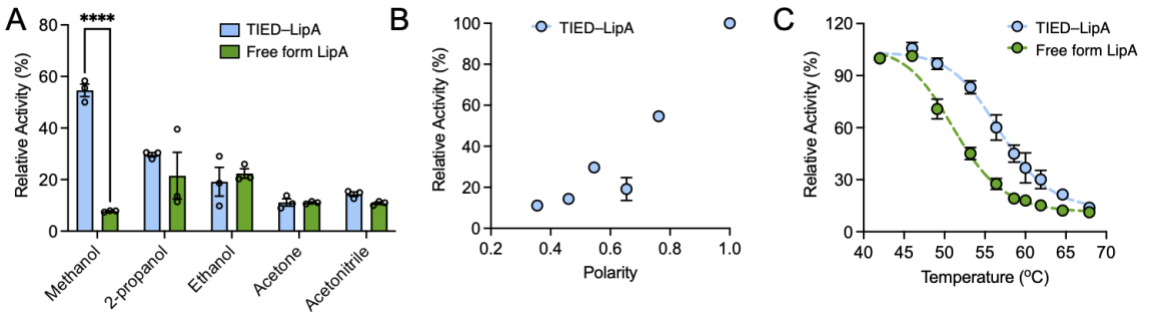

Figure 3.6. Resilience of TIED-LipA. (**A**), Relative activities of TIED-LipA (combination of P_{CotV} and CotZ fusion partner, OD_{600} of 0.5) and the free-form LipA (100 μg mL^{-1}) for hydrolysis of C16 in organic solvents, normalized to their respective activities in Tris-HCl (pH 8.0) buffer. (**B**), Relative activities of TIED-LipA (combination of P_{CotV} and CotZ fusion partner) as a function of solvent polarity (n = 3 biological replicates). (**C**), Relative activities of TIED-LipA (combination of P_{CotV} and CotZ fusion partner, OD_{600} of 0.5) and the free-form LipA (100 μg mL^{-1}) for hydrolysis of C16 at temperatures from 42 to 68 °C, normalized to their respective activities at 42 °C. The half-inactivation temperature was determined by fitting a simple Boltzmann sigmoid function (n = 3 biological replicates). P values were determined by two-tail t-tests. *$P < 0.05$, **$P < 10^{-2}$, ***$P < 10^{-3}$, ****$P < 10^{-4}$.

3.2.3 Catalytic Performance of TIED-APEX2

To demonstrate the capability of TIED technology to synthesize and immobilize heterologous enzymes that are non-native to *B. subtilis*, we chose APEX2, an engineered ascorbate peroxidase, as our last target. In addition to extensive applications in proximity-based protein labeling and electron microscopy,[34] APEX2 has recently been shown to enable conductive polymer synthesis *in vivo*.[35] Analogous to TIED-LipB and TIED-LipA, all TIED-APEX2 constructs (**Figure 3.7A**) yield typical spore formation (**Figures 3.7B**, **S3.1B**). Western blot analysis of the spore coat and crust proteome revealed the presence of full-length APEX2 in all TIED-APEX2 variants, except for the P_{cotZ} and CotZ combination (**Figure 3.7C**). The lower molecular weight product observed in this combination indicates possible protease-mediated cleavage of the fusion protein. The loading densities of the full-length APEX2 in the successful TIED-APEX2 constructs, measured by quantitative western blot analyses, range from 2.85×10^6 to 1.71×10^7 (**Figures S3.3**, **S3.4E-H**). In the presence of H_2O_2, APEX2 rapidly converts Amplex Red substrate into a fluorogenic product, resorufin

(**Figure 3.7D**). Corresponding to the western blot results, TIED-APEX2 spores with a high loading density (> 10^6 enzymes per spore) all showed robust enzymatic activity as probed by Amplex Red conversion (**Figures 3.7E**, **3.7F**). In addition, kinetic analysis of these TIED-APEX2 variants revealed K_m values similar to the free-form APEX2, indicating similar substrate affinity (**Figures 3.7G**, **3.7H**, and **S3.8A-G**). We note that TIED-APEX2 performs slightly better at 30–45 °C but did not result in a meaningful increase in half-inactivation temperature compared to its free form (**Figure S3.8H**). These results demonstrate that TIED technology can effectively accommodate target enzymes that are completely foreign to *B. subtilis*.

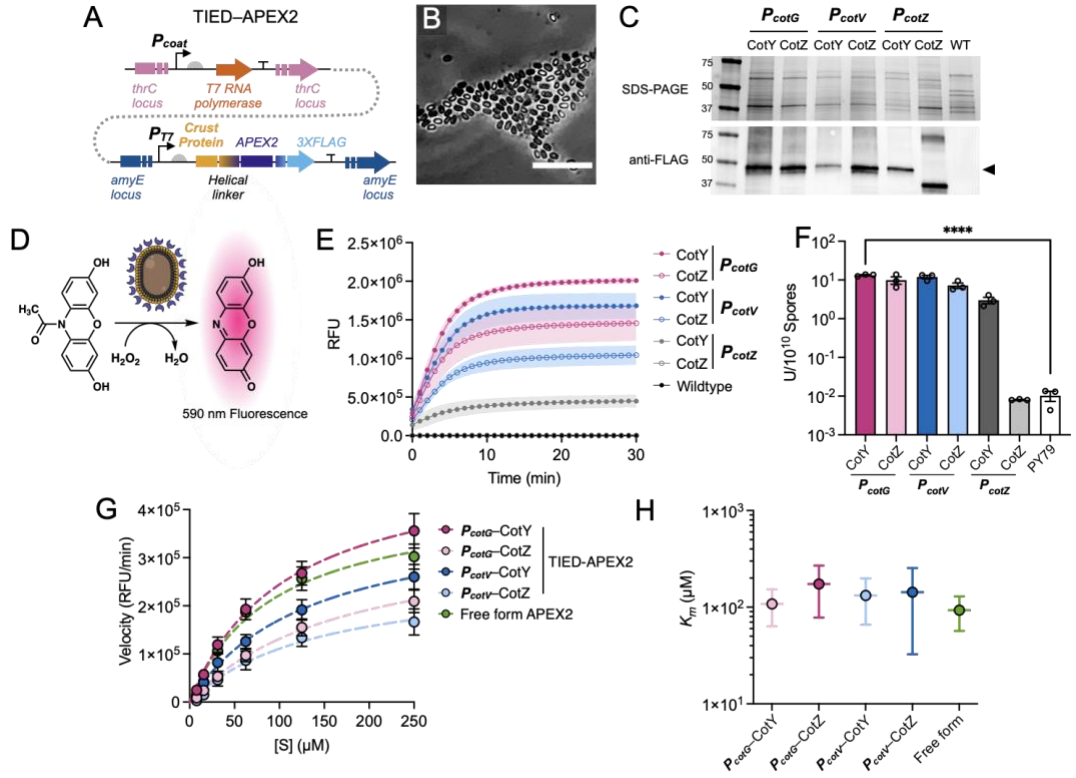

Figure 3.7. Catalytic performance of TIED-APEX2 (**A**), Genetic constructs of TIED-APEX2. (**B**), A representative phase-contrast image of TIED-APEX2 (with the combination of promoter P_{cotG} and CotY fusion partner) after lysozyme digestion. Scale bar, 10 μm. (**C**), SDS-PAGE gel and western blot images of spore lysates of each variant and their parental strain PY79 (WT). Lysate of PY79 (WT) was included as a negative control. The protein content of each lysate, measured by BCA assay, was normalized to 20 μg for loading in each lane. Resolved proteins were transferred for western blot analysis with primary anti-FLAG and secondary Alexa Fluor 647-conjugated antibodies. Bands corresponding to monomers of the respective fusion proteins were indicated by the black triangle. (**D**), Schematic illustration of the TIED-APEX2 catalyzed conversion of Amplex Red to resorufin. (**E**), Fluorescence time trace resulting from resorufin formation catalyzed by TIED-APEX2 variants and PY79. (**F**), Enzymatic activity of TIED-APEX2 variants and PY79 spores for conversion of Amplex Red (125 μM). The enzyme activity unit, U is defined as the conversion of 1 μmol of Amplex Red to resorufin in 1 h at 25 °C. (**G**), Reaction velocities of TIED-APEX2 variants (OD_{600} of 0.5) and the free-form APEX2 (1 μg mL^{-1}) as a function of substrate concentration. Dotted lines indicate fitting with Michaelis Menten model (n = 3 biological replicates, see full kinetics data in Extended Data Fig. 8). (**H**), The Michaelis Menten constant, K_m, of TIED-APEX2 variants and the free-form APEX2 for Amplex Red conversion, determined from Michaelis Menten fitting. (Error bar indicates ± 90% confidence interval). P values were determined by two-tail t-tests. *P < 0.05, **P < 10^{-2}, ***P < 10^{-3}, ****P < 10^{-4}.

2.2.4 Recycling and Renewal of TIED Enzymes

The design of the TIED system allows recycling and renewal of enzymes to fully recover original activity on-demand, enabling theoretically infinite reuse of biocatalysts (**Figure 3.8A**). We first set out to test the recyclability of TIED-enzymes, which is one of the major known advantages of enzyme immobilization. After each reaction cycle, TIED-LipA was immediately recollected by centrifugation and subjected to the next cycle. With C8 and C12 substrates, TIED-LipA maintains almost 100% activity for at least 20 cycles (**Figure S3.9**). In the case of the C16 substrate, the enzymatic conversion diminished to below 50% after 10 rounds of recycling. Similar to TIED-LipA, conversion of C8 by TIED-LipB was maintained for at least 20 cycles, while conversion of C16 declined after 5 rounds of recycling (**Figure S3.10**). TIED-APEX2 retained 84% of its original activity after 10 consecutive cycles (**Figure S3.11**).

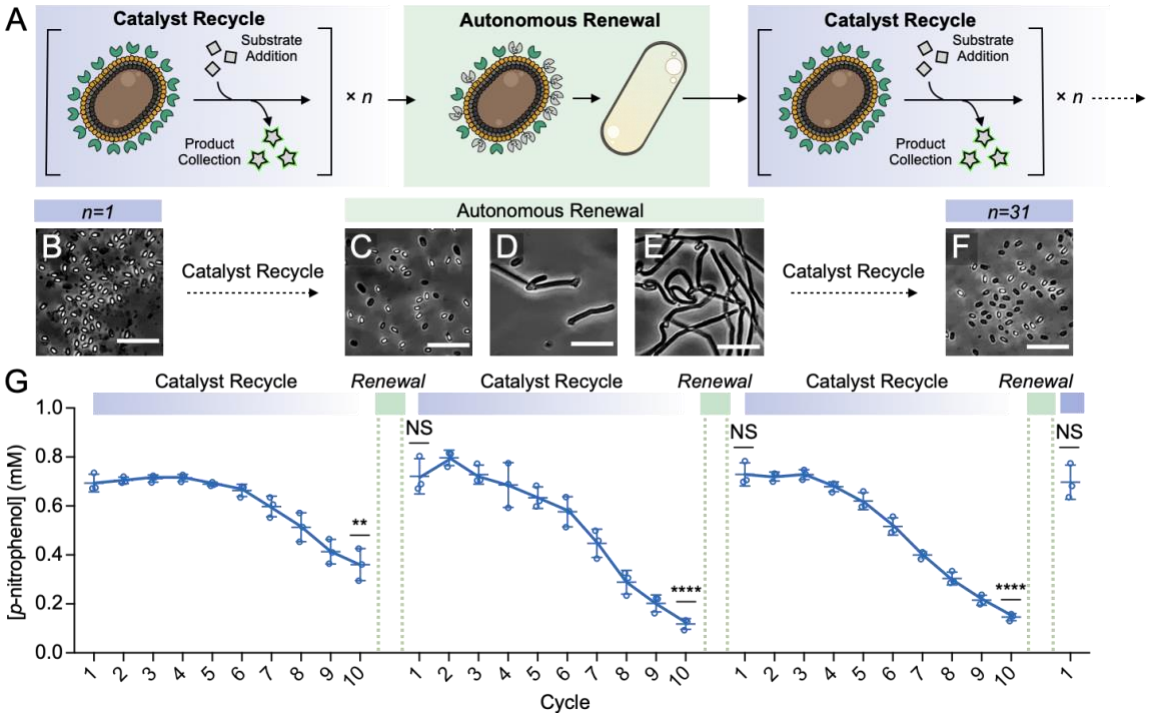

Figure 3.8. Recycling and renewal of TIED-LipA in aqueous phase. (**A**), Schematic illustration of recycling and renewal of TIED-enzymes. (**B-F**), A representative phase-contrast microscopic image of TIED-LipA (combination of P_{cotV} and CotZ fusion partner) spore germination in LB medium after (B), the 1st cycle of reaction with *p*-nitrophenyl palmitate (C16, 0.8 mM) in Tris-HCl buffer (pH 8.0). (C) 2 h. (D), 3 h. (E), 4 h. and (F), the completion of the 31st cycle of reaction with C16. Scale bar, 10 μm (G), Recycling and renewal of TIED-LipA (combination of P_{cotV} and CotZ fusion partner, OD_{600} = 1) spores catalyzing the conversion of C16 (0.8 mM) in Tris-HCl buffer. Each reaction cycle lasts 10 min (n = 3 biological replicates). *P* values were determined by two-tail t-tests against the pristine activity of TIED-LipA (1st cycle). $*P < 0.05$, $**P < 10^{-2}$, $***P < 10^{-3}$, $****P < 10^{-4}$.

Another obvious merit of the TIED system is that the synthesis and assembly of recombinant enzymes are completely autonomous. Therefore, once the activity is reduced to a critical point, TIED enzymes can be fully renewed by germinating spores into cells, growing cells, and subsequently triggering sporulation. We demonstrated this novel concept with TIED-LipA for conversion of C16, the substrate that causes attrition of enzymatic activity after 10 cycles. After completion of the first 10 cycles, TIED-LipA spores (**Figure 3.8B**) were germinated in nutrient-rich media (**Figure 3.8C-E**), after which sporulation was induced by

medium shift. The catalytic performance of renewed TIED-LipA in cycle 11 is fully comparable to the pristine TIED-LipA in cycle 1 (**Figure 3.8G**). Renewals after consecutive 10 cycles of TIED-LipA (cycle 21 and cycle 31) all result in full recovery of activity (**Figure 3.8G**). Similar to TIED-LipA, TIED-LipB also recovered its full activity upon renewal after cycle 6, allowing multiple recycling and renewal rounds (**Figure S3.10B**). Recycling and renewal ability of TIED-LipA were observed even in methanol, albeit with a lower enzymatic conversion and more rapid loss of activity than in aqueous solutions (**Figure 3.9**). Multiple renewals of TIED-LipA after 5 consecutive cycles result in full recovery of enzymatic activity, which is consistent with the known tolerance of *B. subtilis* spores against organic solvents.

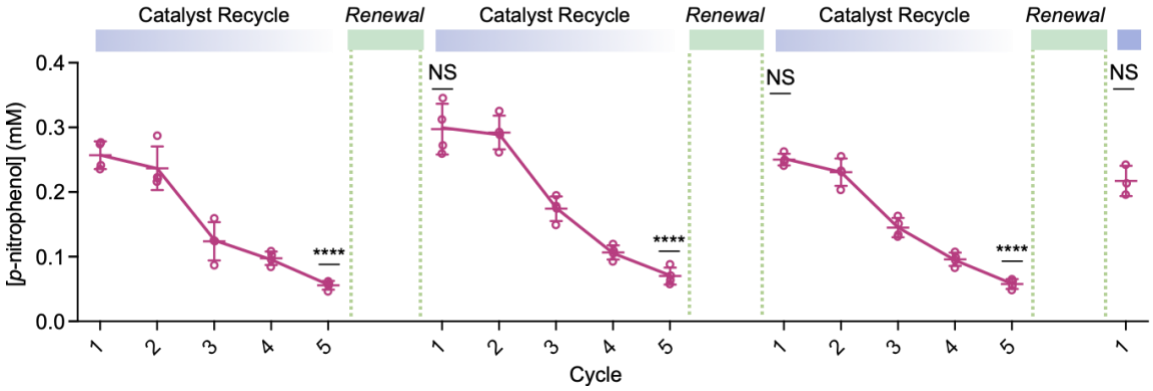

Figure 3.9. Recycling and renewal of TIED-LipA (combination of P_{cotV} and CotZ fusion partner, OD_{600} = 1) spores catalyzing the conversion of C12 (0.8 mM) in methanol. Each reaction cycle lasts 20 min (n = 4 biological replicates). P values were determined by two-tail t-tests against the pristine activity of TIED-LipA (1st cycle). $*P < 0.05$, $**P < 10^{-2}$, $***P < 10^{-3}$, $****P < 10^{-4}$.

3.3 Conclusions

We developed TIED technology to immobilize enzymes in high density on bacterial spores leveraging a T7 RNAP expression system active specifically during sporulation. The versatility and utility of this platform are demonstrated with three different enzymes – two endogenous lipases from *B. subtilis* and an engineered peroxidase APEX2 – all exhibiting efficient substrate conversion comparable to the respective free enzymes. Compared to the previously reported spore display systems, TIED significantly enhances the loading capacity of recombinant enzymes (10^6–10^7 per spores). Enhanced thermal stability of displayed lipases was observed. In addition, TIED-lipases show high activity in methanol and a positive correlation between enzymatic activity and solvent polarity. This feature makes TIED technology desirable for practical applications, such as biodiesel synthesis. Departing from all previously reported enzyme immobilization strategies, TIED-enzymes are not only recyclable, but are fully renewable. The high efficiency from the high loading density, improved stability in harsh conditions, recyclability, and renewability of the TIED system compare favorably to existing enzyme immobilization technologies, making TIED a powerful and sustainable biocatalyst platform.

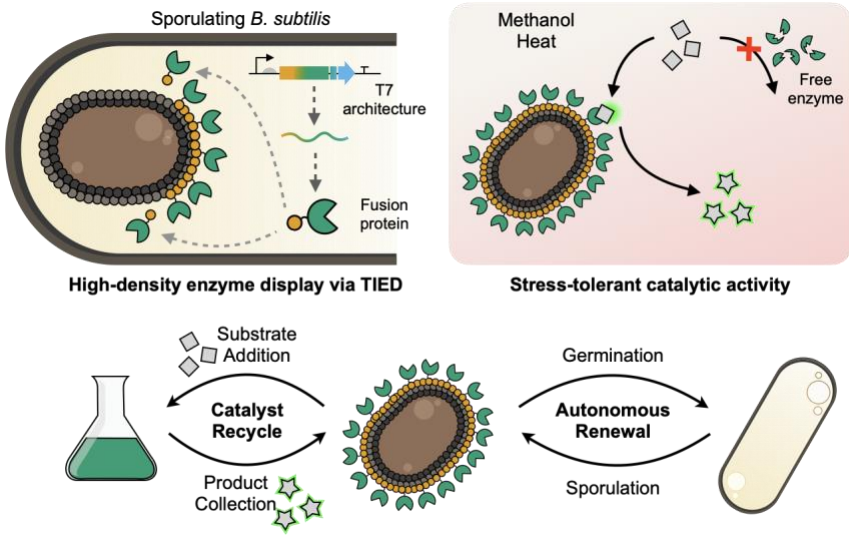

Figure 3.10. Illustration of the T7 RNA polymerase-enabled high-density protein display (TIED) on bacterial spores and its unique features as a biocatalyst platform.

Our current work lays the foundation for expanding the scope of the TIED technology. Because of the highly interconnected nature of spore coat proteins,[12] the maximum level of one anchor protein may be limited by the availability of their interaction partners. For example, co-expression of fusion proteins harnessing a well-known interaction pair, CotY and CotZ,[36,37] may further enhance the loading capacity. In addition, different local environments that individual coat proteins reside in may have unexpected implications for enzyme thermostability and activity in organic solvents. With more varieties and combinations of anchor proteins, TIED can potentially offer a higher loading density and meet requirements for specific applications for end-users. Moreover, future generations of TIED will enable multifunctional biocatalysts by displaying more than one type of enzyme. Engineering enzymatic cascades on a single spore surface could be pursued by displaying all involved enzymes in close proximity. Another useful application is to display enzymes having different substrate preferences on a single spore. This new version of TIED will enable a fast and convenient approach for generating one-for-all biocatalysts useful for multiple chemical transformations.

While in this work we compared the performance of TIED to free-form enzymes, it is worth noting additional advantages of spore-surface display over cell-surface display. Genetically encoding heterologous enzymes usually reduces growth rate, viability, and cell density relative to parental nonproducing cells, which gives a strong selection pressure for mutations eliminating the burden. In the TIED system, burdensome expression of genetically-encoded fusion proteins occurs only after *B. subtilis* cells have committed to sporulation. Because the burden and cellular growth are decoupled in the TIED system, the selective pressure for mutations debilitating the enzymatic functionality is largely or entirely mitigated. This evolutionary stability is another strong merit for the TIED system as it allows for the unlimited renewal of biocatalysts. Overall, we believe that TIED technology will generate a large portfolio of biocatalysts useful in various practical applications and advance the field of sustainable catalysis.

3.4 Materials and Methods

Design and cloning of genetic constructs in *B. subtilis*. Gene sequences of lipase A, lipase B, CotY, and CotZ were obtained from genes *estA*, *estB*, *cotY*, and *cotZ*, respectively, from the genome of *B. subtilis* PY79. The secretion signal sequences of estA and estB were excluded. The gene sequence of APEX2 was codon-optimized (IDT Codon Optimization Tool) based on its protein sequence.[34,38] Gene sequences of T7 RNAP and the T7 promoter, along with the lac operator and hammerhead ribozyme were amplified from a previously reported construct (GenBank MN005204).[39] The endogenous promoters, P_{cotG}, P_{cotZ}, and P_{cotV}, were amplified from the genome of *B. subtilis* PY79. A strong synthetic ribosomal binding site (RBS), MF001, was inserted between the promoter region and start codon.[39] Between the target protein and the C terminus of CotY/CotZ, an 11-amino-acid spacer that forms a stable α-helical structure was placed.[40] Three repeats of the FLAG tag were introduced to the C terminus of the fusion construct for immunostaining.

PCR-amplified DNA fragments were assembled using Golden Gate Assembly and inserted into plasmid backbones (New England Biolabs).[41] The T7 driven gene circuits for fusion protein expression were inserted into vector PBS1C,[42] which carries homology sites of the *amyE* locus and a chloramphenicol resistance selection marker. The T7 RNAP expression circuit was cloned into the PBS4S backbone,[43] which contains the spectinomycin resistance gene, flanked by sequences homologous to the *thrC* locus. The resultant plasmids were transformed into *E. coli* DH10B (New England Biolabs, C3019) through electroporation and selected by carbenicillin resistance (100 μg mL^{-1}). Clones carrying plasmids with correct sequences were isolated for DNA extraction (QIAGEN, 56604785).

Purified plasmids were linearized by restriction enzyme digestion for the transformation of *B. subtilis*. Chromosomal integration into the *B. subtilis* PY79 genome via double cross-over was performed according to the reported two-step method.[44] The resulting *B. subtilis* clones were selected on lysogeny broth (LB) agar plates supplemented with chloramphenicol (5 μg mL^{-1}) or (and) spectinomycin (100 μg mL^{-1}). To generate strains carrying TIED constructs with engineered circuits in two loci, *B. subtilis* PY79 was transformed first with the T7-

driven fusion protein expression circuit into the *amyE* locus. Competence was induced in selected clones for the subsequent transformation of the construct for T7 RNAP expression.

The construct for expressing free enzymes contained a fusion protein sequence with a 6×His tag appended to the N terminus of the genes encoding lipase A, lipase B, or APEX2 and three repeats of FLAG tag on the C terminus. The assembled DNA-of-interest was inserted into a pET22b expression vector containing a T7 promoter and lac operon (Novagen). Ligated plasmids were electroporated into *E. coli* BL21 (DE3) competent cells (Invitrogen). Clones were selected on LB agar plates supplemented with carbenicillin (100 μg mL^{-1}). The complete list of plasmids used and created in this study is provided in Table S1.

Protein expression and purification. For expression of free-form LipA, LipB, and APEX2, the respective expression strain of *E. coli* was inoculated in 10 mL of LB, supplemented with 100 μg mL^{-1} carbenicillin, and grown for 14 h at 37 °C. The saturated starter culture was then diluted into 500 mL Terrific Broth (Sigma-Aldrich) in 2800 mL baffled Erlenmeyer flask and allowed to grow at 37 °C (200 rpm) till OD_{600} of reached 0.5. The culture was cooled on ice for 10 min and induced with 1 mM IPTG. The induced culture was grown at 25 °C for 20 h (120 rpm). Cells were pelleted and resuspended in lysis buffer (50 mM NaH_2PO_4, 300 mM NaCl, 10 mM imidazole, pH 8.0) supplemented with 1 mg mL^{-1} lysozyme, and incubated on ice for 1 h. Cells were disrupted by sonication (Qsonica, Q125, 5s on, 5s off, 5 min, 100% amplitude), and the debris was pelleted by centrifugation (40,000 g, 1 h, 4 °C) and discarded. The lysate (20 mL) was incubated with 10 mL of Ni-NTA agarose (QIAGEN, 30230) for 30 min at room temperature. The protein-bound agarose resin was washed with 60 mL of wash buffer (50 mM NaH_2PO_4, 300 mM NaCl, 20 mM imidazole, pH 8.0) and eluted with 20 mL of elution buffer (50 mM NaH_2PO_4, 300 mM NaCl, 250 mM imidazole, pH 8.0). The eluted fraction was analyzed by SDS-PAGE to confirm the protein size and purity. Purified proteins were then flash-frozen at -80 °C and lyophilized for 48 h.

Lipase activity assay. Spores with TIED-lipases were harvested by lysozyme treatment and resuspended in Tris-HCl buffer (50 mM pH 8.0, supplemented with 0.3% Triton-X). The lipase activity assay was conducted based on previously established protocols.[45] 10 mM

stock solutions of lipase substrates, C8, C12, and C16 were prepared in isopropanol. Enzymatic activities of TIED variants were evaluated by reacting spore suspensions normalized to OD_{600} of 0.5 with 1 mM substrate C16 in 1 mL total volume for 1 h at 42 °C with agitation (800 rpm). After the reaction, spores were spun down, and 100 μL of the supernatant containing the reaction product was loaded onto a 96-well microplate. The absorbance of each well at 410 nm was measured by a microplate reader (BioTek Synergy H1 Hybrid Multi-Mode, gain = 100). To convert the absorbance at 410 nm to product concentration, a calibration curve of *p*-nitrophenol concentration versus absorbance was plotted using solutions prepared with a standard compound (Sigma-Aldrich) (Extended Data Fig. 3b). The enzyme activity unit, U, is defined as the conversion of 1 μmol of a substrate into *p*-nitrophenol in 1 h at 42 °C.

To compare the activity of TIED-LipB to free form LipB, spore-displayed enzyme concentration (using 1 mL spore suspension of OD_{600} = 0.3) was calculated from quantitative western blot analysis. Purified and lyophilized free-form LipB was dissolved in Tris-HCl buffer (50 mM pH 8.0, supplemented with 0.3% Triton-X) to match the enzyme concentrations of the spore suspensions. With each substrate, reaction was performed at 42 °C for 1 h.

The kinetics assay was performed on a microplate reader. Each of the three substrates was serially diluted to concentrations ranging from 10 mM to 71.825 μM in isopropanol. Spore suspension (OD_{600} = 0.5) was transferred to a 96-well microplate and pre-incubated at 42 °C for 10 min. Substrates of varying concentrations were then simultaneously diluted 1:10 to a final volume of 100 μL. The absorbance at 410 nm in each well was continuously measured till the absorbance readouts plateaued.

Lipase activity assays in organic solvents. For TIED-lipases, spores in 1 mL PBS (OD_{600} = 0.5) were pelleted and placed in a vacuum desiccator for 3 h to remove residual water. Dried spores were suspended in the respective organic solvents by brief sonication (VWR Symphony Ultrasonic Cleaner). Stock solutions of lipase substrates C8, C12, and C16 were diluted 1:10 into spore suspensions to a final concentration of 1 mM in 1 mL total volume.

Lyophilized free-form enzymes (100 μg mL^{-1}) were directly dissolved in the respective solvents containing 1 mM substrates. Reactions were performed at 42 °C for 1 h, followed by centrifugation (10^4 g, 10 min). The supernatants containing the reaction product were collected and heated at 80 °C for 10 min to deactivate any carried-over enzymes. Solvents in the supernatant were completely evaporated by a rotary evaporator (Buchi R-100, < 30 kPa), and the dried residues were dissolved in an equal volume of Tris-HCl buffer for colorimetric quantification.

Thermal stability of lipases. Temperatures used in the assays were implemented by a user-defined gradient protocol on a thermocycler (Bio-Rad, C1000). TIED-lipases (spore OD_{600} = 0.5) and the free-form lipases (100 μg mL^{-1}) dissolved in Tris-HCl buffer were preincubated at each temperature for 5 min to reach equilibrium. Reactions (total volume of 100 μL) were initiated by spiking in C16 substrate to the final concentration of 1 mM and allowed to proceed for 1 h. Supernatants were collected for colorimetric measurements. Activities of LipA and LipB at elevated temperatures were determined relative to those at their respective optimal temperatures, 42 °C for LipA and 30 °C for LipB.

APEX2 activity assay. Amplex Red reagent (Invitrogen, A12222) was dissolved in DMSO ($\geqslant$ 99.7%) to prepare a 10 mM stock solution. Reactions were performed in a 96-well plate with 100 μL total volume. Spores with TIED-APEX2 were suspended in PBS (pH 7.2). H_2O_2 was added from a 20 mM stock solution to the final concentration of 1 mM. Spore suspensions (OD_{600} = 0.1) were transferred onto a microplate. The enzymatic reaction was initiated by adding Amplex Red stock solution to a final concentration of 125 μM in each well, followed by manual mixing and immediate fluorescence monitoring (λ_{ex} = 530 nm, λ_{em} = 590 nm) for 1 h. The enzyme activity unit, U, is defined as the conversion of 1 μmol of Amplex Red to resorufin in 1 h at 25 °C. For the kinetics assay, the Amplex Red stock solution was serially diluted to concentrations ranging from 10 mM to 71.825 μM in DMSO. Substrates with varying concentrations were added 1:10 to each well containing TIED-APEX2 (in PBS with 1 mM H_2O_2). Fluorescence was continuously monitored under constant shaking till the emission readouts plateaued. To convert the fluorescence emission (RFU) to

product concentration, a calibration curve of resorufin concentrations versus RFU was plotted using solutions prepared with a standard compound (Sigma-Aldrich, 635-78-9) (Extended Data Fig. 3c).

Preparation of spore lysate and western blot analysis. For quantification of TIED-enzyme concentrations, concentrated spore suspensions in PBS were serially diluted, and OD_{600} of each dilution was measured. Spores were collected and resuspended in an equal volume of a decoating buffer (100 mM NaOH, 100 mM NaCl, 100 mM dithiothreitol, and 10 g L^{-1} sodium dodecyl sulfate).[46] Spores were decoated for 30 min at 65 °C. After centrifugation (10000g, 15 min), clear lysate containing the solubilized spore coat and crust proteome was collected for western blot analysis. For comparing expression levels in different TIED variants, the protein concentration of each lysate sample was measured by BCA Protein Assay Kit (Thermo Scientific, 23250) according to the manufacturer's manual. The original lysate was diluted 1:20 in PBS to lower the concentration of sodium dodecyl sulfate to below 5 mM. Samples with normalized protein content were loaded into each lane (20 μg/lane) and resolved by SDS-PAGE (Bio-Rad, 456809). Total protein contents were imaged with the Bio-Rad Chemidoc MP Imaging System, and the gels were transferred to a PVDF membrane (Bio-Rad, 1620174) using a western blot transfer system (Trans-Blot Turbo Transfer System, 1.5 mm Gel Protocol). Membranes were blocked with 3% (w/v) BSA (Sigma-Aldrich, A9418) in 0.1% Tween 20 in phosphate buffered saline (PBST) at room temperature for 1 h to prevent non-specific labeling. Primary anti-FLAG antibody (1: 5000, Sigma Aldrich, F1804) was added, and the labeling was allowed to proceed for 1 h at room temperature. Membranes were then washed three times in PBST to remove unbound antibody and incubated with Alexa Fluor 647 conjugated secondary antibody (1: 2000, Goat anti-Mouse IgG (H+L) Highly Cross-Adsorbed Secondary Antibody, Alexa Fluor 647, Invitrogen, A21236) in PBST for 30 min in dark. Stained membranes were rinsed three times in PBST and imaged with Bio-Rad Chemidoc MP Imaging System. Fluorescence signals from each membrane were collected using the Cy5 channel (5 s exposure time, gain = 1), and the resulting images were subjected to the same image processing method with Bio-Rad Image Lab Touch Software to ensure a fair comparison.

Quantification of TIED-enzyme loading density. Western blot images were processed with Image J (Extended Data Fig. 4).[47] Different spore concentrations were used to prepare lysates in each lane. Intensities of all bands within the lane were plotted using the Plot Lanes function in Image J. The area-under-peaks corresponding to the TIED-enzymes were segmented and quantified. To quantify the enzyme loading density in each TIED variant, the intensities of the bands corresponding to the monomer of the fusion protein were plotted against the OD_{600} of the spore suspension used to generate the lysate. The linear range was manually determined and fitted with linear regression (Extended Data Fig. 5). Colony-forming units (CFU) corresponding to each OD_{600} were determined from a CFU-spore OD_{600} calibration curve. Purified spores were diluted in PBS to OD_{600} between 0.1 to 1. Each sample was serially diluted and plated on LB agar plates, and the CFUs were calculated based on the numbers of colonies on the plates. The data were fitted by linear regression (Extended Data Fig. 3a). For each target protein, free enzyme solutions ranging from 1 mg mL^{-1} to 1.56 μg mL^{-1} were prepared with purified and lyophilized protein powder. After SDS-PAGE and subsequent western blot analysis, intensities of the bands corresponding to a specific concentration of free enzymes were quantified. A calibration curve of band intensities versus enzyme concentrations was plotted for each target enzyme. The linear range was determined in each case and fitted by regression (Extended Data Fig. 5). Together with the OD_{600} and CFU conversion plot, TIED-enzyme loading densities for each variant were determined with these calibration curves.

Recycle and renewal of spores with TIED-enzymes. For aqueous phase reactions, spores with TIED-LipA were suspended in 50 mM Tris-HCl buffer (pH 8.0, 0.3% Triton-X). Reactions were conducted using 1 mL of spore suspension (OD_{600} = 1) with 0.8 mM substrates (C8, C12, and C16) in 1.7 mL microcentrifuge tubes. The reaction proceeded for 10 min at 42 °C with agitation (800 rpm) for each cycle. After reactions, the spores were collected by centrifugation (5000 g, 10 min), and the supernatant was decanted for colorimetric analysis. Tris-HCl buffer and fresh substrates were immediately added to the spore pellets to initiate the next cycle. Reaction conditions for all cycles were kept constant. Spores of TIED-LipB were recycled with the same procedure. To reuse TIED-APEX2

(OD_{600} = 1), each reaction cycle was performed with 125 μM Amplex Red in PBS (pH 7.2) for 5 min. For reactions in methanol, spores of TIED-LipA in 1 mL PBS (OD_{600} = 1) were used. Before being subjected to reaction conditions, the harvested spores in 1.7 mL microcentrifuge tubes were placed in a vacuum desiccator for 3 h to remove residual water within pellets. The dried spores were suspended in 1 mL of methanol (Fisher chemical, $\geqslant$ 99.9%) supplemented with 0.8 mM of C12 substrate. Each reaction was performed at 42 °C for 20 min before collecting spores by centrifugation (5000 g, 10 min). To renew spores with TIED-LipA, 2 μL of spore suspension after the last reaction cycle was diluted in 5 mL of LB supplemented with the appropriate antibiotics. The starter culture was grown to saturation, and sporulation was induced as described in previous sections.

Statistical analysis. All experimental data were plotted as mean ± s. e. m. unless otherwise mentioned. All enzymatic assays were performed with at least three biological replicates. The mean values determined from three biological replicates were fitted to the Michaelis Menten model for kinetics analyses. Error bars for K_m represent the 90% confidence interval (CI) of the fitting (Fig. 2i, 3g, and 4h). The thermal stability of lipases (Fig. 2l and 3j) was determined by fitting a Boltzmann sigmoid function to the experimental data. Statistical significance and *P* values were derived from two-tailed t-tests.

3.5 Supplementary Tables and Figures

Table S3.1. Protein sequences

CotY	MSCGKTHGRHENCVCDAVEKILAEQEAVEEQCPTGCYTNLLNPTIA GKDTIPFLVFDKKGGLFSTFGNVGGFVDDMQCFESIFFRVEKLCDCC ATLSILRPVDVKGDTLSVCHPCDPDFFGLEKTDFCIEVDLGCFCAIQC LSPELVDRTSPHKDKKHHHNG
CotZ	MSQKTSSCVREAVENIEDLQNAVEEDCPTGCHSKLLSVSHSLGDTVP FAIFTSKSTPLVAFGNVGELDNGPCFNTVFFRVERVHGSCATLSLLIA FDEHKHILDFTDKDTVCEVFRLEKTNYCIEVDLDCFCAINCLNPRLIN RTHHH
Lipase A	MEHNPVVMVHGIGGASFNFAGIKSYLVSQGWSRDKLYAVDFWDKT GTNYNNGPVLSRFVQKVLDETGAKKVDIVAHSMGGANTLYYIKNL DGGNKVANVVTLGGANRLTTGKALPGTDPNQKILYTSIYSSADMIV MNYLSRLDGARNVQIHGVGHIGLLYSSQVNSLIKEGLNGGGQNTN
Lipase B	MESVHNPVVLVHGISGASYNFFAIKNYLISQGWQSNKLYAIDFYDKT GNNLNNGPQLASYVDRVLKETGAKKVDIVAHSMGGANTLYYIKYL GGGNKIQNVVTLGGANGLVSSTALPGTDPNQKILYTSIYSLNDQIVIN SLSRLQGARNIQLYGIGHIGLLSNSQVNGYIKEGLNGGGLNTN
APEX2	MVSKGEETTMGVIKPDMKIKLKMEGNVNGHAFVIEGEGEGKPYDG TNTINLEVKEGAPLPFSYDILTTAFSYGNRAFTKYPDDIPNYFKQSFPE GYSWERTMTFEDKGIVKVKSDISMEEDSFIYEIHLKGENFPPNGPVM QKETTGWDASTERMYVRDGVLKGDVKMKLLLEGGGHHRVDFKTI YRAKKAVKLPDYHFVDHRIEILNHDKDYNKVTVYEIAVARNSTDG MDELYK

Table S3.2. Genetic constructs

Plasmid name	**Description**	**Promoter**	**Tags**	**Integration**
PBS1C-CotY-LipB-3XFLAG	TIED-LipB fused to CotY	P_{T7}, LacO	3XFLAG at C terminus; helical linker between CotY and LipB	*amyE*
PBS1C-CotZ-LipB-3XFLAG	TIED-LipB fused to CotZ	P_{T7}, LacO	3XFLAG at C terminus; helical linker between CotZ and LipB	*amyE*
PBS1C-CotY-LipA-3XFLAG	TIED-LipA fused to CotY	P_{T7}, LacO	3XFLAG at C terminus; helical linker between CotY and LipA	*amyE*
PBS1C-CotZ-LipA-3XFLAG	TIED-LipA fused to CotZ	P_{T7}, LacO	3XFLAG at C terminus; helical linker between CotZ and LipA	*amyE*
PBS1C-CotY-APEX2-3XFLAG	TIED-APEX2 fused to CotY	P_{T7}, LacO	3XFLAG at C terminus; helical linker between CotY and LipB	*amyE*
PBS1C-CotZ-APEX2-3XFLAG	TIED-APEX2 fused to CotZ	P_{T7}, LacO	3XFLAG at C terminus; helical linker between CotY and LipB	*amyE*

PBS4S-P_{cotG}-T7 RNAP	T7 RNAP expression	P_{cotG}		*thrC*
PBS4S-P_{cotV}-T7 RNAP	T7 RNAP expression	P_{cotV}		*thrC*
PBS4S-P_{cotZ}-T7 RNAP	T7 RNAP expression	P_{cotZ}		*thrC*
PET22b-6XHis-LipB-3XFLAG	LipB expression	P_{T7}, LacO	3XFLAG at C terminus 6XHis at N terminus	
PET22b-6XHis-LipA-3XFLAG	LipA expression	P_{T7}, LacO		
PET22b-6XHis-APEX2-3XFLAG	APEX2 expression	P_{T7}, LacO		

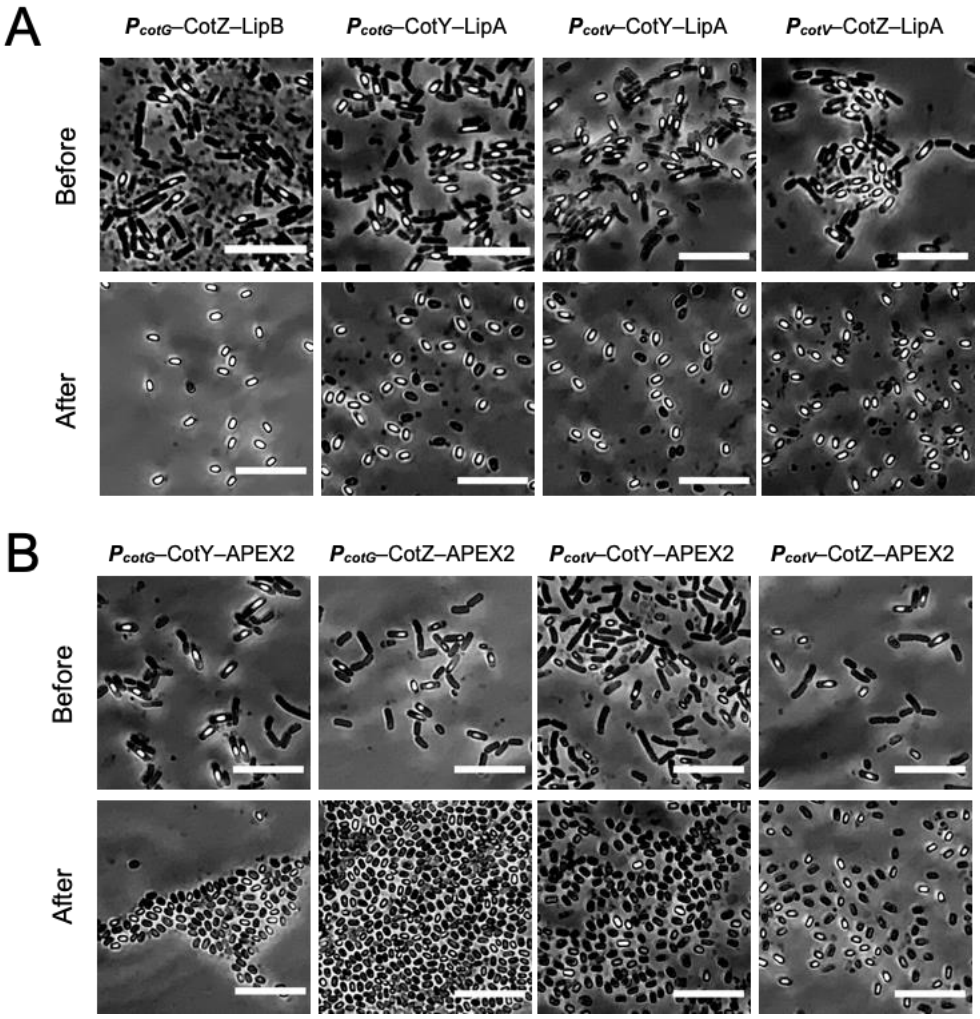

Figure S3.1. Spores of TIED variants. (**A**), Representative phase-contrast microscopic images of spores and cells of TIED-LipB and TIED-LipA variants. (**B**), Representative phase-contrast microscopic images of spores and cells of TIED-APEX2 variants. Top panel: before lysozyme digestion. Bottom panel: after lysozyme digestion.

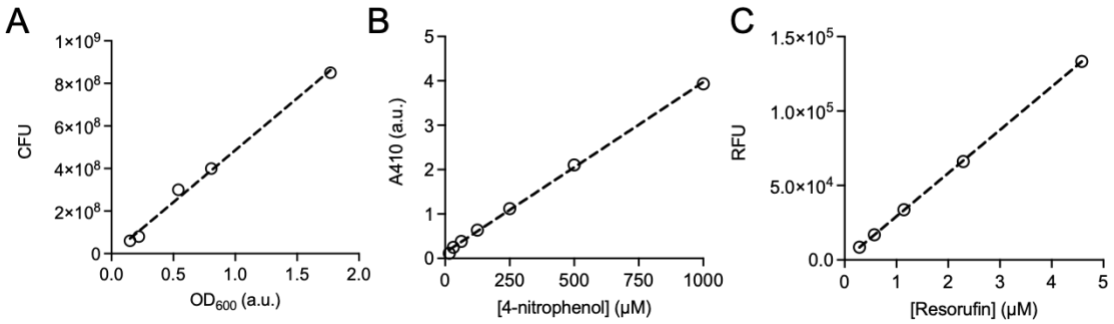

Figure S3.2. Calibration curves. (**A**), OD_{600}–CFU standard calibration curve. (**B**), Absorbance at 410 nm as a function of *p*-nitrophenol concentration. (**C**), Relative fluorescence emission unit ($\lambda_{ex}/\lambda_{em}$ = 530/590 nm) as a function of sodium resorufin concentration.

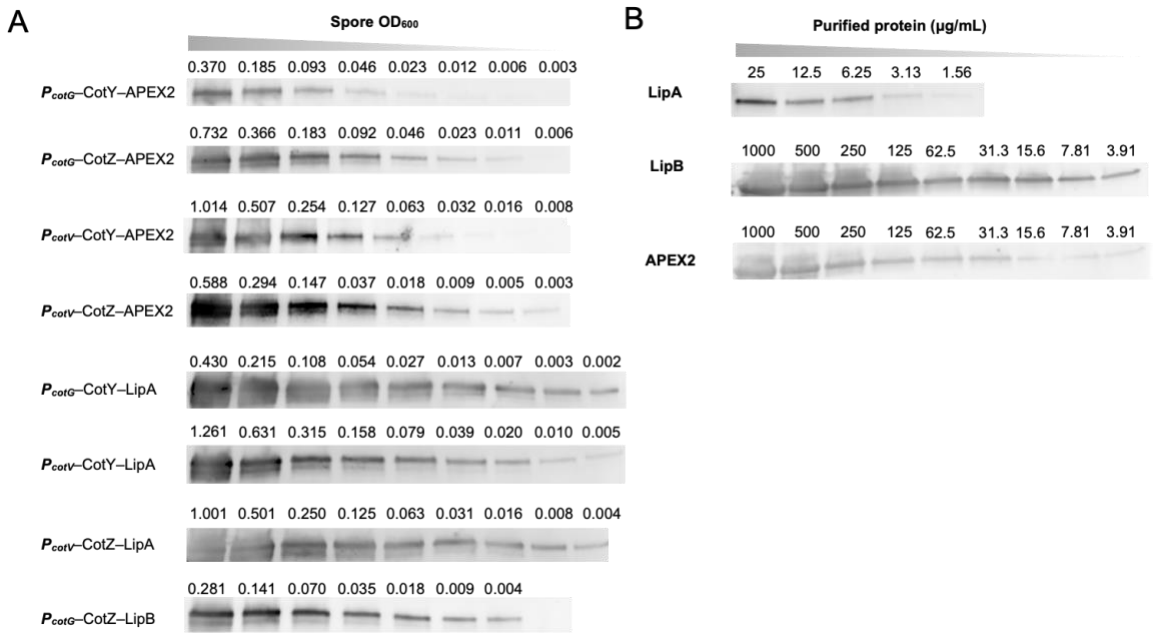

Figure S3.3. Western blot analysis. (**A**), Western blot images of lysates prepared from spores of TIED variants with the indicated OD_{600}. Bands correspond to the monomers of the respective fusion protein. (**B**), Western blot images of solutions of purified enzymes (PBS) with the indicated concentrations. Bands correspond to the size of the respective enzyme.

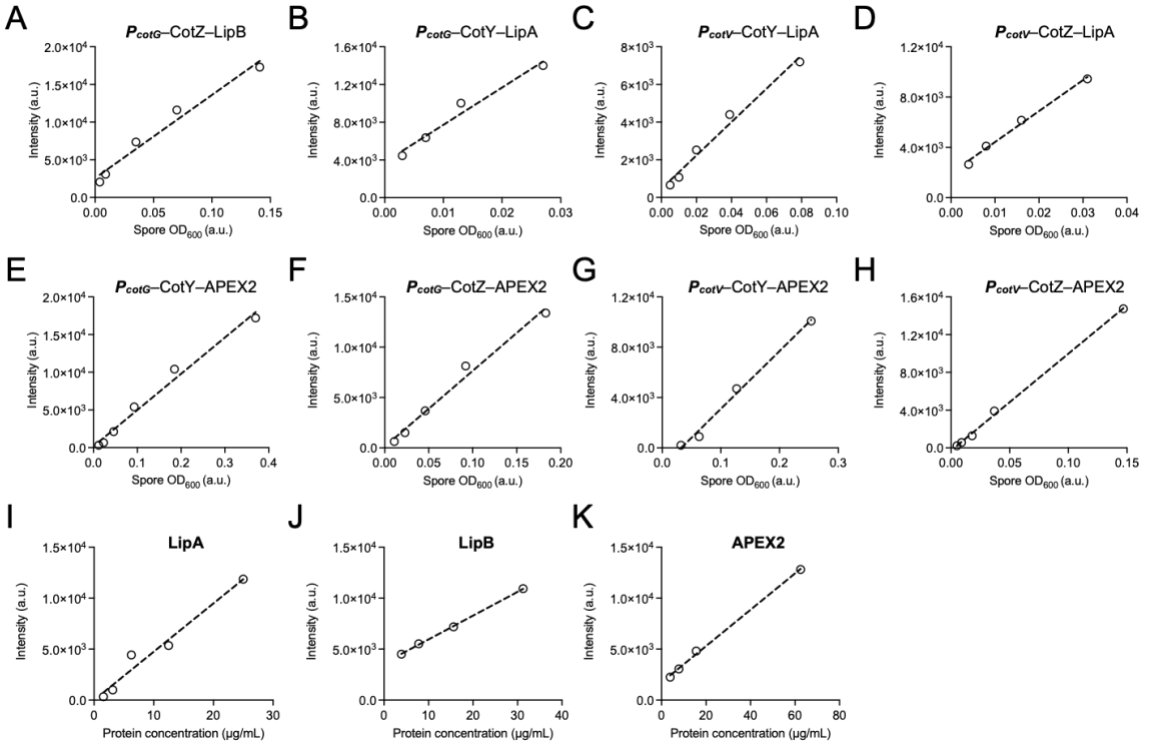

Figure S3.4. Quantitative western blot analysis. (**A-H**), Quantified band intensities of spore lysates as a function of spore OD_{600}. (**I-K**), Quantified band intensities of purified free enzymes as a function of their concentration. Bands corresponding to the fusion proteins (Extended Data Fig. 4) were quantified with Image J and fitted with linear regression (dotted lines).

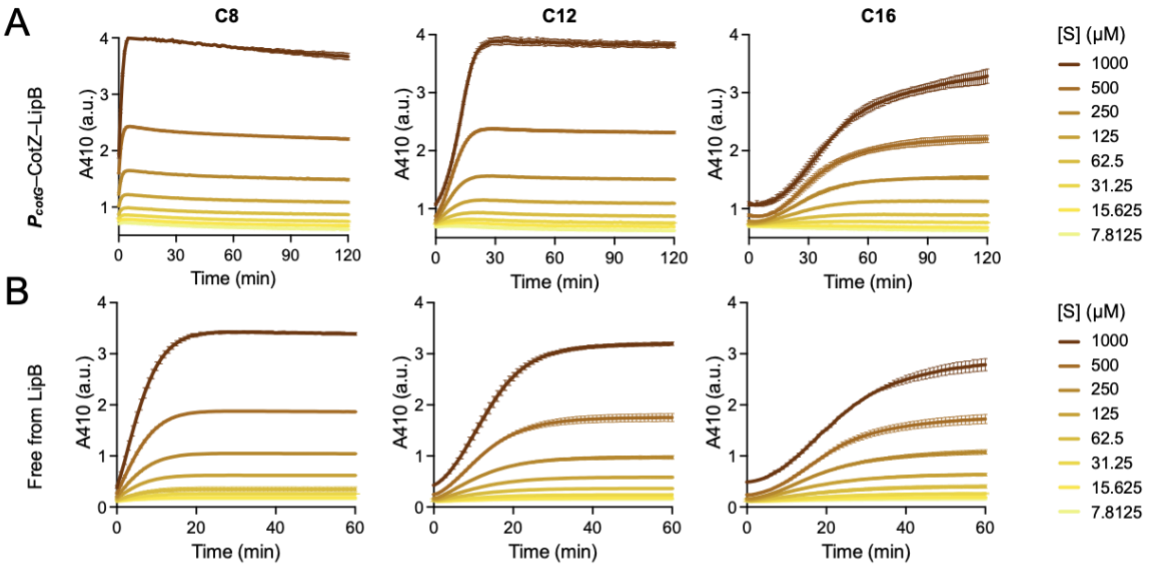

C

Entry	Loading (enzyme/spore)	S	V_{max} (μM/min)	K_m (μM)
P_{cotG} CotZ–LipB	1.75×10^7	C8	379±47.1	1370±259
		C12	80.6±5.76	1120±129
		C16	25.2±41.9	1090±294
Free form LipB	N/A	C8	152±17.0	1390±234
		C12	91.5±19.4	1900±559
		C16	30.9±3.00	599±114

Figure S3.5. Kinetics study of TIED-LipB and free-form LipB. (**A**), TIED-LipB (combination of P_{cotG} promoter and CotZ fusion partner, spore OD_{600} of 0.5) catalyzed conversion of C8, C12, and C16 over time. The absorbance of the reaction product, *p*-nitrophenol, at 410 nm was monitored on a microplate reader (n = 3 biological replicates). (**B**), Free form LipB (1 μg mL^{-1}) catalyzed conversion of C8, C12, and C16 over time (n = 3 biological replicates). (**C**), The maximum rate of reaction (V_{max}) and the Michaelis Menten constant (K_m) of the reactions catalyzed by TIED-LipB and free form LipB. The constants were determined by fitting the rates of reaction at various substrate concentrations with the Michaelis Menten model.

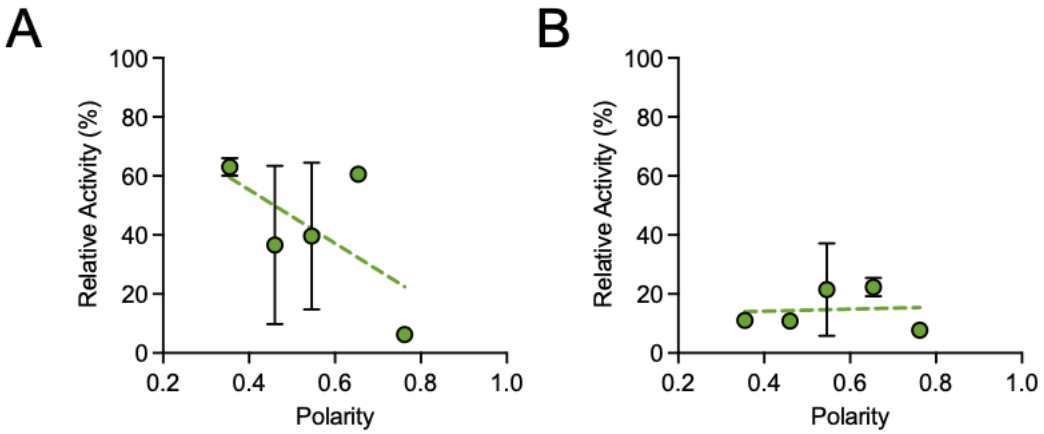

Figure S3.6. Relative activities of free-form lipases in organic solvents. (**A**), Relative activities of free-form LipB in polar organic solvents (methanol, ethanol, 2-propanol, acetone, and acetonitrile) as a function of the normalized empirical solvent polarity (water has a polarity of 1), based on the intramolecular CT absorption of a pyridinium-*N*-phenolate betaine dye.[26] The dotted line indicates fitting with linear regression (n = 3 biological replicates). (**B**), Relative activities of free-form LipA in polar organic solvents (methanol, ethanol, 2-propanol, acetone, and acetonitrile) as a function of solvent polarity. The dotted line indicates fitting with linear regression (n = 3 biological replicates).

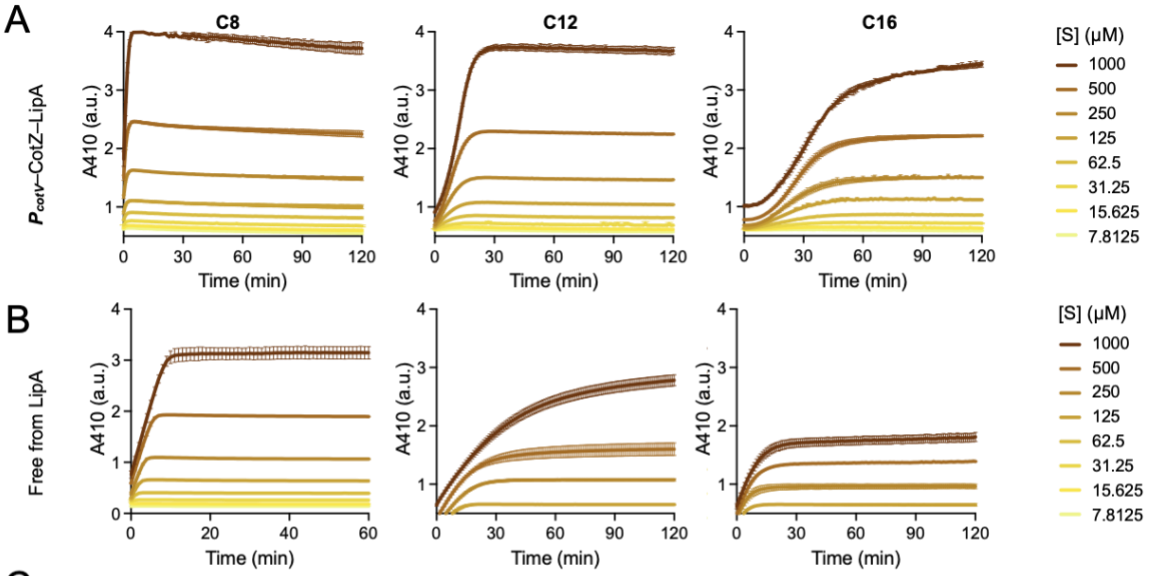

C

Entry	Loading (enzyme/spore)	S	V_{max} (μM/min)	K_m (μM)
P_{cotV} CotZ–LipA	2.93×10^7	C8	511±90.4	1490±392
		C12	129±0.860	1890±178
		C16	30.0±3.57	926±188
Free form LipA	N/A	C8	84.1±17.0	163±35.5
		C12	16.2±1.34	86.1±25.4
		C16	26.4±3.02	69.6±19.1

Figure S3.7. Kinetics study of TIED-LipA and free-form LipA. (**A**), TIED-LipA (combination of P_{cotV} promoter and CotZ fusion partner, spore OD_{600} of 0.5) catalyzed conversion of C8, C12, and C16 over time. The absorbance of the reaction product, *p*-nitrophenol, at 410 nm was monitored on a microplate reader (n = 3 biological replicates). (**B**), Free-form LipA (1 μg mL^{-1}) catalyzed conversion of C8, C12, and C16 over time (n = 3 biological replicates). (**C**), The maximum rate of reaction (V_{max}) and the Michaelis Menten constant (K_m) of the reactions catalyzed by TIED-LipA and free-form LipA. The constants were determined by fitting the rates of reaction at various substrate concentrations with the Michaelis Menten model.

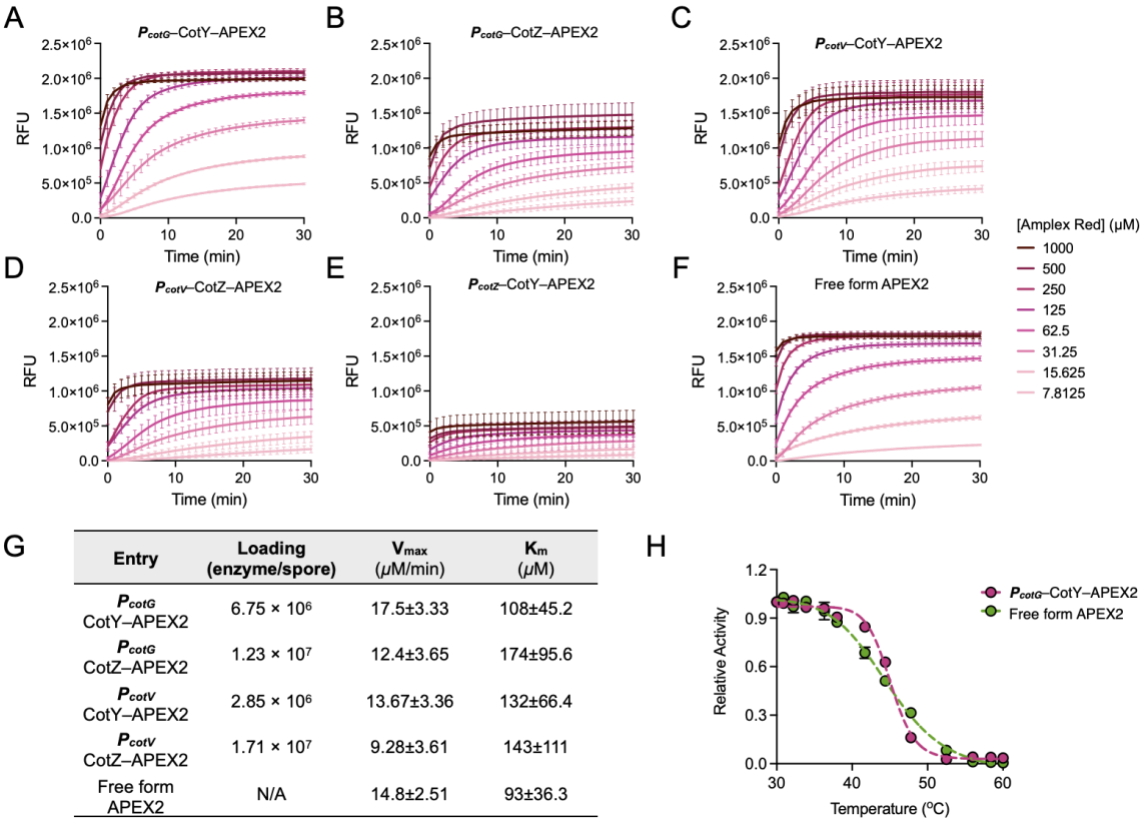

Entry	Loading (enzyme/spore)	V_{max} (μM/min)	K_m (μM)
P_{cotG} CotY–APEX2	6.75 × 10^6	17.5±3.33	108±45.2
P_{cotG} CotZ–APEX2	1.23 × 10^7	12.4±3.65	174±95.6
P_{cotV} CotY–APEX2	2.85 × 10^6	13.67±3.36	132±66.4
P_{cotV} CotZ–APEX2	1.71 × 10^7	9.28±3.61	143±111
Free form APEX2	N/A	14.8±2.51	93±36.3

Figure S3.8. Kinetics and resistance analysis of TIED-APEX2 and free-form APEX2. (**A**), Conversion of Amplex Red to resorufin over time by TIED-APEX2 with the combination of P_{cotG} promoter and CotY fusion partner. (**B**), Conversion of Amplex Red to resorufin over time by TIED-APEX2 with the combination of P_{cotG} promoter and CotZ fusion partner. (**C**), Conversion of Amplex Red to resorufin over time by TIED-APEX2 with the combination of P_{cotV} promoter and CotY fusion partner. (**D**), Conversion of Amplex Red to resorufin over time by TIED-APEX2 with the combination of P_{cotV} promoter and CotZ fusion partner. (**E**), Conversion of Amplex Red to resorufin over time by TIED-APEX2 with the combination of P_{cotZ} promoter and CotY fusion partner. (**F**), Conversion of Amplex Red to resorufin over time by free-form APEX2 (1 μg mL^{-1}). TIED-APEX2 with spore OD_{600} of 0.1 was used for each reaction. (**G**), The maximum rate of reaction (V_{max}) and the Michaelis Menten constant (K_m) of the reactions catalyzed by TIED-APEX2 and free-form APEX2. The constants were determined by fitting the rates of reaction at various substrate concentrations with the Michaelis Menten model. (**H**), Relative activities of TIED-APEX2 (combination of PCotG and CotY fusion partner, OD600 of 0.5) and the free-form APEX2 (100 μg mL−1) for conversion of Amplex Red (125 μM) from 30 to 60 °C, normalized to their respective activities at 30 °C (n = 3 biological replicates).

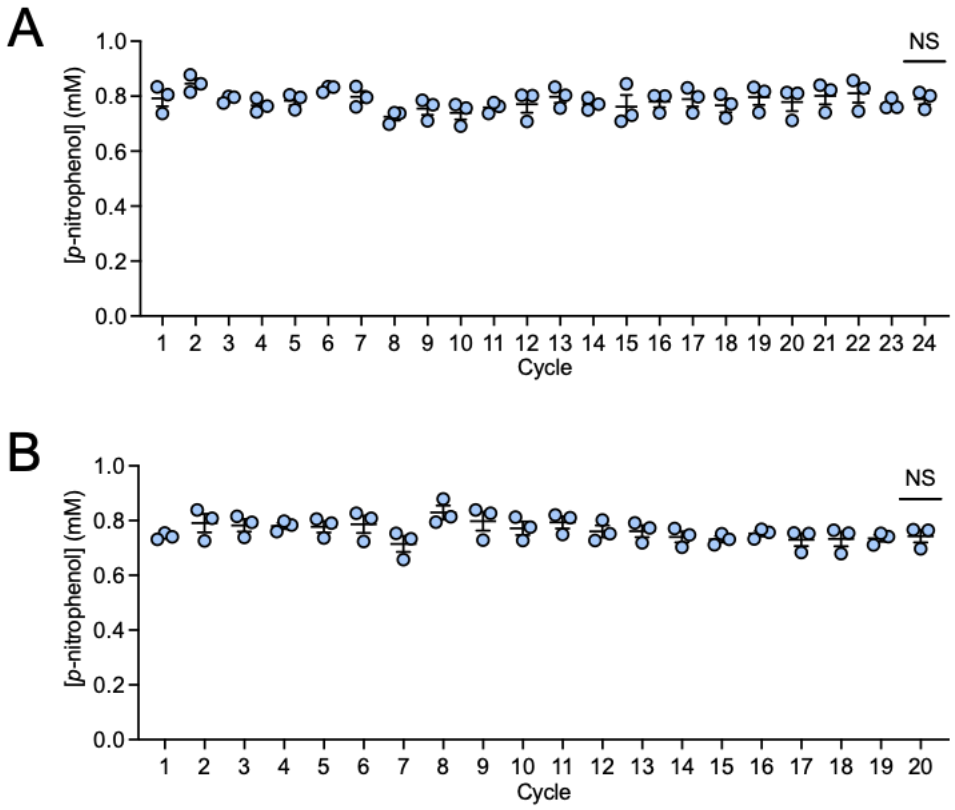

Figure S3.9. Recycling of TIED-LipA. **(A)**, Recycling TIED-LipA (combination of P_{cotV} promoter and CotZ fusion partner, spore OD_{600} of 1.0) for conversion of C8 (0.8 mM) in Tris-HCl (50 mM, pH 8.0). **(B)**, Recycling TIED-LipA (combination of P_{cotV} promoter and CotZ fusion partner, spore OD_{600} of 1.0) for conversion of C12 (0.8 mM) in Tris-HCl. *P* values were determined by two-tail t-tests against the pristine activity of TIED-enzymes (1st cycle). $*P < 0.05$, $**P < 10^{-2}$, $***P < 10^{-3}$, $****P < 10^{-4}$.

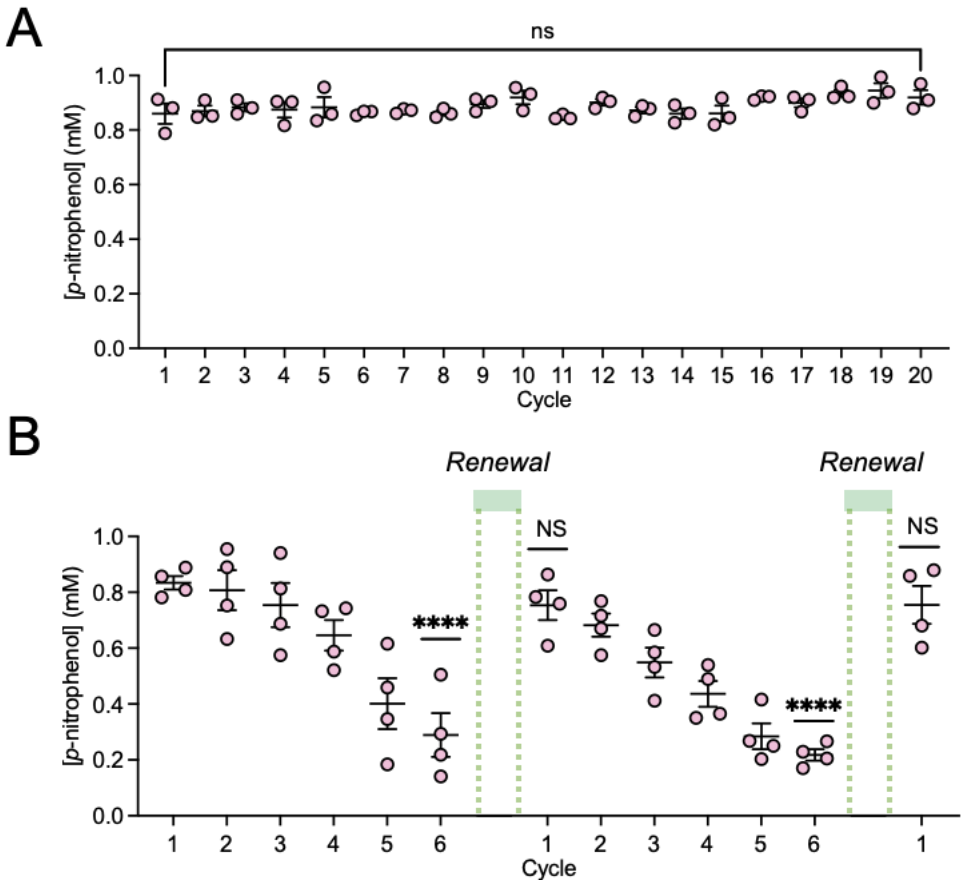

Figure S3.10. Recycling and renewal of TIED-LipB. (**A**), Recycling of TIED-LipB (combination of PcotG promoter and CotZ fusion partner, spore OD600 of 1.0) for conversion of C8 (1.0 mM) in Tris-HCl. (**B**), Recycling and renewal of TIED-LipB (combination of PcotG promoter and CotZ fusion partner, spore OD600 of 1.0) for conversion of C16 (0.8 mM) in Tris-HCl. *P* values were determined by two-tail t-tests against the pristine activity of TIED-enzymes (1st cycle). $*P < 0.05$, $**P < 10^{-2}$, $***P < 10^{-3}$, $****P < 10^{-4}$.

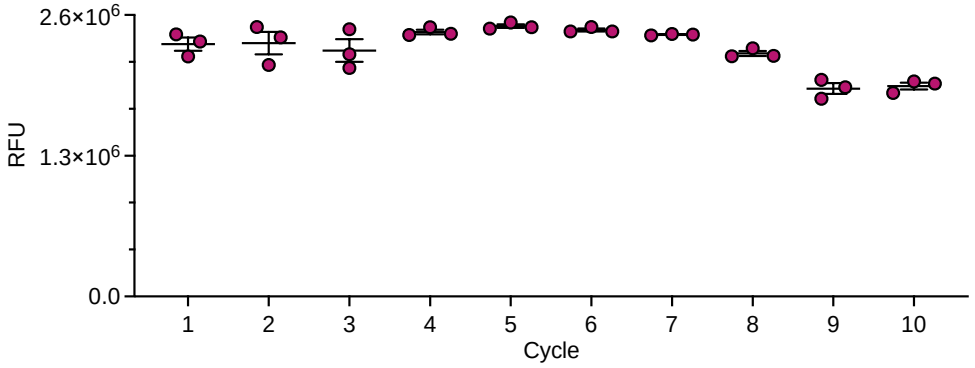

Figure S3.11. Recycling of TIED-APEX2 (combination of PcotG promoter and CotY fusion partner, spore OD600 of 1.0) for conversion of Amplex Red (0.125 mM) in PBS (pH 7.2). *P* values were determined by two-tail t-tests against the pristine activity of TIED-enzymes (1st cycle). $*P < 0.05$, $**P < 10-2$, $***P < 10-3$, $****P < 10-4$.

3.6 Acknowledgements

We thank Professors David Tirrell and Jennifer Prescher for their helpful comments. This work was supported by Defense Advanced Research Projects Agency Engineered Living Materials Agreement HR0011-17-2-0037, by the Institute for Collaborative Biotechnologies through cooperative agreement W911NF-19-2-0026 from the U.S. Army Research Office, and by the start-up funds (S. S.) from the University of California, Irvine. The content of the information does not necessarily reflect the position or the policy of the Government, and no official endorsement should be inferred.

3.7 References

1 Hauer, B. Embracing nature's catalysts: A viewpoint on the future of biocatalysis. *ACS Catalysis* **10**, 8418-8427 (2020).

2 Bell, E. L. *et al.* Biocatalysis. *Nature Reviews Methods Primers* **1**, 1-21 (2021).

3 Winkler, C. K., Schrittwieser, J. H. & Kroutil, W. Power of biocatalysis for organic synthesis. *ACS Central Science* **7**, 55-71 (2021).

4 Yi, D. *et al.* Recent trends in biocatalysis. *Chemical Society Reviews* **50**, 8003-8049 (2021).

5 Mazurenko, S., Prokop, Z. & Damborsky, J. Machine learning in enzyme engineering. *ACS Catalysis* **10**, 1210-1223 (2019).

6 Arnold, F. H. Directed evolution: bringing new chemistry to life. *Angewandte Chemie International Edition* **57**, 4143-4148 (2018).

7 Qu, G., Li, A., Acevedo-Rocha, C. G., Sun, Z. & Reetz, M. T. The crucial role of methodology development in directed evolution of selective enzymes. *Angewandte Chemie International Edition* **59**, 13204-13231 (2020).

8 Yang, K. K., Wu, Z. & Arnold, F. H. Machine-learning-guided directed evolution for protein engineering. *Nature Methods* **16**, 687-694 (2019).

9 Sheldon, R. A. & Woodley, J. M. Role of biocatalysis in sustainable chemistry. *Chemical Reviews* **118**, 801-838 (2018).

10 Sheldon, R. A., Basso, A. & Brady, D. New frontiers in enzyme immobilisation: robust biocatalysts for a circular bio-based economy. *Chemical Society Reviews* **50**, 5850-5862 (2021).

11 Garcia-Galan, C., Berenguer-Murcia, Á., Fernandez-Lafuente, R. & Rodrigues, R. C. Potential of different enzyme immobilization strategies to improve enzyme performance. *Advanced Synthesis & Catalysis* **353**, 2885-2904 (2011).

12 Bartels, J., López Castellanos, S. n., Radeck, J. & Mascher, T. Sporobeads: The utilization of the Bacillus subtilis endospore crust as a protein display platform. *ACS Synthetic Biology* **7**, 452-461 (2018).

13 Chen, L., Holmes, M., Schaefer, E., Mulchandani, A. & Ge, X. Highly active spore biocatalyst by self-assembly of co-expressed anchoring scaffoldin and multimeric enzyme. *Biotechnology and Bioengineering* **115**, 557-564 (2018).

14 Wang, F. *et al.* Bacillus subtilis spore surface display of haloalkane dehalogenase DhaA. *Current Microbiology* **76**, 1161-1167 (2019).

15 Gashtasbi, F., Ahmadian, G. & Noghabi, K. A. New insights into the effectiveness of alpha-amylase enzyme presentation on the Bacillus subtilis spore surface by adsorption and covalent immobilization. *Enzyme and Microbial Technology* **64**, 17-23 (2014).

16 Kim, J. Surface display of lipolytic enzyme, Lipase A and Lipase B of Bacillus subtilis on the Bacillus subtilis spore. *Biotechnology and Bioprocess Engineering* **22**, 462-468 (2017).

17 Kwon, S. J., Jung, H.-C. & Pan, J.-G. Transgalactosylation in a water-solvent biphasic reaction system with β-galactosidase displayed on the surfaces of Bacillus subtilis spores. *Applied and Environmental Microbiology* **73**, 2251-2256 (2007).

18 Houde, A., Kademi, A. & Leblanc, D. Lipases and their industrial applications. *Applied Biochemistry and Biotechnology* **118**, 155-170 (2004).

19 Gorman, L. A. S. & Dordick, J. S. Organic solvents strip water off enzymes. *Biotechnology and Bioengineering* **39**, 392-397 (1992).

20 Cui, H. *et al.* Enzyme hydration determines resistance in organic cosolvents. *ACS Catalysis* **10**, 14847-14856 (2020).

21 Laane, C., Boeren, S., Vos, K. & Veeger, C. Rules for optimization of biocatalysis in organic solvents. *Biotechnology and Bioengineering* **30**, 81-87 (1987).

22 Kulschewski, T., Sasso, F., Secundo, F., Lotti, M. & Pleiss, J. Molecular mechanism of deactivation of C. antarctica lipase B by methanol. *Journal of Biotechnology* **168**, 462-469 (2013).

23 Lotti, M., Pleiss, J., Valero, F. & Ferrer, P. Effects of methanol on lipases: molecular, kinetic and process issues in the production of biodiesel. *Biotechnology Journal* **10**, 22-30 (2015).

24 Yang, K. S., Sohn, J.-H. & Kim, H. K. Catalytic properties of a lipase from Photobacterium lipolyticum for biodiesel production containing a high methanol concentration. *Journal of Bioscience and Bioengineering* **107**, 599-604 (2009).

25 Korman, T. P. *et al.* Dieselzymes: development of a stable and methanol tolerant lipase for biodiesel production by directed evolution. *Biotechnology for Biofuels* **6**, 1-13 (2013).

26 Reichardt, C. & Welton, T. *Solvents and Solvent Effects in Organic Chemistry*. (John Wiley & Sons, 2011).

27 Zhang, X., Cunningham, M. M. & Walker, R. A. Solvent polarity at polar solid surfaces: The role of solvent structure. *The Journal of Physical Chemistry B* **107**, 3183-3195 (2003).

28 Singappuli-Arachchige, D., Manzano, J. S., Sherman, L. M. & Slowing, I. I. Polarity control at interfaces: quantifying pseudo-solvent effects in nano-confined systems. *ChemPhysChem* **17**, 2982-2986 (2016).

29 Li, Y. *et al.* Solvent effects on heterogeneous catalysis in the selective hydrogenation of cinnamaldehyde over a conventional Pd/C catalyst. *Catalysis Science & Technology* **8**, 3580-3589 (2018).

30 Le, Q. A. T., Joo, J. C., Yoo, Y. J. & Kim, Y. H. Development of thermostable Candida antarctica lipase B through novel in silico design of disulfide bridge. *Biotechnology and Bioengineering* **109**, 867-876 (2012).

31 Han, Z.-l., Han, S.-y., Zheng, S.-p. & Lin, Y. Enhancing thermostability of a Rhizomucor miehei lipase by engineering a disulfide bond and displaying on the yeast cell surface. *Applied Microbiology and Biotechnology* **85**, 117-126 (2009).

32 Xie, Y. *et al.* Enhanced enzyme kinetic stability by increasing rigidity within the active site. *Journal of Biological Chemistry* **289**, 7994-8006 (2014).

33 Eggert, T., van Pouderoyen, G., Dijkstra, B. W. & Jaeger, K.-E. Lipolytic enzymes LipA and LipB from Bacillus subtilis differ in regulation of gene expression, biochemical properties, and three-dimensional structure. *FEBS letters* **502**, 89-92 (2001).

34 Lam, S. S. *et al.* Directed evolution of APEX2 for electron microscopy and proximity labeling. *Nature Methods* **12**, 51-54 (2015).

35 Liu, J. *et al.* Genetically targeted chemical assembly of functional materials in living cells, tissues, and animals. *Science* **367**, 1372-1376 (2020).

36 Liu, H. *et al.* Investigating interactions of the Bacillus subtilis spore coat proteins CotY and CotZ using single molecule force spectroscopy. *Journal of Structural Biology* **192**, 14-20 (2015).

37 Krajčíková, D., Forgáč, V., Szabo, A. & Barák, I. Exploring the interaction network of the Bacillus subtilis outer coat and crust proteins. *Microbiological Research* **204**, 72-80 (2017).

38 Kozlowski, M. T., Silverman, B. R., Johnstone, C. P. & Tirrell, D. A. Genetically Programmable Microbial Assembly. *ACS Synthetic Biology* **10**, 1351-1359 (2021).

39 Castillo-Hair, S. M., Fujita, M., Igoshin, O. A. & Tabor, J. J. An engineered B. subtilis inducible promoter system with over 10 000-fold dynamic range. *ACS Synthetic Biology* **8**, 1673-1678 (2019).

40 Hinc, K., Iwanicki, A. & Obuchowski, M. New stable anchor protein and peptide linker suitable for successful spore surface display in B. subtilis. *Microbial Cell Factories* **12**, 1-8 (2013).

41 Engler, C., Gruetzner, R., Kandzia, R. & Marillonnet, S. Golden gate shuffling: a one-pot DNA shuffling method based on type IIs restriction enzymes. *PloS One* **4**, e5553 (2009).

42 Popp, P. F., Dotzler, M., Radeck, J., Bartels, J. & Mascher, T. The Bacillus BioBrick Box 2.0: expanding the genetic toolbox for the standardized work with Bacillus subtilis. *Scientific Reports* **7**, 1-13 (2017).

43 Radeck, J. *et al.* The Bacillus BioBrick Box: generation and evaluation of essential genetic building blocks for standardized work with Bacillus subtilis. *Journal of Biological Engineering* **7**, 1-17 (2013).

44 Bennallack, P. R., Burt, S. R., Heder, M. J., Robison, R. A. & Griffitts, J. S. Characterization of a novel plasmid-borne thiopeptide gene cluster in Staphylococcus epidermidis strain 115. *Journal of Bacteriology* **196**, 4344-4350 (2014).

45 Kumar, A. *et al.* A broad temperature active lipase purified from a psychrotrophic bacterium of sikkim himalaya with potential application in detergent formulation. *Frontiers in Bioengineering and Biotechnology*, 642 (2020).

46 Isticato, R. *et al.* Flexibility of the prograamme of spore coat formation in Bacillus subtilis: bypass of CotE requirement by over-production of CotH. *Plos One* **8**, e74949 (2013).

47 Schindelin, J. *et al.* Fiji: an open-source platform for biological-image analysis. *Nature Methods* **9**, 676-682 (2012).

Chapter 4

LEAK-FREE CELLULAR COMPOSITES FOR PRODUCTION OF RECOMBINANT PROTEINS

Abstract

The incorporation of living cells into materials promises both significant challenges and new possibilities. Although recent years have seen important advances in this field, there is still much to be learned about engineering interfaces between cells and materials. Here we present a new class of living composite materials, based on poly(*N*-hydroxymethylacrylamide) (PNHMAA), in which the spore-forming bacterium *Bacillus subtilis* is effectively crosslinked into the surrounding polymeric scaffold. After dehydration and subsequent re-swelling in nutrient-rich media, embedded cells and spores remain metabolically active and are capable of heterologous protein production and secretion. Strikingly, the leak-free scaffold allows protein production while preventing escape of embedded cells, suggesting utility in a broad range of applications.

4.1 Introduction

Biological materials such as wood, bone, and skin are composites of cells, polymeric scaffolds, and effector biomolecules. The cellular components of these materials are responsible for critical functions, including molecular synthesis, self-regulation, and response to environmental signals. Recent advances in synthetic biology have expanded our ability to engineer cells for specific functional outcomes that may transcend those of natural systems.[1,2] Inspired by the possibility of engineering 'living' materials, several strategies to incorporate cells into smart 3-dimensional materials have been explored.[3-10] One of the remaining challenges in this field is developing methods to achieve secure cellular confinement, such that cells do not escape into the environment, while permitting the functional biomacromolecules produced to readily diffuse from materials and be collected for use. A recent strategy using a hydrogel with a core-shell architecture was shown to achieve effective biocontainment; however, the crosslinked network was designed to be permeable to nutrients, but not to biomacromolecules, including proteins.[11] Finding molecular design principles for scaffolds that provide secure confinement of cells while allowing permeation of recombinant proteins will open new possibilities for the application of engineered living materials.

This work describes a novel synthetic platform to generate living composite materials (LCM) through light-triggered polymerizations of monomers mixed with the spore-forming microbe *B. subtilis*. The method results in successful immobilization of viable *B. subtilis* cells and spores in polymeric scaffolds. The resulting LCMs can be dried to yield portable materials. When re-immersed in aqueous media, entrapped cells and spores in previously-dried LCMs exhibit metabolic activity, including synthesis and secretion of recombinant proteins. Notably, one of the scaffolds developed in this study, based on photopolymerization of *N*-(hydroxymethyl)acrylamide (NHMAA), achieves effective cellular confinement, showing no evidence of cellular leakage over a period of 72 h.

4.2 Results and Discussion

We evaluated covalently crosslinked hydrogel scaffolds prepared by photopolymerization of two water-soluble acrylamide monomers: NHMAA and *N*-isopropylacrylamide (NIPAM). Notably, the reactive side chain of NHMAA has prompted its use as a crosslinking reagent in textiles, protective coatings, and adhesives.[12-14] The pre-polymerization mixture included xanthan (1% w/v) to control cellular sedimentation, *N*,*N*'-methylenebisacrylamide (26 mM) as crosslinker, lithium phenyl-2,4,6-trimethylbenzoylphosphinate (3 mM) as initiator, and acrylamide monomer (1 M) dissolved in phosphate buffered saline (pH 7). *B. subtilis* cells were harvested from overnight cultures, washed, resuspended in PBS, and added to the pre-polymerization mixture. Colony-forming unit (CFU) assays (**Figure S4.1**) were used to determine and control the number of viable cells added to each pre-polymerization mixture. Upon UV irradiation (25 °C, 10 mW/cm^2 at 365 nm and 16 mW/cm^2 at 405 nm, 300 s), viscoelastic pre-polymerization mixtures became self-standing hydrogels (**Figures 4.1A**, **4.1B**). PNHMAA hydrogels prepared in this way were transparent (**Figure 4.1B**, upper image) whereas the PNIPAM hydrogels were turbid (**Figure 4.1B**, lower image), presumably because the high concentration and high molecular weight of the polymer depress the lower critical solution temperature (LCST) of the sample.[15] Confocal laser scanning microscopy was performed on LCMs prepared from PNHMAA and PNIPAM scaffolds (designated **PNHMAA$_{Cell}$** and **PNIPAM$_{Cell}$**, respectively). Samples were stained with the BacLight LIVE/DEAD^{TM} reagent, a mixture of SYTO-9 and propidium iodide. In both samples, the majority of cells showed emission from the SYTO-9 dye (**Figures 4.1C**, **4.1F**) and well-defined cell shapes, suggesting high cell viability after photopolymerization. In scanning electron microscopy (SEM) analysis, **PNHMAA$_{Cell}$** exhibited characteristics of ductile fracture (**Figure 4.1D**), with cells apparently enmeshed in the polymer matrix (**Figure 4.1E**). In contrast, **PNIPAM$_{Cell}$** showed features of brittle fracture (**Figure 4.1G**), and the encapsulated cells showed no signs of interaction with the scaffold (**Figure 4.1H**).

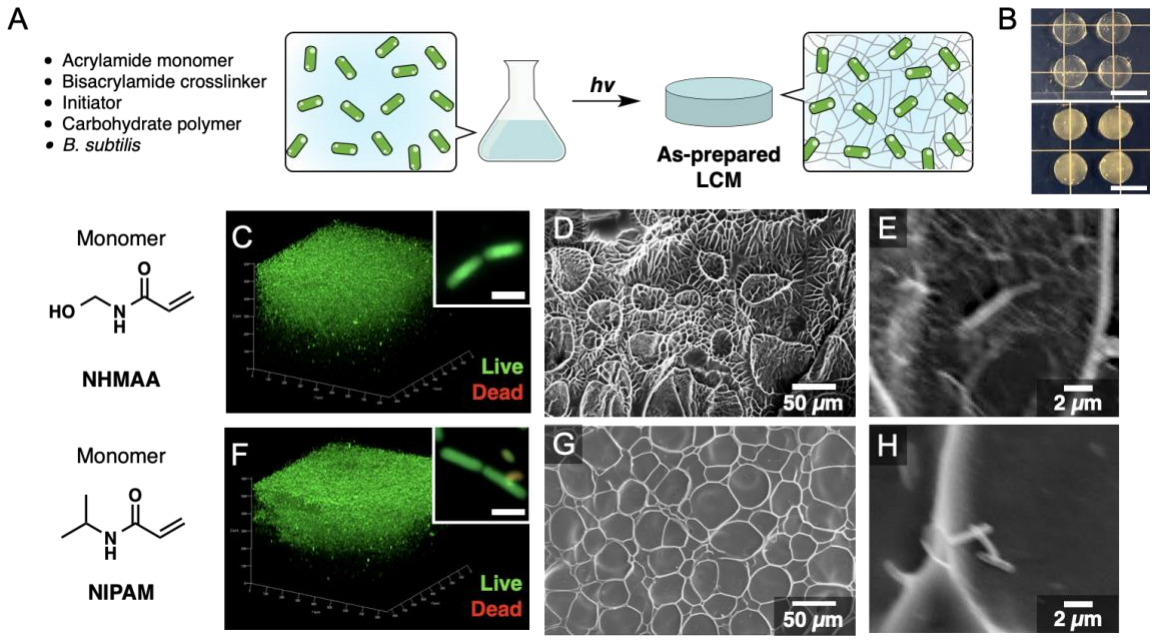

Figure 4.1. Characterization of pristine LCMs encasing *B. subtilis* cells. (**A**), Schematic illustration of the light-initiated radical polymerization process. (**B**), Photographic images of the composite materials immediately after photo-polymerization: **PNHMAA$_{Cell}$** (upper) and **PNIPAM$_{Cell}$** (lower). Scale bars = 10 mm (**C**), Representative confocal laser scanning microscopy image stacks (inset: high-resolution, scale bar: 2 μm) of pristine **PNHMAA$_{Cell}$** after staining with LIVE/DEAD™ reagent. The average percentage of green pixels in low-resolution image stacks is 90% for NHMAA (n=3). (**D, E**), Representative scanning electron microscopy (SEM) images of **PNHMAA$_{Cell}$**. (**F**), Representative confocal image stacks (inset: high-resolution) of pristine **PNIPAM$_{Cell}$**. The average percentage of green pixels is 94% (n=3). (**G, H**), Representative scanning electron microscopy (SEM) images of **PNIPAM$_{Cell}$**.

PNHMAA$_{Cell}$ and **PNIPAM$_{Cell}$** samples were desiccated on polytetrafluoroethylene (PTFE) plates. After 36 h of desiccation, the dried materials were immersed in either nutrient-deficient PBS or nutrient-rich LB medium for 12 h at 37 °C (**Figure 4.2A**). In confocal microscopic analysis of samples stained with the LIVE/DEAD™ reagent, re-swollen **PNHMAA$_{Cell}$** samples exhibited lower SYTO-9 emission than pristine samples (**Figures 4.1C**, **4.2B**, and **4.2C**). Image analysis on z-stacks indicated that 64% of the emission signals arose from SYTO-9 in samples re-swollen in LB medium vs 21% after re-swelling in PBS (**Figures 4.2B, 4.2C**). Consistent with this result, high-resolution confocal imaging revealed that most cells in **PNHMAA$_{Cell}$** samples re-swollen in PBS

showed emission only from propidium iodide (**Figure 4.2C,** inset). In contrast, in **PNHMAA$_{Cell}$** samples re-swollen in LB, a characteristic pattern of alternating red and green stains was observed in high-resolution imaging (**Figure 4.2B**, inset). In **PNIPAM$_{Cell}$** samples re-swollen in LB, we observed permeable spores marked by propidium iodide emission and vegetative cells stained with SYTO-9 adjacent to one other (**Figure 4.2E**, inset), capturing different stages in the sporulation – germination life cycle of *B. subtilis*.[16,17] The same material re-swollen in PBS showed irregular cell shapes with patches of SYTO-9 and propidium iodide staining, presumably due to a large amount of cellular debris (**Figure 4.2F**, inset).

To better understand the characteristic patterns observed in confocal imaging analysis, LCMs were prepared from a *B. subtilis* strain lacking Spo0A,[18] an upstream regulator of the spore formation pathway. The corresponding LCMs were designated **PNHMAA$_{Spo0A}$** and **PNIPAM$_{Spo0A}$**. Interestingly, Spo0A knock-out cells in either **PNHMAA$_{Spo0A}$** or **PNIPAM$_{Spo0A}$** re-swollen in LB did not show the red-green alternating pattern (**Figures S4.2B**, **S4.2D**). These results strongly suggest that the characteristic staining pattern is a consequence of spore formation in the PNHMAA network. The relatively high percentage of the Spo0A KO mutant exhibiting SYTO-9 signal, compared to **PNHMAA$_{Cell}$** and **PNIPAM$_{Cell}$**, in the course of the dehydration and re-swelling process may be due to persister-like slow growth.[19] To investigate retention of cells and their cytoplasmic biomacromolecules in PNHMAA scaffolds upon dehydration and re-swelling, we prepared LCMs (**PNHMAA$_{mRFP}$** and **PNIPAM$_{mRFP}$**) with *B. subtilis* cells engineered for cytoplasmic expression of the red fluorescent protein (mRFP). Upon dehydration and re-swelling in either PBS or LB, emission from mRFP in **PNHMAA$_{mRFP}$** remained similar to that observed for the pristine sample (**Figures 4.2D**, **S4.3A**). In contrast, emission from **PNIPAM$_{mRFP}$** was significantly diminished upon re-swelling (**Figures 4.2G**, **S4.3B**). These results, together with the confocal observations of LCMs stained with LIVE/DEAD^{TM} reagent, suggest that the PNHMAA scaffold retains encapsulated cells upon dehydration and re-swelling. In contrast, in all experiments with PNIPAM LCMs re-swollen in LB, we observed cell growth outside the material within 18 h. *B. subtilis* cells

in the PNIPAM scaffold freely form spores upon dehydration, escape from the scaffold as it re-swells, and undergo cell division.

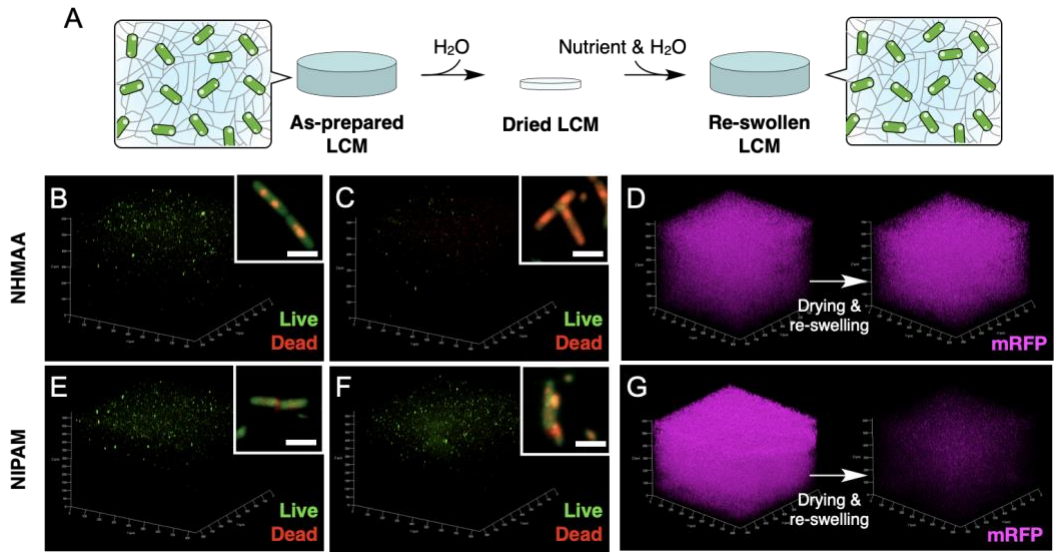

Figure 4.2. Characterization of LCMs re-swollen after dehydration. (**A**), Schematic illustration of the process: pristine LCMs were desiccated on PTFE plate for 36 h and re-immersed in solutions. (**B, C**), Representative confocal laser scanning microscopy image stacks (inset: high-resolution, scale bar = 2 μm) of the re-swollen **PNHMAA$_{Cell}$** in (**B**), LB and (**C**), PBS for 12 h. The LCMs were stained with LIVE/DEAD™ reagent. The average percentages of green pixels in low-resolution image stacks are 63% for **PNHMAA$_{Cell}$** re-swollen in LB and 21% for **PNHMAA$_{Cell}$** re-swollen in PBS (n=3). (**D**), Representative confocal image stacks of **PNHMAA$_{mRFP}$** before (left) and after (right) dehydration and re-swelling in LB. (**E, F**), Representative confocal laser scanning microscopy image stacks (inset: high-resolution, scale bar = 2 μm) of re-swollen **PNIPAM$_{Cell}$** in (**E**), LB and (**F**), PBS for 12 h. The average percentages of green pixels in low-resolution image stacks are 65% for LB-reswollen **PNIPAM$_{Cell}$** and 54% for PBS-reswollen **PNIPAM$_{Cell}$** (n=3). (**G**), Representative confocal image stacks of **PNIPAM$_{mRFP}$** before (left) and after (right) dehydration and re-swelling in LB.

We induced sporulation in *B. subtilis* cell cultures and generated spore-based LCMs designated **PNHMAA$_{Spore}$** and **PNIPAM$_{Spore}$** (**Figure 4.3A**). SEM images (**Figures 4.3B**, **4.3C**) of **PNHMAA$_{Spore}$** and **PNIPAM$_{Spore}$** show characteristics similar to those of **PNHMAA$_{Cell}$** and **PNIPAM$_{Cell}$**, with evidence of polymer chains associated with the spore surface in **PNHMAA$_{Spore}$**. To monitor the fraction of mature spores and vegetative cells

in the matrix, we constructed a double fluorescence strain of *B. subtilis* that expresses both a C-terminal fusion of mWasabi with the spore coat protein CotG (CotG-mWasabi), and mRFP under control of the P_{veg} promoter, which is active during vegetative growth (**Figure 4.3D**). The vegetative cells and fully matured spores of this strain are easily identified by emission of the expected fluorescence signals (**Figure 4.3E-H**). More cells were observed in **PNHMAA$_{Spore}$** samples re-swollen in LB medium (**Figure 4.3J**) than in those re-swollen in PBS (**Figure 4.3K**) or in pristine materials (**Figure 4.3I**), indicating increased germination upon re-swelling in rich medium. In **PNIPAM$_{Spore}$,** cells were detected primarily on the sample surface, where they formed biofilms (**Figures S4.4C, S4.6D**).

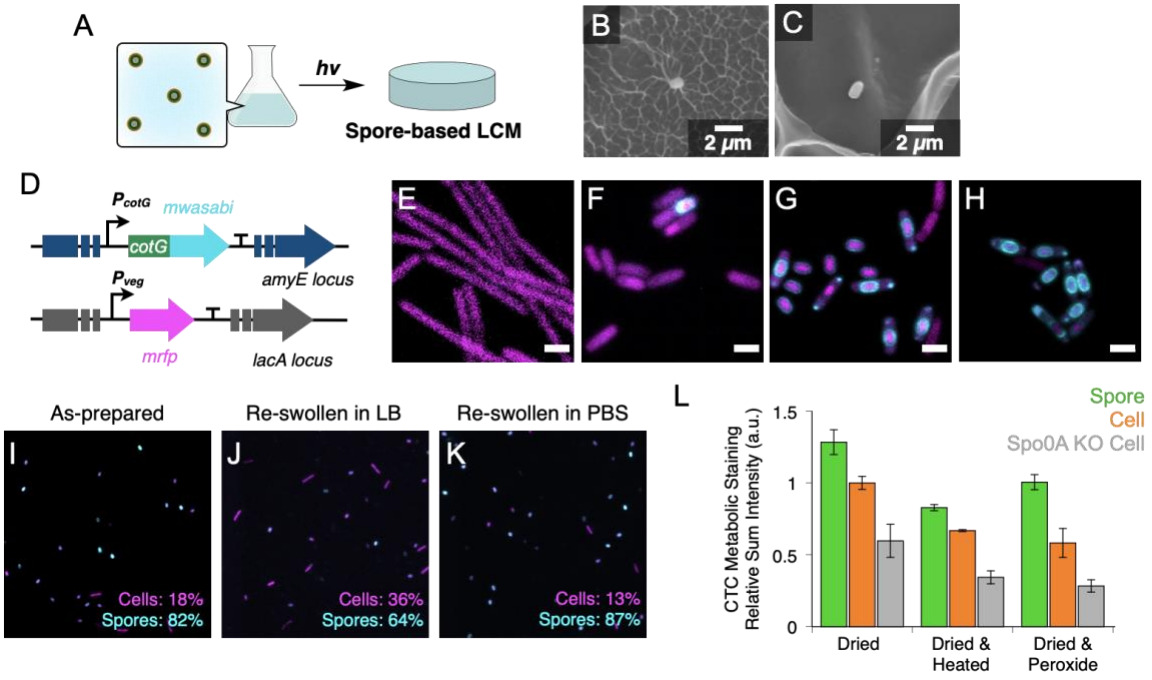

Figure 4.3. Characterization of spore-based LCMs. (**A**), Schematic illustration of the preparation of spore-based LCMs. (**B**, **C**), Representative scanning electron microscopy (SEM) images of pristine (**B**) **PNHMAA$_{Spore}$** and (**C**) **PNIPAM$_{Spore}$** samples. (**D**), Schematic illustration of the genetic construct for the doubly-fluorescent *B. subtilis* strain. (**E-H**), Confocal images of doubly-fluorescent *B. subtilis* cells (**E**), immediately after resuspension in sporulation-inducing SM medium and grown for (**F**), 6 h, (**G**), 16 h, and (**H**), 24 h. Scale bars = 2 μm. (**I–K**), Representative confocal laser scanning microscopy images of **PNHMAA$_{Spore}$** containing spores of the double-fluorescence strain. (**I**), Pristine **PNHMAA$_{Spore}$**, (**J**), **PNHMAA$_{Spore}$** re-swollen in LB after dehydration, and (**K**), **PNHMAA$_{Spore}$** re-swollen in PBS after dehydration. Fractions of spores and cells were calculated from high-resolution images (n > 150). (**L**), Metabolic activities probed by CTC staining of **PNHMAA$_{Spore}$**, **PNHMAA$_{Cell}$**, and **PNHMAA$_{Spo0A}$** after treating the dried LCMs with stressors– heat (80 °C, 10 min) and peroxide (1 M, 25 °C, 30 min) and subsequent rescue by immersing them in LB (12 h). 5-cyano-2,3-ditolyl tetrazolium chloride (CTC) dye was used to probe the respiratory activity in the LCMs. Relative sum fluorescence intensities are collected from confocal microscopy image stacks (n=3) and normalized based on the average intensity of **PNHMAA$_{Cell}$** after dehydration treatment. Data from three samples were used. Error bars represent ± s.e.m.

PNHMAA LCMs were subjected to a variety of stresses, including dehydration, dehydration followed by heat treatment (80 °C, 10 min), and dehydration followed by severe oxidative stress (hydrogen peroxide 1 M, 30 min, 25 °C). Samples were then

allowed to recover for 12 h in LB medium. Metabolic activity was measured using the redox dye 5-cyano-2,3-ditolyl tetrazolium chloride (CTC), which probes respiratory activity in bacterial cells. After exposure to each of these stressors and subsequent recovery, **PNHMAA$_{Spore}$** samples showed the highest metabolic activity, followed by **PNHMAA$_{Cell}$** and **PNHMAA$_{Spo0A}$**. This result confirms the value of sporulation in preserving the functional capacity of living materials under stress (**Figure 4.3L**).[20-22]

To evaluate cellular escape from LCMs, we immersed **PNHMAA$_{Cell}$** and **PNIPAM$_{Cell}$** samples in LB (15 mL, 37 °C) with agitation (250 rpm) and measured the optical density of the medium (OD_{600}) over 72 h (**Figure 4.4A**). Cells in **PNIPAM$_{Cell}$** escaped from the scaffold and proliferated in the surrounding medium within 12 h. On the other hand, cells in **PNHMAA$_{Cell}$** showed no evidence of escape from the composite even after 72 h. Image analysis of the dehydrated and re-swollen **PNHMAA$_{Cell}$** samples further suggest that crosslinked cells do not divide in LB (**Figure S4.5**). In contrast to the cell-based LCMs, agitation of spore-based LCMs in LB resulted in increased OD_{600} over time in both cases (**Figure 4.4B**). Notably, the average time required for cells to emerge and propagate is longer for **PNHMAA$_{Spore}$** than for **PNIPAM$_{Spore}$**, consistent with weaker interaction with the PNIPAM scaffold. We speculate that a few germinated cells from crosslinked spores near the material surface escape and proliferate in LB media.

When **PNHMAA$_{mRFP}$** and **PNIPAM$_{mRFP}$**, which express cytoplasmic mRFP, were dehydrated and re-swollen in LB for 12 h, they showed slightly higher fluorescence emission in comparison with pristine samples and PBS-reswollen LCMs (**Figures S4.7**, **S4.8**). Motivated by this observation, we constructed a plasmid that directs *B. subtilis* cells to express mRFP outfitted with the N-terminal secretion sequence AmyQ[23] so that the fluorescent protein would be exported to the extracellular space (**Figure 4.4C**). Pristine LCMs prepared from cells bearing this plasmid (designated **PNHMAA$_{mRFP_s}$** and **PNIPAM$_{mRFP_s}$**) showed low fluorescence intensities compared to **PNHMAA$_{mRFP}$** or **PNIPAM$_{mRFP}$**, respectively, as AmyQ-tagged mRFP was secreted to the extracellular space and washed away prior to photo-polymerization. Upon re-swelling in LB for 12 h, **PNHMAA$_{mRFP_s}$** and **PNIPAM$_{mRFP_s}$** showed significantly stronger fluorescence

emission than the corresponding pristine or PBS-reswollen materials (**Figures S4.9**, **S4.10**), indicating resumption of mRFP expression and secretion. When **PNHMAA$_{mRFP_s}$** was immersed in LB and shaken for 72 h, the fluorescence associated with the material decreased, consistent with diffusional loss of mRFP. We quantified the amount of mRFP in the media as samples of **PNHMAA$_{mRFP_s}$** and **PNIPAM$_{mRFP_s}$** were shaken for 72 h in LB. For **PNHMAA$_{mRFP_s}$**, the fluorescence intensity gradually increased over 72 h (**Figure 4.4D**); during this time OD_{600} did not increase, indicating good cellular retention. In contrast, **PNIPAM$_{mRFP_s}$** showed increases in both fluorescence and OD_{600}, owing to cellular escape, proliferation and production of protein by free cells (**Figure S4.10**).

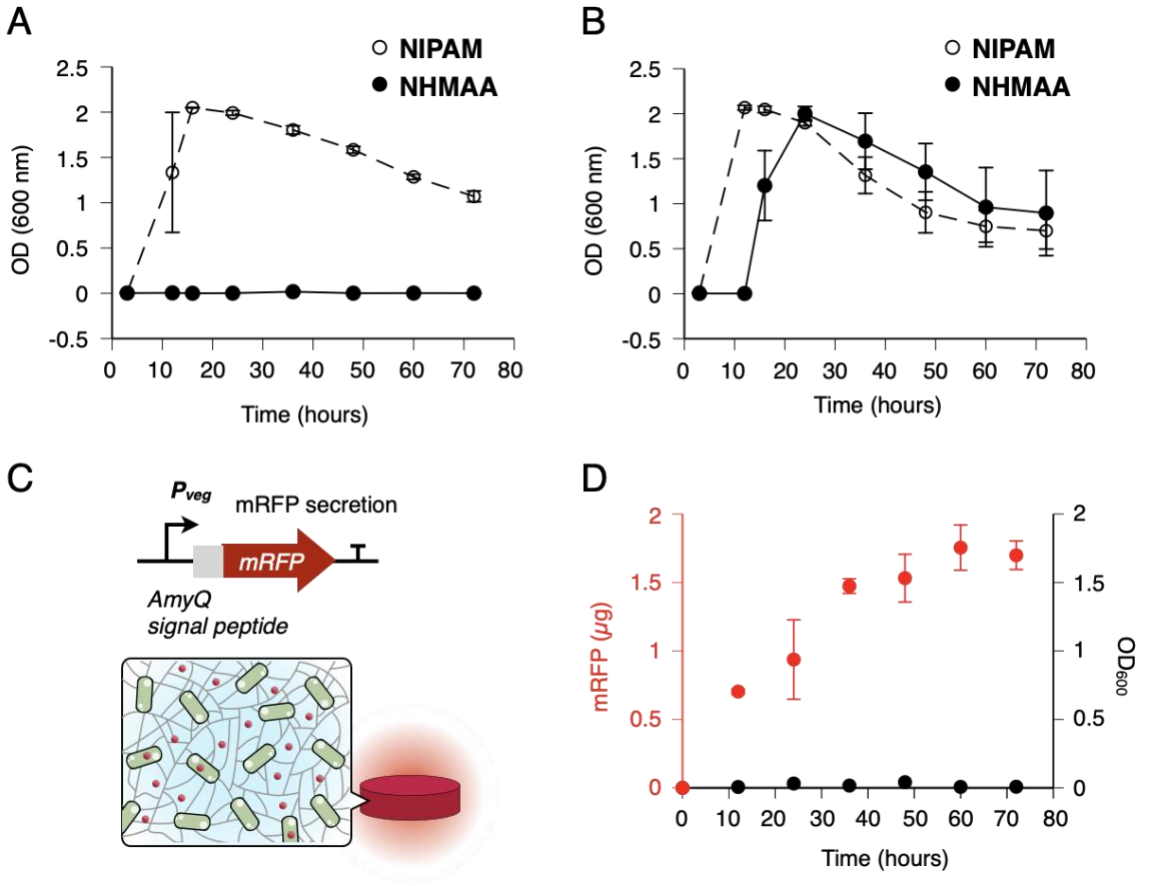

Figure 4.4. Properties of re-swollen LCMs. (**A**), Time trace of optical density at 600 nm of LB media in which dried **PNHMAA**$_{\mathbf{Cell}}$ (filled symbols) or **PNIPAM**$_{\mathbf{Cell}}$ (unfilled symbols) were immersed and shaken (250 rpm, 37 °C, 72 h, n=3). (**B**), Time trace of optical density at 600 nm in LB media in which dried **PNHMAA**$_{\mathbf{Spore}}$ (filled symbols) or **PNIPAM**$_{\mathbf{Spore}}$ (unfilled symbols) were immersed and shaken (250 rpm, 37 °C, 72 h, n=3). (**C**), Schematic illustration of the plasmid construct for expression and secretion of mRFP bearing an AmyQ signal sequence. (**D**), Time trace of optical density at 600 nm and the amount of mRFP in LB media in which dried **PNHMAA**$_{\mathbf{mRFP}}$ samples were immersed and shaken (250 rpm, 37 °C, 72 h). Signals were averaged from 3 measurements. Error bars represent ± s.e.m.

4.3 Conclusions

In summary, we have established a platform for generating LCMs encasing *B. subtilis* cells and spores with good control of 3-dimensional structure. The reactive nature of NHMAA enables effective cross-linking and immobilization of cellular material within the polymer scaffold. *In situ* photo-polymerization of NHMAA yields leak-free scaffolds that confine cells and retain the capacity to produce functional proteins, even after dehydration and subsequent re-swelling. The methods described here provide a promising route to functional living materials engineered for biomedical and other applications.

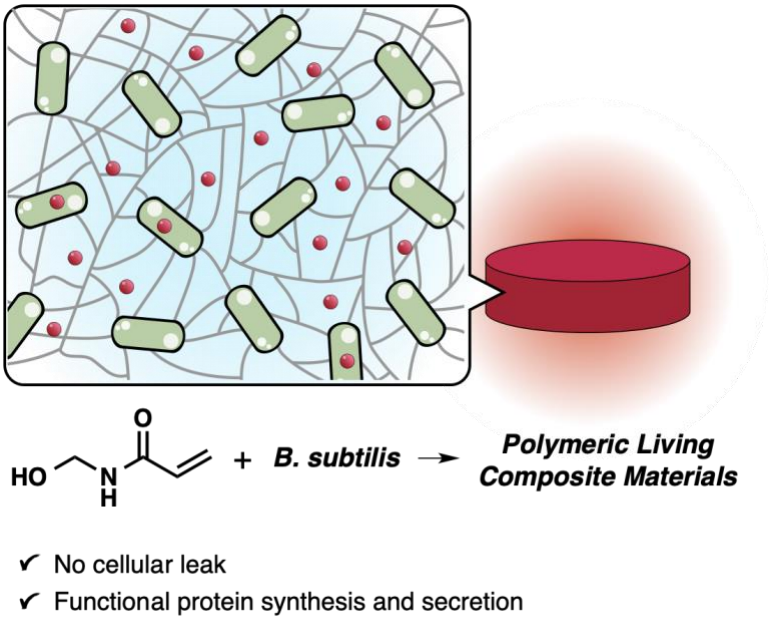

Figure 4.5. Illustration of polymeric living composite materials encasing *B. subtilis*

4.4 Materials and Methods

Bacterial growth conditions. *B. subtilis* strains PY79 and *spo0A* knockout mutant (*spo0A:: kan W168*) were obtained from the Bacillus Genetic Stock Center at the Ohio State University. Pre-cultures of *B. subtilis* and *E. coli* (Turbo, New England Biolabs) were prepared by inoculating a single colony in Lysogeny broth (LB) at 37 °C and growing for 14 h. Strains carrying an antibiotic resistance marker were selected by supplementing the growth medium with chloramphenicol (5 μg ml^{-1}) or erythromycin (1 μg ml^{-1}). All genetic manipulations were carried out in *E. coli* and verified by sequencing (Laragen, USA). Verified constructs were subsequently transformed into PY79 following previous protocols.[24]

Spore preparation for LCMs. A fresh colony of *B. subtilis* was inoculated in Difco sporulation (DS) medium and grown to mid-exponential phase (37 °C, 150 rpm). Cells were subsequently resuspended in an equal volume of Sterlini-Mendalstam (SM) medium.[25] Spores were harvested 36 h after resuspension. Remaining vegetative cells were deactivated by heating at 80 °C for 30 m. Spores after heat treatment were further purified by washing three times in deionized water and resuspended in PBS to final volume.

Composite material preparation. A premix solution of xanthan polymer (Spectrum Chemicals, final concentration: 1% w/v), *N*,*N'*-methylenebisacrylamide (Sigma-Aldrich, final concentration: 26 mM), and *N*-(hydroxymethyl)acrylamide (NHMAA) or *N*-isopropylacrylamide (NIPAM) monomers (Sigma-Aldrich, final concentration: 1 M) in PBS was prepared. For cell and spore-containing materials, culture solutions of known colony-forming units CFU per mL (**Figure S4.1**) were centrifuged to harvest cells, which were subsequently washed, suspended in PBS, and added to the premix solution. Lithium phenyl-2,4,6-trimethylbenzoylphosphinate (Sigma-Aldrich, final concentration: 3 mM) was used as photo-initiator and added to the premix right before UV irradiation. We used commercially available gaskets (Press-to-Seal™, ThermoFisher Scientific, 9 mm diameter, 500 μm thickness) to seal the premix between glass slides. Upon UV spot irradiation (Omnicure s2000, 300 s), hydrogels of uniform size were obtained. The irradiance at the reaction site

was measured to be 14–18 mW/cm^2 at 405 nm and 8–12 mW/cm^2 at 365 nm (G & R Labs, model 202 UV meter). To minimize variability, photo-polymerization of NIPAM mixtures were performed on ice. The resulting NHMAA hydrogels were transparent; NIPAM hydrogels were turbid.

Genetic construction. The expression plasmid was constructed based on pLIKE-rep backbone by replacing P_{lia} with P_{veg}.[25] The SpoVG ribosomal binding site was cloned downstream of the promoter with standard BioBrick RFC spacers.[26] Sequences along with RBS was amplified from a previous template with primer YH110 and YH119 and digested with *EcoRI* and *BsaI*. The sequence of *mrfp* along with the double transcriptional terminators was amplified directly from pBS1C with primer YH120 and YH108 (**Table S4.1**). The PCR product was then digested with *BsaI* and *SphI* and ligated to the backbone. Sequence of the secretion signal peptide, *AmyQ* was amplified from vector pHT43 (MoBiTec, GmbH) with primer YH134 and YH135, digested with *EcoRI* and *BsaI* prior to ligation. Chromosomal co-expression of mWasabi and mRFP was achieved by integrating P_{veg}-*mrfp* and *cotG-mWasabi* into *amyE* and *lacA* locus using vector pBS1C and pBS2E, respectively into the genome of PY79. Sequence of *cotG* along with its endogenous promoter and ribosomal binding regions was amplified from PY79 genome using primer YH178 and YH180. Purified plasmids were linearized by digesting with *SacI* before transformation (**Table S4.1**).

CFU assay. Aliquots of overnight cell cultures grown in LB were diluted in PBS to generate 10-100 colonies on LB agar plates. Colonies were subsequently counted and averaged among three biological replicates. For spore cultures, aliquots were first heated to 80 °C for 30 min to kill remaining vegetative cells. The heated samples were then diluted as described to obtain CFU.

Confocal laser scanning microscopy and image analysis. Samples were imaged on a Zeiss Upright Axio Examiner Fixed stage confocal laser scanning microscope at the Biological Imaging Facility of the Beckman Institute at Caltech. For low-resolution imaging, a Plan-Apochromat 10×/0.45 M27 objective lens (850.19 µm × 850.19 µm) was used. For LIVE/DEAD^{TM} BacLight (Thermofischer, USA) staining, samples were

immersed in the working solutions for 4 h and washed twice with phosphate buffered saline to remove excess staining reagent. A 488 nm laser line (2.0 %) with 523–597 nm (green) and 597–651 nm (red) bandpass filters was used for detection of live and dead cellular entities. Images were taken as Z-stacks (1 μm per stack). 3D reconstructions of the Z-stacks were performed by using the Zeiss Zen software. ImageJ (NIH) was used to quantify the fraction of green pixels (particle analysis plugin) after applying appropriate thresholds to discern red and green pixels. The means and standard errors were calculated from 3 z-stacks. For CTC staining, the BacLight redoxSensor CTC vitality kit (Thermofischer, USA) was used. Samples were immersed in 100 μL working CTC solution (5 mM), incubated at 37°C for 30 min, and subsequently washed with PBS before imaging. A 488 nm laser line (5%) with a 597–651 nm (red) bandpass filter was used for collecting fluorescence signals. The total intensity for each sample was calculated by ImageJ (NIH) and normalized with respect to the average total intensity of the cell–NHMAA composite. High-resolution single-cell images of living composite materials were obtained by using a Plan-Apochromat 100×/1.45 Vis-IR objective lens. For imaging, the mRFP-mWasabi double fluorescence strain, a 488 nm laser line (1.0%) with a 410-546 nm bandpass filter and a 561 nm laser (1.5%) with a 600-700 nm bandpass filter were used for detection. To minimize overlapping cells and spores in the z-direction, images spanning 10 μm in the z-direction were taken as 50 stacks, with 0.2 μm per stack. 2D reconstruction was done using ImageJ (NIH) with drift correction (StackReg) when necessary. Percentages of cells and spores were quantified by manual counting of more than 150 cellular entities within each sample. High resolution images of samples stained with LIVE/DEAD™ BacLight stains were obtained using same laser settings as described above.

Scanning electron microscopy. Experiments were performed on a ZEISS 1550VP Field Emission Scanning Electron Microscope at the Caltech Division of Geological and Planetary Sciences Analytical Facility. Cell and spore composites were immersed in a 2.5% glutaraldehyde solution in 50 mM sodium cacodylate buffer for 2 h at 37 °C. After dialyzing in DI water 3 times (2 h each), the samples were freeze-dried. Before the measurement,

freeze-dried samples were transferred to a conductive carbon tape, fractured with a blade, and coated with a Pd layer 10 nm in thickness before imaging.

Transmission electron cryo-microscopy. Experiments were performed on a ZEISS 1550VP Field Emission Scanning Electron Microscope at the Caltech Division of Geological and Planetary Sciences Analytical Facility. Cell and spore composites were immersed in a 2.5% glutaraldehyde solution in 50 mM sodium cacodylate buffer for 2 h at 37 °C. After dialyzing in DI water 3 times (2 h each), the samples were freeze-dried. Before the measurement, freeze-dried samples were transferred to a conductive carbon tape, fractured with a blade, and coated with a Pd layer 10 nm in thickness before imaging.

Re-swelling of composite materials. After dehydration on PTFE plates for 36 h with desiccants (Drierite®), composites were immersed in LB or PBS (1.5 mL/composite) at 37 °C for 12 h.

Shaking experiments. Three dehydrated cell or spore composites were immersed in 15 mL LB and placed in a shaking incubator set at 37 °C, 250 rpm. The optical density of the medium was measured over 72 h.

Epifluorescence imaging. A Bio-Rad ChemiDoc™ imager equipped for epifluorescence illumination was used for imaging cell composites expressing AmyQ-mRFP (exposure time 10 s) or mRFP (exposure time 1 s). Using ImageJ (NIH) software, the areas of interest were selected and the total fluorescent intensity in each area was calculated. The intensity was normalized based on the average total fluorescence intensity of the as-prepared composites. For blank subtraction, NHMAA and NIPAM scaffolds without cells were prepared, dehydrated, immersed in LB or PBS, and imaged with the same settings.

mRFP quantification in shaking experiments. Twelve dried cell composites bearing AmyQ-mRFP or mRFP expressing cells were immersed in 5 mL LB. The culture tube was shaken at 37 °C in 250 rpm for 72 h. Aliquots (150 µL) were collected every 12 h to measure the total fluorescence intensity and optical density. For fluorescence measurements, samples

were excited with a 584 nm laser (10 nm bandwidth), and emission was recorded at 607 nm (10 nm bandwidth) with manually adjusted gain (100 or 150), using a Varioskan multimode plate reader at 25 °C. The amount of mRFP was quantified using a standard curve generated from known concentrations of mRFP (Clontech). Signals from 3 measurements were averaged.

mRFP quantification of liquid culture. A saturated culture of cells expressing AmyQ-mRFP was collected by centrifugation, washed with PBS, and cells were resuspended in the same volume of either LB or PBS. The culture tube was shaken at 37 °C in 250 rpm for 72 h. Aliquots (150 µL) were collected after 12, 24, 48, and 72 h to measure the total fluorescence intensity after removing the cell pellet. For fluorescence measurements, samples were excited with a 584 nm laser (10 nm bandwidth), and emission was recorded at 607 nm (10 nm bandwidth) with manually adjusted gain (100 or 150), using a Varioskan multimode plate reader at 25 °C. The amount of mRFP was quantified using a standard curve generated from known concentrations of mRFP (Clontech).

4.5 Supplementary Tables and Figures

Table S4.1. Primers

Primers	Sequence
YH110	GATCGAATTCGGAGTTCTGAGAATTGGT
YH119	GATCGGTCTCCCACCTTTCTCTAGTAACATTTATTGTACAACACGAGCC
YH120	GATCGGTCTCAGGTGGTGAATACTAGATGGCTTCCTCCGAAGA
YH108	GATCGCATGCTATAAACGCAGAAAGGCCCAC
YH134	GATCGGTCTCAGGTGGTGAATACTAGATGATTCAAAAACGAAAGCG
YH135	GATCGGTCTCTACGGCTGATGTTTTTG
YH178	AAAAAAGAATTCTTGATTTACCTTCATCACAGCTG
YH180	GATCGGTCTCCTCCACCTTTGTATTTCTTTTTGACTACCCAGCA

* enzyme recognition sites were underlined

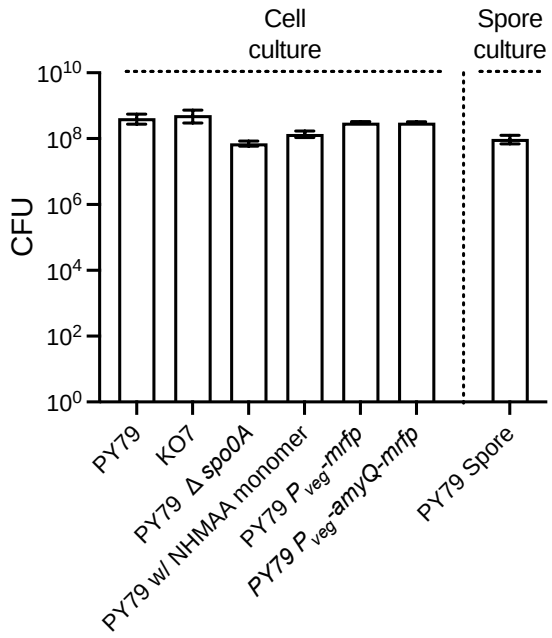

Figure S4.1. Colony-forming units (CFU) per mL of PY79 *B. subtilis* cell cultures grown in LB for 14 h and PY79 spore culture grown in SM medium for 36 h.

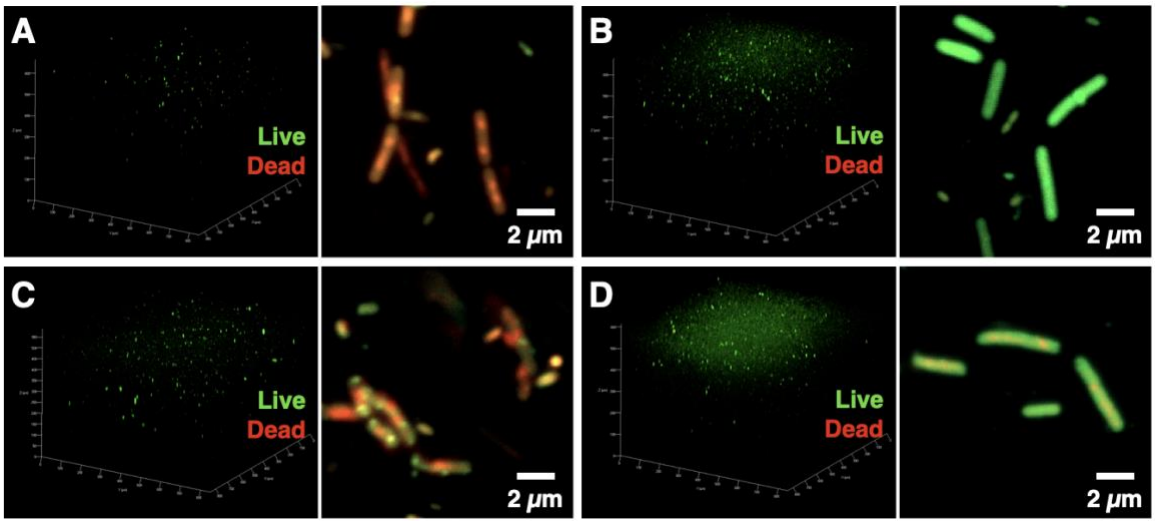

Figure S4.2. Viability analysis of cell-based (Spo0A knock-out) LCMs. Representative confocal laser scanning microscopy image stacks (left: low-resolution, right: high-resolution) of re-swollen LCMs containing a Spo0A knock-out mutant of *B. subtilis*. (**A**), **PNHMAA$_{Spo0A}$** re-swollen in PBS; average percentage of green pixels: 34%, (**B**), **PNHMAA$_{Spo0A}$** re-swollen in LB; average percentage of green pixels: 65%, (**C**), **PNIPAM$_{Spo0A}$** re-swollen in PBS; average percentage of green pixels: 66%, and (**D**), **PNIPAM$_{Spo0A}$** in LB; average percentage of green pixels: 70%. Samples were stained with LIVE/DEAD™ reagent and washed prior to imaging.

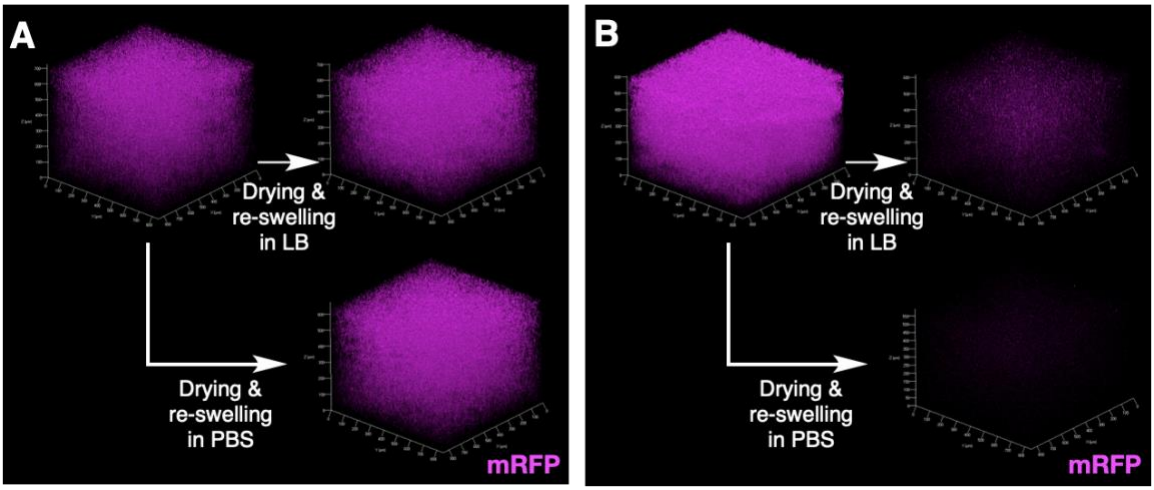

Figure S4.3. mRFP expression in cell-based LCMs. Representative confocal laser scanning microscopy image stacks of LCMs prepared with *B. subtilis* cells expressing mRFP intracellularly (without secretion tag). (**A**), Pristine **PNHMAA$_{mRFP}$**, **PNHMAA$_{mRFP}$** re-swollen in LB after drying, and **PNHMAA$_{mRFP}$** re-swollen in PBS after drying. (**B**), Pristine **PNIPAM$_{mRFP}$**, **PNIPAM$_{mRFP}$** re-swollen in LB after drying, and **PNIPAM$_{mRFP}$** re-swollen in PBS after drying.

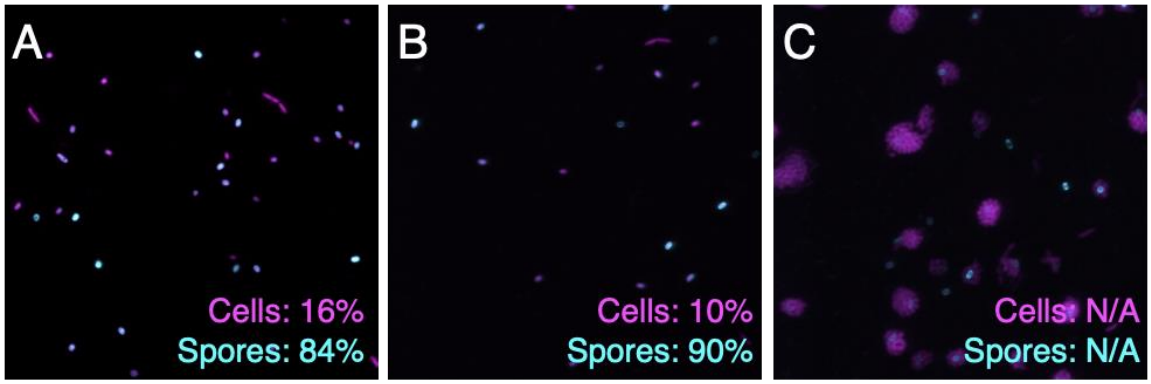

Figure S4.4. Characterization of **PNIPAM$_{Spore}$** Representative confocal laser scanning microscopy images of **PNIPAM$_{Spore}$** samples prepared from the dual-fluorescence (DF) strain. (**A**), Pristine **PNIPAM$_{Spore}$**, (**B**), **PNIPAM$_{Spore}$** re-swollen in PBS after dehydration and (**C**), **PNIPAM$_{Spore}$** re-swollen in LB after dehydration. Re-swelling **PNIPAM$_{Spore}$** in LB for 12 h resulted in biofilm formation on the surface: Percentages of cells and spores were not determined for samples that contained large cell clusters. Fractions of spores and cells were calculated from high-resolution image stacks ($n > 100$).

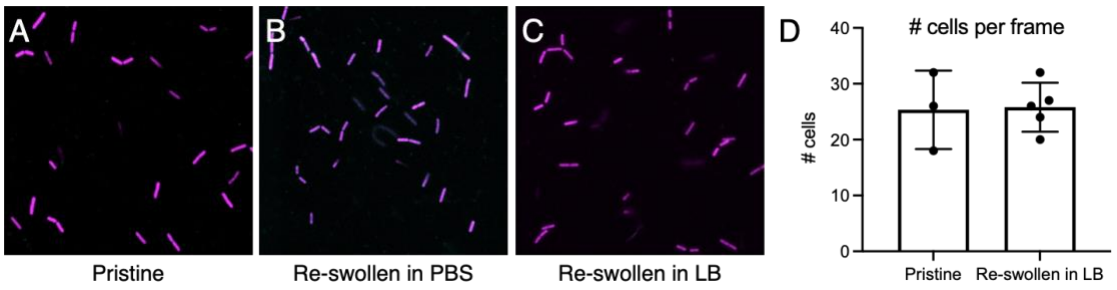

Figure S4.5. Characterization of **PNHMAA$_{Cell}$**. Representative confocal laser scanning microscopy images of **PNHMAA$_{Cell}$** samples prepared from the dual-fluorescence (DF) strain. (**A**), Pristine **PNHMAA$_{Cell}$**, (**B**), **PNHMAA$_{Cell}$** re-swollen in PBS after dehydration and (**C**), **PNHMAA$_{Cell}$** re-swollen in LB after dehydration. (**D**), Number of cells per frame calculated from high-resolution image stacks.

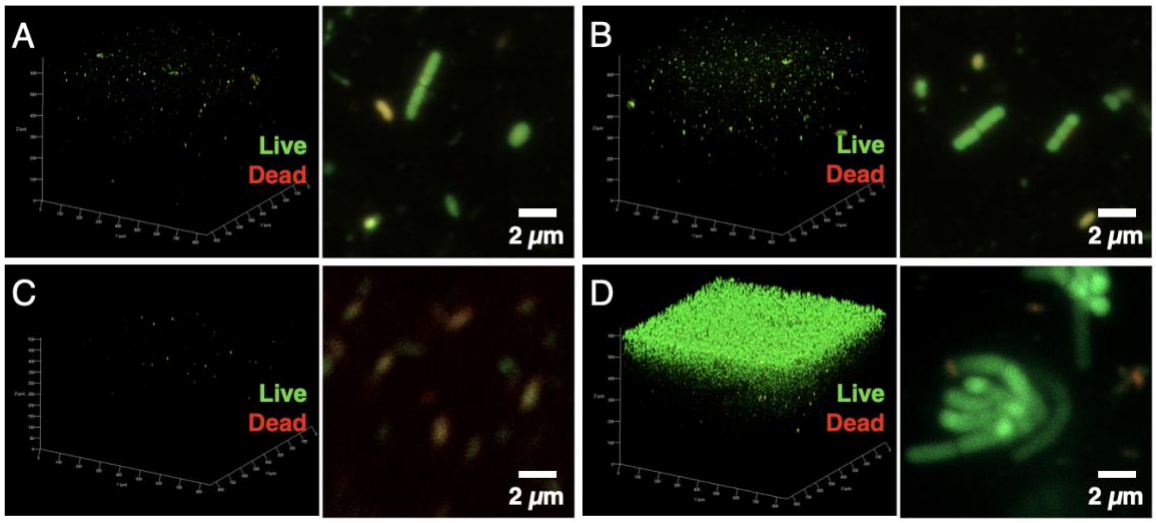

Figure S4.6. Viability analysis of spore-based LCMs. Representative confocal laser scanning microscopy image stacks (left: low-resolution, right: high-resolution) after 12 h of re-swelling of dehydrated LCMs prepared with *B. subtilis* spores. (**A**), **PNHMAA$_{Spore}$** re-swollen in PBS, (**B**), **PNHMAA$_{Spore}$** re-swollen in LB, (**C**), **PNIPAM$_{Spore}$** re-swollen in PBS, and (**D**), **PNIPAM$_{Spore}$** in LB. Re-swelling **PNIPAM$_{Spore}$** in LB resulted in biofilm formation on the surface of the sample. Samples were stained with LIVE/DEAD™ reagent and washed prior to imaging.

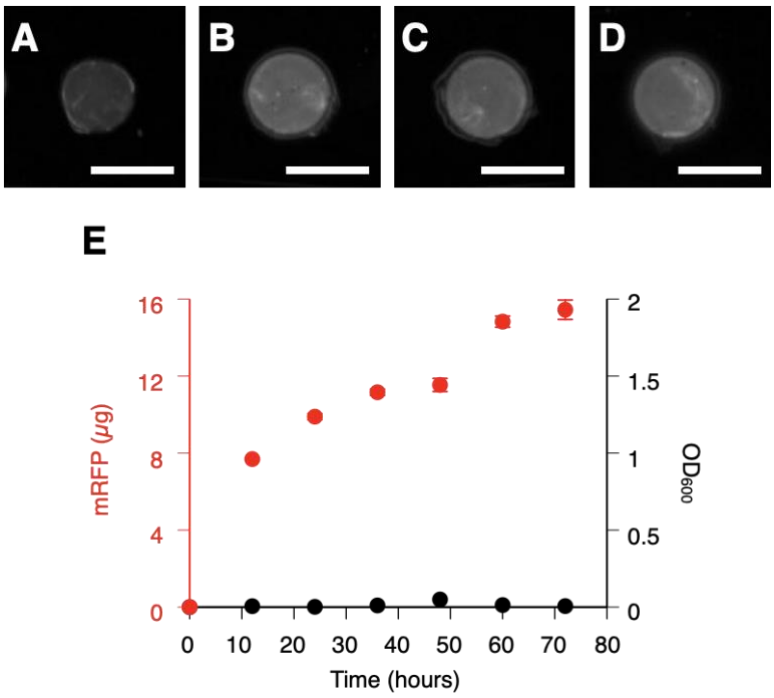

Figure S4.7. Protein synthesis and cell leakage from **PNHMAA$_{mRFP}$**. (**A–D**), Epifluorescence images of **PNHMAA$_{mRFP}$** containing *B. subtilis* cells expressing cytoplasmic mRFP. (**A**), pristine **PNHMAA$_{mRFP}$**, (**B**), **PNHMAA$_{mRFP}$** re-swollen for 12 h in LB after dehydration, (**C**), **PNHMAA$_{mRFP}$** re-swollen for 12 h in PBS after dehydration, and (**D**), **PNHMAA$_{mRFP}$** re-swollen after dehydration and shaken in LB for 72 h. Scale bars: 1 cm. (**E**), The amount of mRFP in the media and OD time trace over 72 h after adding 12 samples of **PNHMAA$_{mRFP}$** to 5 mL LB (37 °C, 250 rpm).

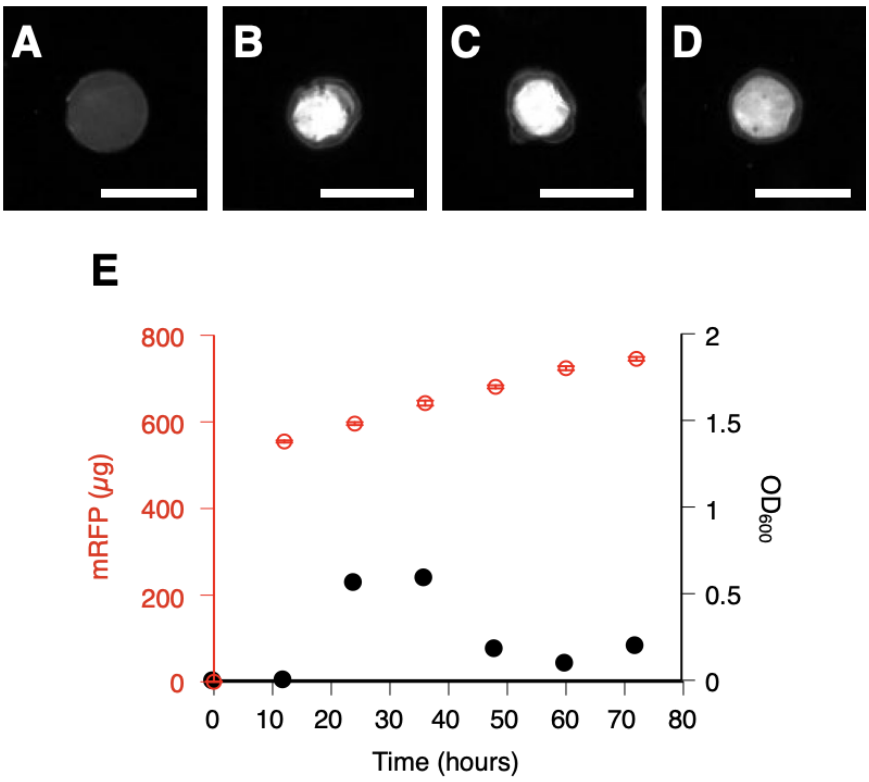

Figure S4.8. Protein synthesis and cell leakage from **PNIPAM$_{mRFP}$**. (**A–D**), Epifluorescence images of **PNIPAM$_{mRFP}$** containing *B. subtilis* cells expressing cytoplasmic mRFP. (**A**), pristine **PNIPAM$_{mRFP}$**, (**B**), **PNIPAM$_{mRFP}$** re-swollen for 12 h in LB after dehydration, (**C**), **PNIPAM$_{mRFP}$** re-swollen for 12 h in PBS after dehydration, and (**D**), **PNIPAM$_{mRFP}$** re-swollen after dehydration and shaken in LB for 72 h. Scale bars: 1 cm. (**E**), The amount of mRFP in the media and OD time trace over 72 hours after adding 12 samples of **PNIPAM$_{mRFP}$** to 5 mL LB (37 °C, 250 rpm).

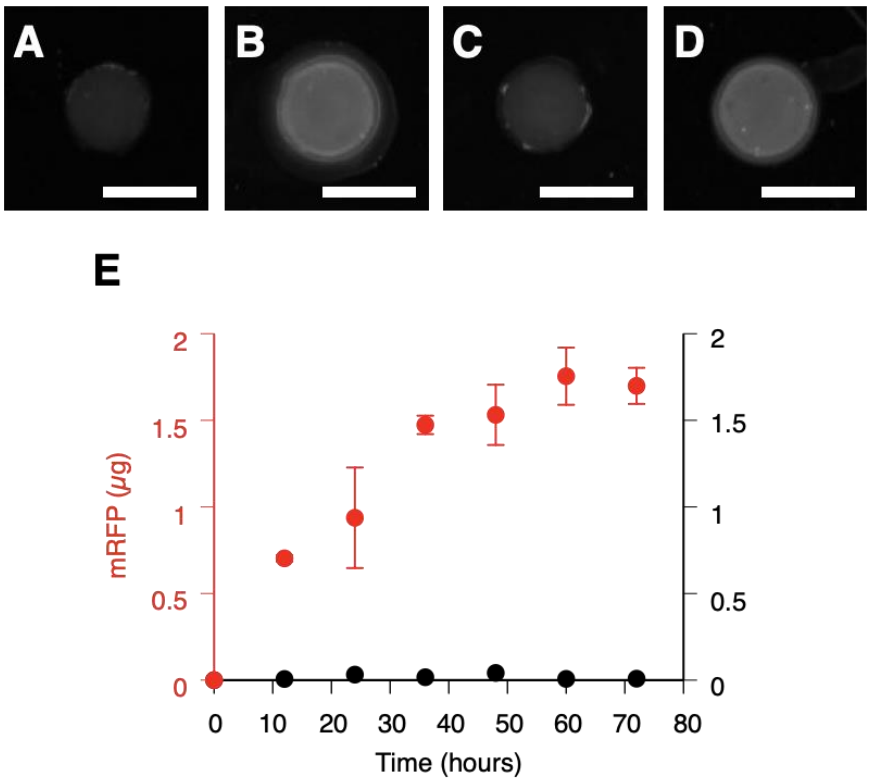

Figure S.4.9. Protein synthesis and cell leakage from **PNHMAA$_{mRFP_s}$**. (**A–D**), Epifluorescence images of **PNHMAA$_{mRFP_s}$** containing *B. subtilis* cells expressing and secreting AmyQ-mRFP. (**A**), pristine **PNHMAA$_{mRFP_s}$**, (**B**) **PNHMAA$_{mRFP_s}$** re-swollen for 12 h in LB after dehydration, (**C**), **PNHMAA$_{mRFP_s}$** re-swollen for 12 h in PBS after dehydration, and (**D**), **PNHMAA$_{mRFP_s}$** re-swollen after dehydration and shaken in LB for 72 h. Scale bars: 1 cm. (**E**), The amount of mRFP in the media and OD time trace over 72 hours after adding 12 samples of **PNHMAA$_{mRFP_s}$** to 5 mL LB (37 °C, 250 rpm).

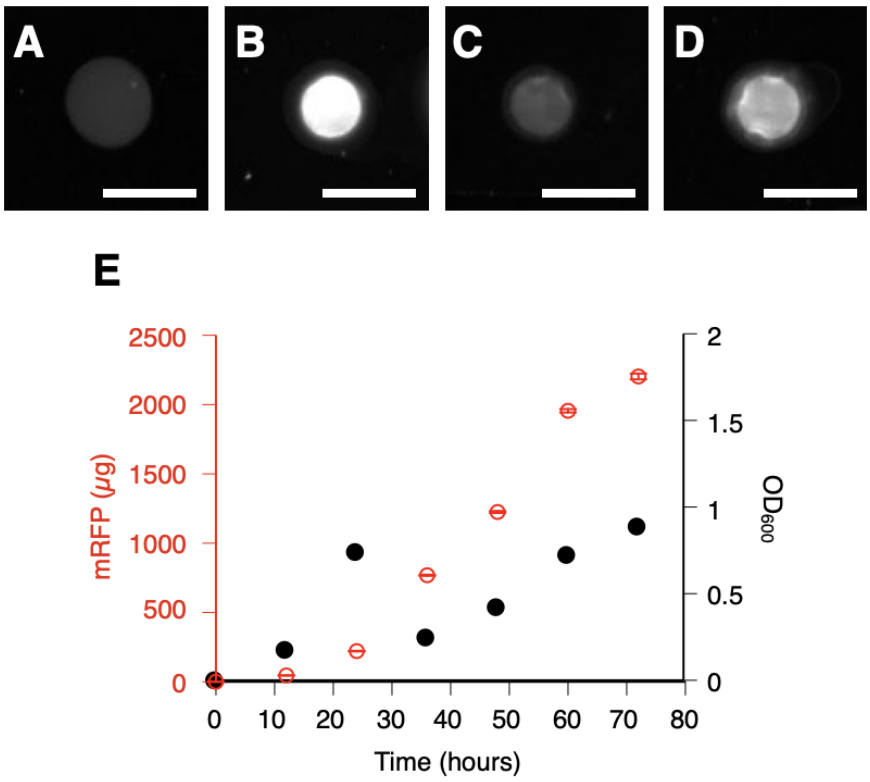

Figure S4.10. Protein synthesis and cell leakage from **PNIPAM$_{mRFP_s}$**. (**A–D**), Epifluorescence images of **PNIPAM$_{mRFP_s}$** containing *B. subtilis* cells expressing and secreting AmyQ-mRFP. (**A**), pristine **PNIPAM$_{mRFP_e}$**, (**B**), **PNIPAM$_{mRFP_s}$** re-swollen for 12 h in LB after dehydration, (**C**), **PNIPAM$_{mRFP_s}$** re-swollen for 12 h in PBS after dehydration, and (**D**), **PNIPAM$_{mRFP_s}$** re-swollen after dehydration and shaken in LB for 72 h. Scale bars: 1 cm. (**E**), The amount of mRFP in the media and OD time trace over 72 hours after adding 12 samples of **PNIPAM$_{mRFP_s}$** to 5 mL LB (37 °C, 250 rpm).

4.6 Acknowledgements

S.S. and Y.H. contributed equally to this work. This work was supported by Defense Advanced Research Projects Agency Engineered Living Materials Agreement HR0011-17-2-0037, and by the Institute for Collaborative Biotechnologies through cooperative agreement W911NF-19-2-0026 from the U.S. Army Research Office. The content of the information does not necessarily reflect the position or the policy of the Government, and no official endorsement should be inferred. Confocal imaging was performed in the Biological Imaging Facility, with the support of the Caltech Beckman Institute and the Arnold and Mabel Beckman Foundation. Scanning Electron Microscopy was performed at the Caltech Division of Geological and Planetary Sciences Analytical Facility.

4.7 References

1 Smanski, M. J. *et al.* Synthetic biology to access and expand nature's chemical diversity. *Nature Reviews Microbiology* **14**, 135-149 (2016).

2 Nguyen, P. Q., Courchesne, N. M. D., Duraj-Thatte, A., Praveschotinunt, P. & Joshi, N. S. Engineered living materials: prospects and challenges for using biological systems to direct the assembly of smart materials. *Advanced Materials* **30**, 1704847 (2018).

3 Cao, Y. *et al.* Programmable assembly of pressure sensors using pattern-forming bacteria. *Nature biotechnology* **35**, 1087-1093 (2017).

4 Connell, J. L., Ritschdorff, E. T., Whiteley, M. & Shear, J. B. 3D printing of microscopic bacterial communities. *Proceedings of the National Academy of Sciences* **110**, 18380-18385 (2013).

5 Schaffner, M., Rühs, P. A., Coulter, F., Kilcher, S. & Studart, A. R. 3D printing of bacteria into functional complex materials. *Science advances* **3**, eaao6804 (2017).

6 Liu, X. *et al.* 3D printing of living responsive materials and devices. *Advanced Materials* **30**, 1704821 (2018).

7 Balasubramanian, S., Aubin-Tam, M.-E. & Meyer, A. S. Vol. 8 1564-1567 (ACS Publications, 2019).

8 Huang, J. *et al.* Programmable and printable Bacillus subtilis biofilms as engineered living materials. *Nature chemical biology* **15**, 34-41 (2019).

9 Priks, H. *et al.* Physical confinement impacts cellular phenotypes within living materials. *ACS applied bio materials* **3**, 4273-4281 (2020).

10 González, L. M., Mukhitov, N. & Voigt, C. A. Resilient living materials built by printing bacterial spores. *Nature chemical biology* **16**, 126-133 (2020).

11 Tang, T.-C. *et al.* Hydrogel-based biocontainment of bacteria for continuous sensing and computation. *Nature Chemical Biology* **17**, 724-731 (2021).

12 Krishnan, S., Klein, A., El-Aasser, M. S. & Sudol, E. D. Influence of chain transfer agent on the cross-linking of poly (n-butyl methacrylate-co-N-methylol acrylamide) latex particles and films. *Macromolecules* **36**, 3511-3518 (2003).

13 Brown, N. R., Loferski, J. R. & Frazier, C. E. Cross-linking poly (vinyl acetate-co-N-methylolacrylamide) latex adhesive performance Part II: Fracture mechanics and microscopic durability studies. *International journal of adhesion and adhesives* **27**, 554-561 (2007).

14 Chen, T., Fang, Q., Zhong, Q., Chen, Y. & Wang, J. Synthesis and thermosensitive behavior of polyacrylamide copolymers and their applications in smart textiles. *Polymers* **7**, 909-920 (2015).

15 Heskins, M. & Guillet, J. E. Solution properties of poly (N-isopropylacrylamide). *Journal of Macromolecular Science—Chemistry* **2**, 1441-1455 (1968).

16 Stocks, S. Mechanism and use of the commercially available viability stain, BacLight. *Cytometry Part A: The Journal of the International Society for Analytical Cytology* **61**, 189-195 (2004).

17 Pandey, R. *et al.* Live cell imaging of germination and outgrowth of individual Bacillus subtilis spores; the effect of heat stress quantitatively analyzed with SporeTracker. *PloS one* **8**, e58972 (2013).

18 Molle, V. *et al.* The Spo0A regulon of Bacillus subtilis. *Molecular microbiology* **50**, 1683-1701 (2003).

19 Gray, D. A. *et al.* Extreme slow growth as alternative strategy to survive deep starvation in bacteria. *Nature communications* **10**, 1-12 (2019).

20 Riesenman, P. J. & Nicholson, W. L. Role of the spore coat layers in Bacillus subtilis spore resistance to hydrogen peroxide, artificial UV-C, UV-B, and solar UV radiation. *Applied and environmental microbiology* **66**, 620-626 (2000).

21 Setlow, P. Spores of Bacillus subtilis: their resistance to and killing by radiation, heat and chemicals. *Journal of applied microbiology* **101**, 514-525 (2006).

22 Nicholson, W. L., Munakata, N., Horneck, G., Melosh, H. J. & Setlow, P. Resistance of Bacillus endospores to extreme terrestrial and extraterrestrial environments. *Microbiology and molecular biology reviews* **64**, 548-572 (2000).

23 Phan, T. T. P., Nguyen, H. D. & Schumann, W. Novel plasmid-based expression vectors for intra-and extracellular production of recombinant proteins in Bacillus subtilis. *Protein expression and purification* **46**, 189-195 (2006).

24 Harwood, C. R. & Cutting, S. M. *Molecular biological methods for Bacillus*. (Wiley, 1990).

25 Sterlini, J. M. & Mandelstam, J. Commitment to sporulation in Bacillus subtilis and its relationship to development of actinomycin resistance. *Biochemical Journal* **113**, 29-37 (1969).

26 Radeck, J. *et al.* The Bacillus BioBrick Box: generation and evaluation of essential genetic building blocks for standardized work with Bacillus subtilis. *Journal of biological engineering* **7**, 1-17 (2013).